

**Structural analysis of the *Mycobacterium tuberculosis* redox defence network reveals a unique bi-fan motif design associated with hydrogen peroxide reduction**

By

**Nolyn John**

BSc. (*Hons*) Genetics

Submitted in fulfilment of the academic requirements for the degree of Masters of Science in the  
Discipline of Genetics  
School of Life Sciences  
College of Agriculture, Engineering and Science  
University of KwaZulu-Natal  
Pietermaritzburg  
South Africa



As the candidate's supervisor(s) I, have approved this dissertation for submission

**Supervisor:** Dr C. S. Pillay

**Supervisor:** Prof J. M. Rohwer

**Signature:**

**Signature:**



**Date:** 18/04/2017

**Date:** 18/04/2017

## Preface

The research contained in this dissertation was completed by the candidate while based in the discipline of Genetics, School of Life Sciences of the College of Agriculture, Engineering and Science, University of KwaZulu-Natal, Pietermaritzburg, South Africa under the supervision of Dr C. S. Pillay and Prof J. M. Rohwer.

These studies represent original work by the candidate and have not otherwise been submitted in any form to another University. Where use has been made of the work by other authors it has been duly acknowledged in the text.

**Supervisor:** Dr C. S. Pillay

**Supervisor:** Prof J. M. Rohwer

**Signature:**

**Signature:**



**Date:** 18/04/2014

**Date:** 18/04/2017

# College of Agriculture, Engineering, and Science

## Declaration of Plagiarism

I, Nolyn John, declare that:

- (i) the research reported in this dissertation, except where otherwise indicated or acknowledged, is my original work;
- (ii) this dissertation has not been submitted in full or in part for any degree or examination to any other university;
- (iii) this dissertation does not contain other persons' data, pictures, graphs or other information, unless specifically acknowledged as being sourced from other persons;
- (iv) this dissertation does not contain other persons' writing, unless specifically acknowledged as being sourced from other researchers. Where other written sources have been quoted, then:
  - a) their words have been re-written but the general information attributed to them has been referenced;
  - b) where their exact words have been used, their writing has been placed inside quotation marks, and referenced;
- (v) where I have used material for which publications followed, I have indicated in detail my role in the work;
- (vi) this dissertation is primarily a collection of material, prepared by myself, published as journal articles or presented as a poster and oral presentations at conferences. In some cases, additional material has been included;
- (vii) this dissertation does not contain text, graphics or tables copied and pasted from the Internet, unless specifically acknowledged, and the source being detailed in the dissertation and in the References sections.

---

**Signature:** Nolyn John

**Date:** 18/04/2017

*Declaration Plagiarism 22/05/08 FHDR Approved*

## Abstract

*Mycobacterium tuberculosis* (Mtb) infections claim millions of lives per annum and the rise of drug resistance is expected to increase this disease burden particularly in Africa. Several pathogenic targets are consequently being assessed for drug development including the Mtb antioxidant defense network. This conserved network relies on thiol-based moiety couple systems to detoxify harmful reactive oxygen and nitrogen species elicited by the host immune response and both active and latent Mtb appear to be sensitive to redox protein targeting drugs. Curiously, despite the hypoxic granuloma microenvironment, Mtb is proficient in reducing hydrogen peroxide and oxygen radicals generated by host lymphocytes. To systematically uncover the structural properties of this network, the moiety couples within the network were simplified to moiety sums and compared to the antioxidant networks of *E. coli* and baker's yeast using motif detection analysis. Our results show that Mtb has a unique bi-fan motif within the Mtb thioredoxin/peroxiredoxin system in which two peroxiredoxins, thiol peroxidase (Tpx) and the bacterioferritin comigratory protein (BCP), are reduced by both thioredoxin B and C respectively. Characterization of the bi-fan motif using mathematical and computational modelling revealed a greater tolerance to hydrogen peroxide and robustness to changes in thioredoxin B or C concentrations when compared to a bi-parallel motif suggesting that the bi-fan motif could play a critical role in Mtb persistence *in vivo*. Mtb BCP has not previously been kinetically characterized and along with thioredoxin reductase and thioredoxin C were synthesized on pET28a vectors for *in vitro* analysis. Isopropyl  $\beta$ -D-1-thiogalactopyranoside (IPTG) expression of the clones in *E. coli* BL21 and nickel affinity chromatography (Ni-NTA) purification of the His-tagged proteins yielded pure protein samples. Thioredoxin reductase and thioredoxin C were assayed to determine their specific activities while BCPs' kinetics regarding hydrogen peroxide reduction will be tested using a HRP competition assay in future studies. Overall, novel insights into the *M. tuberculosis* redox defence network were obtained through a combination of systems biology techniques and this work serves as a good starting point for further adoption in other diseases.

## Acknowledgements

Upon the completion of my MSc dissertation, I would like to extend the utmost appreciation to the following people:

My supervisor and mentor, Dr Ché S. Pillay, for all your guidance, patience, support and critical analysis of my work all of which not only made me a better scientist but helped me grow into a better and brighter individual. Thank you for awarding me a bursary to carry out my degree, without which I would not have been able to further my studies.

My co-supervisor, Prof Johann M. Rohwer, for your valuable and critical input. Thank you for overlooking the study as well as providing fresh insights towards the research. Thank you, along with Dr Pillay, for awarding me the NRF bursary necessary to carry out my MSc degree.

Thank you to my former and current lab members: Beatrice, Letrisha, Lefenste, Ryan, Jezelle, Diane and Kapil for making the lab a fun-filled and enjoyable place to work in. Aside from the laughs, thank you for lending a helpful hand when experiments failed and contributing to the solutions which ultimately taught and aided me along the path of becoming a better researcher.

To my awesome family: Vimla and Wanita, thank you for the undying support, always bearing with my moods and the hundreds of cups of coffee you guys had to make over these past few years. Without your support through this rough journey, I would have quit a long time ago. Thank you for always having my back no matter the task and always being my pillars of strength. Thank you for making my shoulder injury as comfortable as possible as this was one of the hardest months to deal with throughout this degree.

Last but not least, my bestest friend Ashrenee. Thank you for your patience, support, laughs, believing in me even when I didn't myself and shining the light forward when the path ahead wasn't clear. Thank you for your undying support no matter the time of day, bearing with my moods (I seem to be a really moody person), supporting and helping me recover through my injury during which you took time away from your own work to help me, for that I will be eternally grateful and lastly for being YOU !!! Don't change a damn thing.

*I dedicate this dissertation to Selvin John, a man who I will always thrive to be like, a role-model, father, husband and precious friend.*

## List of Abbreviations

AEBSF	4-(2-aminoethyl)benzenesulfonyl fluoride hydrochloride
AhpC	alkyl hydroperoxidase subunit C
AhpD	alkyl hydroperoxidase subunit D
AhpE	alkyl hydroperoxidase subunit E
AIDS	acquired immunodeficiency syndrome
BCG vaccine	Bacillus Calmette-Guérin vaccine
BCP	bacterioferritin comigratory protein
BSA	bovine serum albumin
CFP-10	culture filtrate protein (10 kDa)
Cys-SO <sub>2</sub> H	cysteine sulfinic acid
Cys-SO <sub>3</sub> H	cysteine sulfonic acid
ddH <sub>2</sub> O	Milli-Q water
dH <sub>2</sub> O	distilled water
ESAT-6	early secretory antigenic target (6 kDa)
DTNB	5,5-dithio-bis-(2-nitrobenzoic acid)
DTT	dithiothreitol
EDTA	ethylene diamine tetraacetic acid
FFL	feed-forward loop
Gor	glutathione reductase
GSH	glutathione
Grx-1	glutaredoxin-1
H <sub>2</sub> O <sub>2</sub>	hydrogen peroxide

HAART	highly active antiretroviral therapy
HIV	human immunodeficiency virus
INH	isoniazid
IPTG	isopropyl $\beta$ -D-1-thiogalactopyranoside
KatG	catalase/peroxidase of <i>M. tuberculosis</i>
LAM	lipoarabinomannan
LM	lipomannan
Mca	mycothiol conjugate amidase
MDR-TB	multidrug-resistant TB
MIM	multiple input module
MR/Mtr	mycothione reductase
Mrx-1	mycoredoxin-1
MSH	mycothiol
MSR	mycothiol mixed compound/disulfide
MSSM	mycothione
Mtb	<i>Mycobacterium tuberculosis</i>
MWM	molecular weight marker
NADPH	nicotinamide adenine dinucleotide phosphate
NO	nitric oxide
Ni-NTA	nickel affinity protein chromatography purification
NP	nanoparticle
O/N	overnight
PIM	phosphatidyl- <i>myo</i> -inositol mannosides

PMSF	phenylmethane sulfonyl fluoride
Prx	peroxiredoxin
PSH/PSS	reduced cellular protein/oxidized cellular protein
PySCeS	Python Simulator for Cellular Systems
ROS	reactive oxygen species
RMP	rifampin
RNS	reactive nitrogen species
SDS-PAGE	sodium dodecyl sulfate-polyacrylamide gel electrophoresis
SIM	single input module
SodA	superoxide dismutase
TB	Tuberculosis
TBDB	The Tuberculosis Database
TEMED	N,N,N',N'-tetramethylethylenediamine
TR	thioredoxin reductase
Trx	thioredoxin
TSA	thiol-specific antioxidant protein
U/I	uninduced
WHO	World Health Organization
XDR-TB	extensively drug-resistant TB

## Table of contents

Preface .....	i
Declaration of Plagiarism .....	ii
Abstract .....	iii
Acknowledgements .....	iv
List of Abbreviations .....	v
List of Tables .....	xii
List of Figures .....	xiii
<b>Chapter One: Literature review</b> .....	1
1. Introduction .....	1
1.1. <i>Mycobacterium tuberculosis</i> , the single celled tank of the infectious disease world .....	1
1.2. Ineffective preventative measures against tuberculosis and its innate ability to evade eradication .....	6
1.2.1. The <i>M. tuberculosis</i> cell wall structure and function .....	7
1.2.2. Secreted Mtb proteins are partially responsible for the bacterium's survival ....	9
1.3. Redox defence networks and the possibility of deciphering drug targets within .....	9
2. Threat of hydrogen peroxide on <i>M. tuberculosis</i> survival during infection .....	12
3. Redoxin defence networks in <i>M. tuberculosis</i> cells .....	12
3.1. The low-molecular-weight thiol mycothiol (MSH) sustains a reduced intracellular environment .....	13
3.2. Central hub of the Mtb redox defence: the thioredoxin (Trx) system .....	15
3.3. Vastly abundant redox defence proteins of Mtb: the Mtb peroxiredoxins .....	17
3.3.1. Thioredoxin-dependent thiol peroxidase (Tpx) of Mtb .....	19

3.3.2. The alkyl hydroperoxidase reductase subunits C, D and E (AhpC, AhpD and AhpD) .....	19
3.3.3. The Bacterioferritin Comigratory Protein (BCP) of Mtb .....	20
3.4. KatG, a system dedicated to the neutralization of hydrogen peroxide .....	20
4. Computational modelling of the <i>M. tuberculosis</i> redox defence systems .....	23
4.1. Genomics and its possible applications in Mtb network biology .....	23
4.2. Proteomic analysis and its role in studying Mtb cellular systems .....	24
4.3. Systems biology computational modelling approaches .....	25
4.3.1. Genome-scale modelling vs. kinetic modelling approaches .....	26
5. Conclusion .....	28
<b>Chapter Two: Structural analysis of the <i>M. tuberculosis</i> redox defence network reveals a unique bi-fan motif design in hydrogen peroxide defence .....</b>	<b>29</b>
2.1. Introduction .....	29
2.2. Methods .....	30
2.2.1. Wire diagram construction and motif detection within the <i>M. tuberculosis</i> redox network .....	30
2.2.2. Analytical solutions and kinetic model simulations for the unique bi-fan motif in <i>M. tuberculosis</i> .....	31
2.3. Results .....	32
2.3.1. Wire diagram construction of the <i>M. tuberculosis</i> redox defence network .....	32
2.3.1.1. Does MtBCP follow a 1- or 2- Cys peroxiredoxin reaction mechanism? .....	32
2.3.1.2. Which of the three thioredoxins of Mtb would be able to reduce MtBCP? ...	33
2.3.2. Motifs detected in the <i>M. tuberculosis</i> H <sub>2</sub> O <sub>2</sub> reduction defence network .....	35
2.3.3. Analytical solutions solved for the bi-parallel and bi-fan motif of Mtb .....	40

2.3.4. Core model simulations to determine dynamics of the bi-parallel and -fan motifs .....	44
2.4. Discussion .....	49
<b>Chapter Three: <i>In vitro</i> analysis of the thioredoxin reductase, thioredoxin C and the bacterioferritin comigratory protein components within the bi-fan motif .....</b>	<b>52</b>
3.1. Introduction .....	52
3.2. Materials .....	52
3.2.1. Preparation of lyophilized plasmid DNA .....	52
3.2.2. Preparation of common reagents .....	53
3.2.2.1. Kanamycin stock solution .....	53
3.2.2.2. IPTG stock solution .....	53
3.2.2.3. DTT stock solution .....	53
3.2.2.4. Bovine pancreas insulin stock solution .....	53
3.2.2.5. DTNB stock solution .....	53
3.2.2.6. NADPH stock solution .....	53
3.2.2.7. 10% (w/v) ammonium persulfate solution .....	54
3.2.2.8. SDS-PAGE sample loading buffer (4×) .....	54
3.2.2.9. SDS-PAGE tank buffer (10×) .....	54
3.2.2.10. Bovine serum albumin standard solution .....	54
3.2.2.11. Bradford reagent .....	54
3.2.3. Bacterial growth media .....	54
3.2.3.1. Luria Bertani (LB) broth .....	54
3.2.3.2. Luria Bertani (LB) agar .....	55
3.2.3.3. Glucose stock solutions .....	55

3.2.3.4. SOC media .....	55
3.3. Methods .....	55
3.3.1. Transformation of pET28a plasmids into <i>E. coli</i> BL21 cells for expression .....	55
3.3.2. Sequencing of gene synthesis products .....	56
3.3.3. SDS-PAGE acrylamide gel electrophoresis .....	56
3.3.4. IPTG expression of the <i>rv3913</i> , <i>rv3914</i> and <i>rv2521</i> genes from <i>M. tuberculosis</i> in host <i>E. coli</i> BL21 cells .....	57
3.3.5. Nickel affinity protein (Ni-NTA) purification .....	57
3.3.6. Specific activity assays of the <i>M. tuberculosis</i> thioredoxin reductase and thioredoxin C proteins .....	58
3.4. Results .....	59
3.4.1. Successful gene synthesis and protein expression of the <i>rv3913</i> , <i>rv3914</i> and <i>rv2521</i> genes from <i>M. tuberculosis</i> .....	59
3.4.2. Successful purification of the thioredoxin reductase, thioredoxin C and BCP proteins using the Ni-NTA purification method and testing of their specific activities .....	61
3.5. Discussion .....	64
<b>Chapter Four:</b> General dissertation overview .....	66
Reference section .....	68
Appendix .....	81

## List of Tables

<b>Table 1.1.</b> Data from the WHO 2015 report highlighting decrease in global TB prevalence and mortality from 1990 until 2015 as well as the milestones and targets set by WHO with the initiation of the END TB strategy beginning in 2015 .....	5
<b>Table 2.1.</b> Common three node motifs in the hydrogen peroxide reduction networks of <i>M. tuberculosis</i> , <i>E. coli</i> and <i>S. cerevisiae</i> generated by both FANMOD and MAVisto motif detection programs .....	36
<b>Table 2.2.</b> Common and unique four node motifs in the hydrogen peroxide reduction networks of <i>M. tuberculosis</i> , <i>E. coli</i> and <i>S. cerevisiae</i> generated by both FANMOD and MAVisto motif detection programs .....	38
<b>Table 2.3.</b> Species concentrations used for the core computational models of the bi-parallel and bi-fan motif designs .....	44
<b>Table 2.4.</b> Reactions and reaction parameters for core computational modelling of both the bi-parallel and bi-fan motif designs .....	45

## List of Figures

<b>Figure 1.1.</b> World map depicting the estimates for TB and HIV prevalence per 100 000 individuals in 2014 .....	3
<b>Figure 1.2.</b> The TB incidence rate (per 100 000 individuals) in South Africa from 2002 up until 2011 .....	6
<b>Figure 1.3.</b> The South African TB cure and mortality rate rates (%) .....	6
<b>Figure 1.4.</b> Components comprising the cell wall of <i>M. tuberculosis</i> .....	8
<b>Figure 1.5.</b> Bar graph depicting the general decreasing trend associated with new drug developments over the past four decades .....	11
<b>Figure 1.6.</b> Summary of the <i>E. coli</i> glutathione S-glutathionylation and the <i>Actinomyces</i> mycothiol S-mycothionylation processes .....	14
<b>Figure 1.7.</b> Diagrammatic representation of the electron flow originating in NADPH and being passed on to protein disulfides via the thioredoxin system .....	16
<b>Figure 1.8.</b> Overview of the three peroxiredoxin mechanisms namely the typical 2-Cys, atypical 2-Cys and the 1-Cys peroxiredoxins .....	18
<b>Figure 1.9.</b> Arrow diagram representation of the redox defence proteins ad mechanisms within the <i>M. tuberculosis</i> cell .....	22
<b>Figure 2.1.</b> Amino acid alignment of the Mtb BCP and <i>E. coli</i> BCP proteins .....	32
<b>Figure 2.2.</b> A proposed reaction scheme for the Mtb BCP based on its sequence alignment with <i>E. coli</i> BCP .....	33
<b>Figure 2.3.</b> Amino acid alignment between the three thioredoxin proteins (TrxA, TrxB and TrxC) found in <i>M. tuberculosis</i> .....	33
<b>Figure 2.4.</b> Wire diagram construction of the redox defence networks belonging to <i>M. tuberculosis</i> , <i>E. coli</i> and <i>S. cerevisiae</i> .....	34
<b>Figure 2.5.</b> Frequencies of the common three node motifs detected for the three redox networks using MAVisto .....	36

<b>Figure 2.6.</b> Frequencies of the common three node motifs detected for the three redox networks using FANMOD .....	37
<b>Figure 2.7.</b> Frequencies of the common and unique four node motifs detected for the three redox networks using MAVisto .....	39
<b>Figure 2.8.</b> Frequencies of the common and unique four node motifs detected for the three redox networks using FANMOD .....	39
<b>Figure 2.9.</b> Diagrammatic representation of the bi-parallel and bi-fan motif designs subjected to mathematical analysis .....	40
<b>Figure 2.10.</b> Core model simulations of the bi-parallel and bi-fan motif designs show that the bi-fan connectivities allow for the system to handle higher hydrogen peroxide concentrations and subsequently takes longer to saturate the Tpx and BCP redox cycles .....	46
<b>Figure 2.11.</b> Steady-state flux analysis of the bi-parallel and bi-fan systems showing the effect of increasing the total thioredoxin moiety pool concentrations on the flux of these two respective systems .....	47
<b>Figure 2.12.</b> Steady-state flux analysis of the bi-parallel and bi-fan systems showing the effect of keeping a constant thioredoxin moiety pool concentration and the effect on the fluxes of the two systems when there is an increased demand for thioredoxin .....	48
<b>Figure 3.1.</b> Amino acid sequence alignments of the transcripts of the Mtb thioredoxin reductase, thioredoxin C and BCP genes housed in the pET28a expression plasmids with their respective sequences from the Tuberculosis Database (TBDB) .....	60
<b>Figure 3.2.</b> Expression profiles of the three Mtb genes transformed into <i>E. coli</i> BL21 cells following IPTG induced expression. Samples were taken hourly and run on 12% acrylamide SDS-PAGE gel .....	61
<b>Figure 3.3.</b> Gel representing the successful Ni-NTA purification of thioredoxin reductase, thioredoxin C and BCP proteins from crude extract samples .....	62
<b>Figure 3.4.</b> Indication of the specific activities of the thioredoxin reductase and thioredoxin C in the DTNB and insulin reduction assays respectively .....	63

# Chapter 1: Literature Review

## 1. Introduction

### 1.1. *Mycobacterium tuberculosis*, the single celled tank of the infectious disease world

Tuberculosis (TB) is caused by a slow growing gram-positive bacterium known as *Mycobacterium tuberculosis* (Mtb) which belongs to the class *Actinomycetes* (Smith, 2003). To a lesser extent, the disease can also be caused by other members of the “*Mycobacterium* complex” namely *M. africanum*, *M. bovis*, *M. canetti* and *M. microti* (Asif, 2013). TB was described by Hippocrates in 400 B.C. where it was identified as “consumption”, “wasting away”, “kings evil”, “lupus vulgaris”, “the white plague” or “phthisis” (Ducati et al., 2006). Remnants of TB infections were found in Egyptian mummies from 2000 B.C. and a rare manifestation of TB, known as Pott’s disease or Gibbous deformity, was revealed amongst several of these mummies which developed into serious spine deformities and subsequent limb paralysis (Ducati et al., 2006). During the European Middle Age TB also manifested itself as Scrofula, a rare form of TB that affects the lymph nodes. The infection was particularly found around the neck and shoulder region and was believed that the cure came from the power of the divine touch of kings. By the beginning of the 20<sup>th</sup> century, TB had claimed many renowned lives including Charlotte Brontë (and most of the Brontë family), John Keats, Lord Byron, George Orwell, Castro Alves and Eleanor Roosevelt among many others (Ducati et al., 2006).

The origin of *M. tuberculosis*, along with other disease causing *Actinomycetes* species like *M. leprae* (Ducati et al., 2006), has been the subject of intense investigation. It is believed that the genus *Mycobacterium* was initially found in soil and that some species evolved to survive within mammals. The fact that TB was so vastly spread throughout the globe roughly 4000 years ago suggested that there was a common vector for transmission (Ducati et al., 2006). The domestication of cattle roughly 10,000 to 25,000 years ago (Smith, 2003) would have allowed the passage of the pathogen from livestock to humans via unpasteurized milk and untreated meat products (Ducati et al., 2006). *M. bovis*, the mycobacterium that causes a TB-like disease in cattle, was initially believed to be the evolutionary precursor to *M. tuberculosis* that developed mechanisms of survival within the human host. However, phylogenetic studies disproved this hypothesis and concluded that the two mycobacteria co-evolved from a common precursor, possibly *M. canetti*, which shows an older genome but retains similar manifestations within the host (Smith, 2003).

The most common clinical manifestations of pulmonary TB include chronic coughing, sputum production, loss of appetite, weight loss, fever leading to night sweats and haemoptysis (the coughing up of blood). Extrapulmonary TB occurs when other organs of the body become infected and is present in 10 to 42% of patients. The development of extrapulmonary TB depends on multiple factors, some of which include ethnic background, age, presence or absence of an underlying disease, immune status and the strain and genotype of *Mtb* causing infection (Zumla et al., 2013). Coinfection with the human immunodeficiency virus (HIV) further complicates management and treatment of TB infection. Once infected with HIV, the patient soon after develops active TB which mimics the early stages of HIV-negative individuals whom are immunocompromised (Zumla et al., 2013).

Tuberculosis is transmitted via aerosolized droplets containing the infectious *M. tuberculosis* bacterial cells which are then inhaled by an uninfected individual where the infection resides before the cycle can continue once more (Smith, 2003). The bacilli, like the majority of *Mycobacteria*, are relatively resistant to drying, alkali and many other chemical disinfectants, making it very difficult to control transmission in urban environments (Ducati et al., 2006). The inability to control this infectious agent has now led to TB being a global threat, infecting one-third of the world's population and claiming approximately 2 million deaths per annum (Karakousis et al., 2004).

The highest TB burden is found in Asia and Africa (Figure 1.1) with India and China collectively accounting for almost 40% of the total world's TB cases. African regions have 24% of the world's total reported cases and the highest rates of death per capita (World Health Organization, 2012). Along with drug-susceptible *Mtb* strains, multidrug-resistant (MDR-TB) (Gomes et al., 2014) and extensively drug-resistant (XDR-TB) strains (Asif, 2013) have developed with India, China, the Russian Federation and South Africa collectively making up almost 60% of the world's total MDR-TB cases (World Health Organization, 2012).

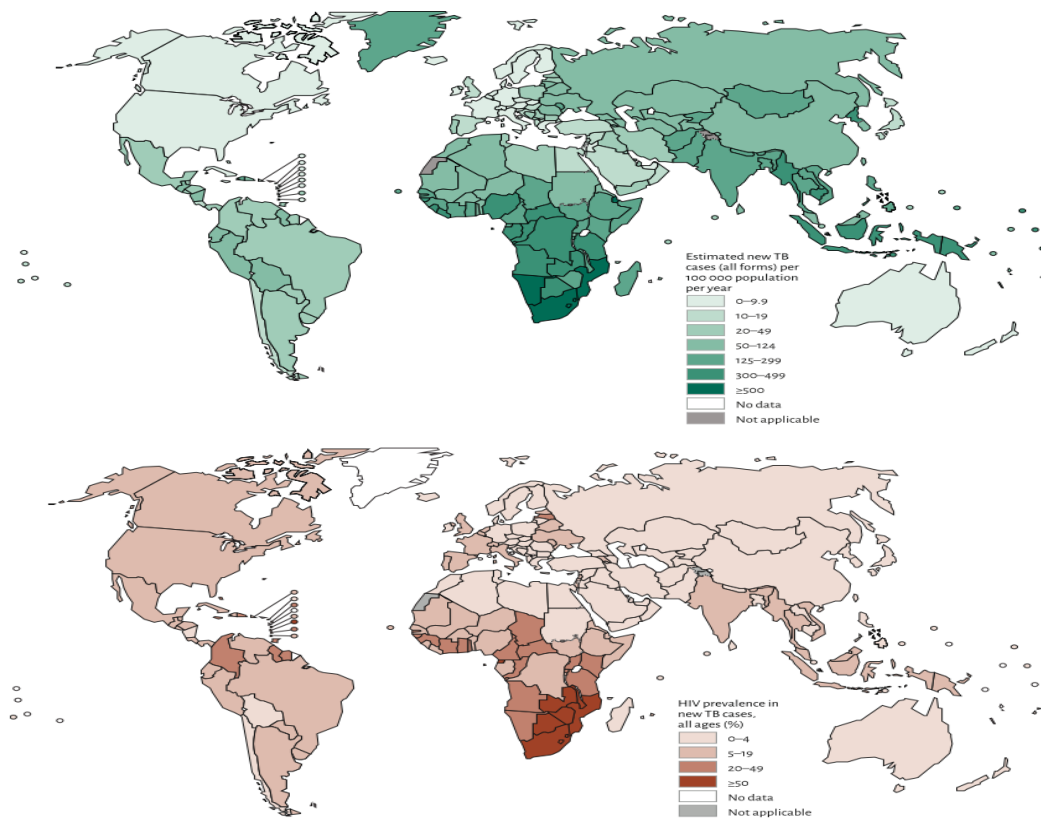


**Figure 1.1.** Estimates of the TB and HIV prevalence per 100 000 individuals in 2014. The increase in the shade of green denotes a higher estimate in reports for new TB cases around the globe while the increase in the shade of brown denotes a higher HIV prevalence percentage amongst all age groups (World Health Organization, 2015). (Permission to reproduce this figure was granted by the World Health Organization Press).

Resistance to the antibiotics isoniazid (INH) and rifampin (RMP), with or without resistance to other first line anti-TB drugs such as pyrazinamide, ethambutol and streptomycin (Gomes et al., 2014) has become the definition of MDR-TB (Campos et al., 2003). XDR-TB refers to strains resistant *in vivo* to at least isoniazid and rifampicin (MDR-TB definition) as well as to three or more of the six main classes of second line anti-TB drugs namely aminoglycosides, polypeptides, fluoroquinolones, thioamides, cycloserine and *p*-aminosalicylic acid. Treatment of patients with MDR- and XDR-TB is significantly more complex, less effective, more toxic and more expensive than that of treatments available against drug-susceptible strains (Gomes et al., 2014). From a clinical perspective, MDR-TB is associated with inadequate treatment regimens, failure to adhere to the treatment for the specified time period, poorly managed TB-control programs and inconsistent hospital infection control programs. While MDR- and XDR-TB are associated with elevated mortality rates,

MDR-TB infections are still manageable with use of second line anti-TB drugs. However, most treatments against XDR-TB are ineffective consequently making it one of the most challenging threats to public health worldwide (Fattorini et al., 2007). The costly and lengthy course of treatment leads to low patient compliance, especially in developing countries, which contributes significantly to the further rise and spread of drug-resistant strains. Clinical cure rates for individuals with MDR-TB in developing areas are less than 50% emphasising the lack of treatment options and adherence, along with the desperate need to find new treatment options (Harbut et al., 2015).

In the South African context, TB along with HIV coinfection poses an enormous threat to the well-being of many individuals. It was recognized that the South African childhood TB burden is one of the largest proportions with regard to the worldwide total TB burden. Disturbingly, 20% of all these cases were estimated to be children of 5 years or younger (Zar et al., 2012). TB prevention can be achieved through various strategies, some of which include improvement of living conditions, immunization, better control and detection methods, use of isoniazid (INH) prophylaxis and highly active antiretroviral therapy (HAART) in HIV-infected individuals (Zar et al., 2012). However, South Africa suffers from the lack of substantial and adequate living conditions along with a lack of access to appropriate treatment (Grange and Zumla, 2008). A study conducted in Cape Town, South Africa, found that INH treatment alone reduced TB incidence and mortality in children by 72 and 54% respectively. A follow-up study placed children on a five year treatment plan with both INH and HAART and yielded promising results with a 90% reduction in TB incidence (Zar et al., 2012). These results suggest that TB treatment alone could play a significant role in controlling the disease provided that patients adhere to the correct treatment regime.

The South African Health Department as well as the World Health Organization (WHO) compile yearly reports for diseases known to be causing great impact and concern in South Africa and the world respectively. These agencies then implement strategies for disease control and set targets by which the disease should be managed and controlled. For example, the WHO aimed to cut total global cases of TB by at least half by 2015 in the STOP TB strategy and totally eradicate the disease from 2015 - 2035 in the END TB strategy (Table 1.1, World Health Organization, 2012 and World Health Organization, 2015). The WHO have successfully implemented their STOP TB strategy as both TB prevalence and mortality have decreased by roughly 50% from 1990 until 2015 (Table 1.1), this also indicates that the END TB strategy can now be implemented with a greater chance of success. The South African department of

Health have also released data showing the number of cases of infected individuals (Figure 1.2) and the TB cure rate and TB mortality (Figure 1.3) with a general trend indicative of increasing TB infections despite strategies put in place to control spread of the disease. Fortunately the cure rate has also increased, revealing increased access to substantial health care and proper TB treatment regimes. Disappointingly, the mortality rate for TB remains constant at roughly 7% (Figure 1.3).

**Table 1.1.** Data from the WHO 2015 report highlighting decrease in global TB prevalence and mortality from 1990 until 2015 as well as the milestones and targets set by WHO with the initiation of the END TB strategy beginning in 2015

<b>Vision</b>		<b>A world free of TB</b>		
		- zero deaths, disease and suffering due to TB		
<b>Global TB reduction and successful regions reaching the target by 2015 since 1990</b>				
	<b>Percentage decrease since 1990</b>		<b>Regions meeting 2015 targets</b>	
<b>TB Prevalence (%)</b>	42%		Americas, South-East Asia, Western Pacific region	
<b>TB mortality (%)</b>	47%		Americas, Eastern Mediterranean region, South-East Asia, Western Pacific region	
<b>Indicators</b>	<b>Milestones</b>		<b>Targets</b>	
	2020	2025	2030	End TB - 2035
Reduce numbers of TB deaths compared to 2015 (%)	35%	75%	90%	95%
Reduce TB incidence rate compared to 2015 (%)	20% (<85/100 000) <sup>a</sup>	50% (<55/100 000) <sup>a</sup>	80% (<20/100 000) <sup>a</sup>	90% (<10/100 000) <sup>a</sup>

<sup>a</sup> represents a value with the decrease in incidence per 100 000 individuals.

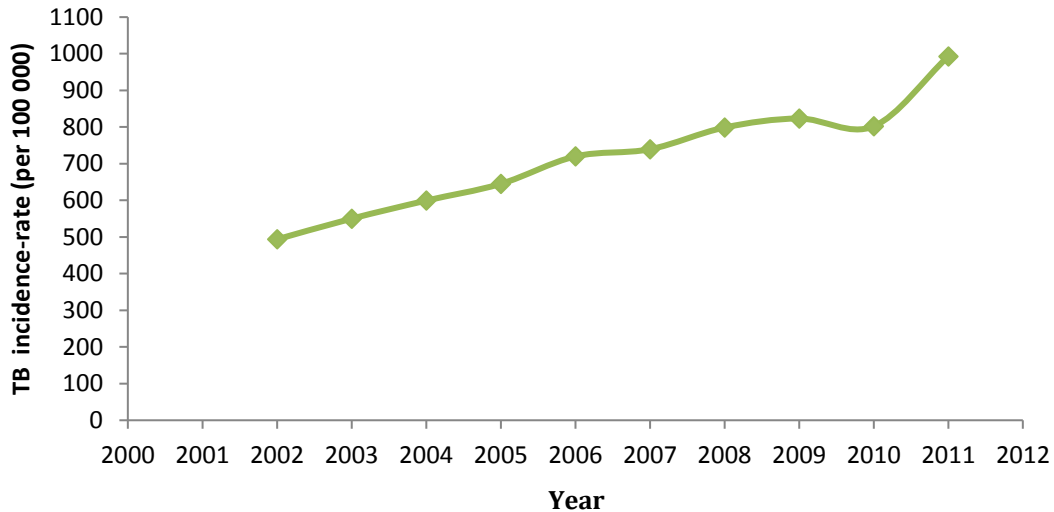


**Figure 1.2.** The TB incidence rate (per 100 000 individuals) in South Africa from 2002 up until 2011. This plot was constructed using data obtained from “Annual Performance Plan 2012/2013-2014/2015”, Department of Health, South Africa. (2012) and “National Strategic Plan on HIV, STI’s and TB 2012 - 2016”, South African National AIDS Council. (2011).

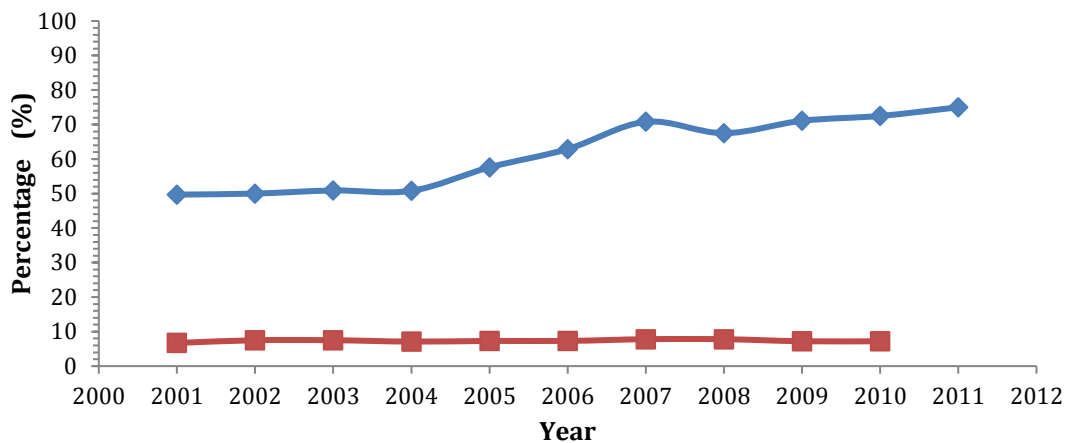


**Figure 1.3.** The South African TB cure rate % (Blue diamond) and TB mortality rate percentage (Red square). This plot was created using data obtained from "National Strategic Plan on HIV, STI's and TB 2012 - 2016", South African National AIDS Council. (2011).

## 1.2. Ineffective preventative measures against tuberculosis and its ability to evade eradication

The risk of developing an active TB infection is significantly increased by co-infection with the acquired immunodeficiency syndrome (AIDS) and other immune-compromising conditions, demonstrating that protective immunity works to suppress the infection in most

Mtb infected individuals. The only recognized vaccine against tuberculosis, the *M. bovis* Bacillus Calmette-Guérin (BCG) vaccine has proved to be inadequate against emerging outbreaks of tuberculosis, particularly in adults (Korbel et al., 2008). The BCG vaccine, although ineffective for adults, is regularly administered to children at birth (Ducati et al., 2006) to protect against severe forms of TB such as TB meningitis and miliary TB (World Health Organization, 2012). When controlled clinical trials were conducted, the BCG vaccine only had an estimated overall efficacy of approximately 50% for the prevention of TB in children (Zumla et al., 2013). Yet another drawback to use of the vaccine is that it is not recommended for use in infants known to be infected with HIV (World Health Organization, 2012). Thus there is a need to develop a better BCG vaccine or create new vaccines entirely, to combat TB in both children and adults. The World Health Organization has described two approaches in achieving these goals. First, develop vaccines that will outperform the ‘old’ BCG vaccine such as an improved version or a new attenuated live *M. tuberculosis* vaccine. The second approach is to develop a “prime boost” strategy in which BCG continues to be given to infants and at a later stage (young adult) a new dose of the BCG vaccine is administered once again to help aid in immunity against development of active TB (World Health Organization, 2012). An updated report from WHO shows that various vaccines are now in phase two and three of clinical trials. These new vaccines namely M72/AS01E, H1:IC31, H4:IC31, H56:IC31, VPM 1002, RUTI, MTBVAC and *M. Vaccae*, are augmentations of the original BCG vaccine aimed at preventing MDR-TB and XDR-TB (World Health Organization, 2015).

Central to the vaccine challenges described above is that Mtb cells have evolved genetic and physiological mechanisms to remain viable within the hostile microenvironment of the host lung tissue. These mechanisms include redox defence gene/protein networks, a relatively impermeable cell wall structure and the secretion of certain proteins to the extracellular environment. These factors work in conjunction with one another to aid in the survival and spread of Mtb within the activated macrophages of the host immune system (Sharma et al., 2012).

### **1.2.1. The *M. tuberculosis* cell wall structure and function**

An interesting feature of the *Mycobacterium* genus is their cell envelope which has a high lipid content and constitutes 40% of the cell’s dry weight. The Mtb cell wall consists of multiple lipoglycans such as lipoarabinomannan (LAM), lipomannan (LM) and phosphatidyl-*myo*-inositol mannosides (PIM) (Figure 1.4) (Forrellad et al., 2013). The function

of the cell wall and outer membrane of any given cell is to protect and enclose its intracellular constituents, but the Mtb cell envelope can also coordinate host-pathogen interactions which aid in the pathogens' ability to avoid suppression by the host immune system (Karakousis et al., 2004).

LAM phosphatidylinositol-anchored lipoglycans are composed of a mannan core with oligoarabinosyl side-chains with diverse biological functions. LAM is the most prominent cell wall component, making up 5 mg.g<sup>-1</sup> of the cell's weight and can be broken down into three sub-types. The three sub-types, each having their own function in protecting the cell, are Man-LAM which is characterized by its extensive mannose capping, phospho-*myo*-inositol capped-LAM (PILAM) and Ara-LAM which lacks mannosylation in the arabinan termini (Karakousis et al., 2004). Another key structural component of the outer membrane of Mtb is mycolic acid, a high molecular weight  $\alpha$ -alkyl  $\beta$ -hydroxy fatty acid tasked with maintaining the structural integrity of the cell wall and membrane and more specifically the cyclopropane rings aid in oxidative stress protection against compounds such as hydrogen peroxide (Figure 1.4 F) (Takayama et al., 2005).

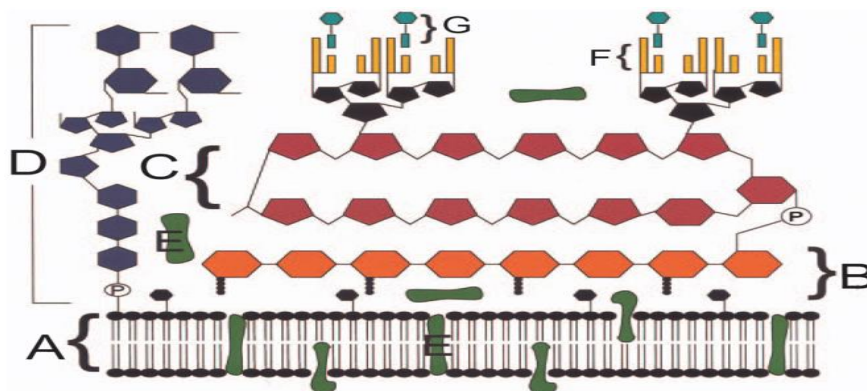


**Figure 1.4.** Cell wall components found in *Mycobacterium tuberculosis* include (A) plasma membrane, (B) peptidoglycans, (C) arabinogalactan, (D) mannose-capped lipoarabinomannan, (E) plasma membrane- and cell envelope-associated proteins, (F) mycolic acids and (G) glycolipid surface molecules associated with mycolic acids (Karakousis et al., 2004). (Permission to reproduce this figure was granted by RightsLink).

This barrier protects against certain antitubercular drugs creating a first-line of defence which contributes to the overall virulence of Mtb (Zumla et al., 2013). With respect to directing macrophage function, mannose capping of LAM seemingly appears to direct the macrophage response by stopping phagosomal maturation and interfering with cell signalling while

Ara-LAM is more effective in eliciting pro-inflammatory cytokine responses (Karakousis et al., 2004).

### **1.2.2. Secreted Mtb proteins are partially responsible for the bacterium's survival**

Mycobacterial survival also depends on protein export and Mtb cells have specialized secretory systems such as the Sec-dependent secretion pathway that transports N-terminal signal sequence containing proteins across the cytosolic membrane and the twin-arginine transporter (Tat) system that is capable of transporting folded molecules across the membrane (Pieters, 2008). Recent studies have shown that mycobacteria, including Mtb, use the ESX-1 system to secrete the 6 kDa early secretory antigenic target (ESAT-6) and the 10 kDa culture filtrate protein (CFP-10) into the extracellular environment (Huppert et al., 2014). Both of these proteins, and possibly other compounds, are important T-cell antigenic targets and are therefore essential for the evasion from the host immune system. Apart from ESX-1, four other systems ESX-2 to ESX-5, are present with independent transport functions and it has been established that they are important for mycobacterial growth (Pieters, 2008). Interestingly, the mycobacterial KatG (catalase/oxidase defence protein) and SodA (superoxide dismutase) enzymes are found in the culture filtrate of Mtb inferring their site of action can also be extracellular (Smith, 2003).

### **1.3. Redox defence networks and the possibility of deciphering drug targets within**

In addition to the aforementioned membrane-dependent survival mechanisms, Mtb has also evolved multiple protein-dependent defensive systems to deal with the continuous oxidative stress experienced from the host immune defence and their microenvironment. During the course of infection, Mtb resides within the macrophages of the granuloma and the cells are constantly exposed to reactive nitrogen species (RNS), reactive oxygen species (ROS) and other toxins released by macrophages for impeding bacterial cell growth. Granuloma formation is a characteristic feature of TB infection and consists of macrophages and T-cells (CD4<sup>+</sup> and CD8<sup>+</sup>) of the host immune system migrating to the site of infection to contain and control the Mtb infection (Tufariello et al., 2003). The granuloma serves as a barrier, protecting the surrounding tissue from the pathogen whilst simultaneously creating a hypoxic microenvironment to curb the growth of the Mtb cells contained within (Hatzios and Bertozzi, 2011). ROS are ultimately generated from O<sub>2</sub> which is abundant within the lung environment and is converted during the oxidative burst within the macrophage into the superoxide ion (O<sub>2</sub><sup>-</sup>), hydrogen peroxide (H<sub>2</sub>O<sub>2</sub>), and the hydroxyl radical (OH<sup>·</sup>) (Ung and Av-Gay, 2006).

Nitric oxide (NO) and related RNS such as the peroxyxynitrite anion (OONO<sup>-</sup>) (Tufariello et al., 2003) are also generated by the enzyme-inducible nitric oxide synthase (NOS2) of activated macrophages. It was found that toxic nitrogen oxides play a significant role in protection against human tuberculosis, with abundant NOS2 protein expression observed within functioning granulomas (Ohno et al., 2003). The main purpose of RNS and ROS are to damage Mtb DNA, lipids and proteins via oxidation reactions (Hemnani and Parihar, 1998; Kashmiri and Mankar, 2014). Mtb cells have nevertheless evolved various detoxification mechanisms to neutralize these reactive species and ensure their survival within the hypoxic granuloma environment. Some of these systems include the thioredoxin/thioredoxin reductase (Trx and TR respectively) system (Lu and Holmgren, 2014), the alkyl hydroperoxidase systems (AhpCDE) (Jaeger and Flohé, 2006), the bacterioferritin comigratory protein (BCP) system (Jeong et al., 2000), the catalase/peroxidase (KatG) system (Chouchane et al., 2000) and the low-molecular-weight thiol, mycothiol/mycoredoxin-1 (MSH and Mrx-1 respectively) network (Antelmann and Hamilton, 2012) which work in conjunction with one another to neutralize the constant threat from the human immune system to ensure Mtb survival.

With the emergence and spread of antibiotic-resistant bacterial infections, there was an increased urgency to find new drugs with novel mechanisms of action. Recent studies have suggested that the activities of some drugs are mediated by the downstream redox effects on metabolic and homeostatic networks within bacteria (Harbut et al., 2015). A possible target pathway in Mtb is the thioredoxin (Trx/TR/NADPH) system which is linked to numerous cellular processes including DNA synthesis (Powis et al., 2000) and protecting the cell from ROS (Zhao et al., 2006). Auranofin, a FDA-approved antirheumatic drug, consists of a gold(I) center coordinated to a thiosugar and triethylphosphine which inhibits the enzyme thioredoxin reductase (TR) by displacing two ligands from gold consequently forming a tight complex between the metal and active site cysteines of thioredoxin reductase (Marzano et al., 2007; Harbut et al., 2015). As dormant Mtb is able to reside within the host for decades (Kumar et al., 2011), auranofin's efficacy against both active and more intriguingly dormant Mtb cells has drawn huge attention to the drug (Harbut et al., 2015). The repurposing of approved drugs provides a more rapid and cost effective route compared to clinical trials that test new drugs (Figure 1.5). Significantly this study also highlighted the vulnerability of the redoxin networks within Mtb.

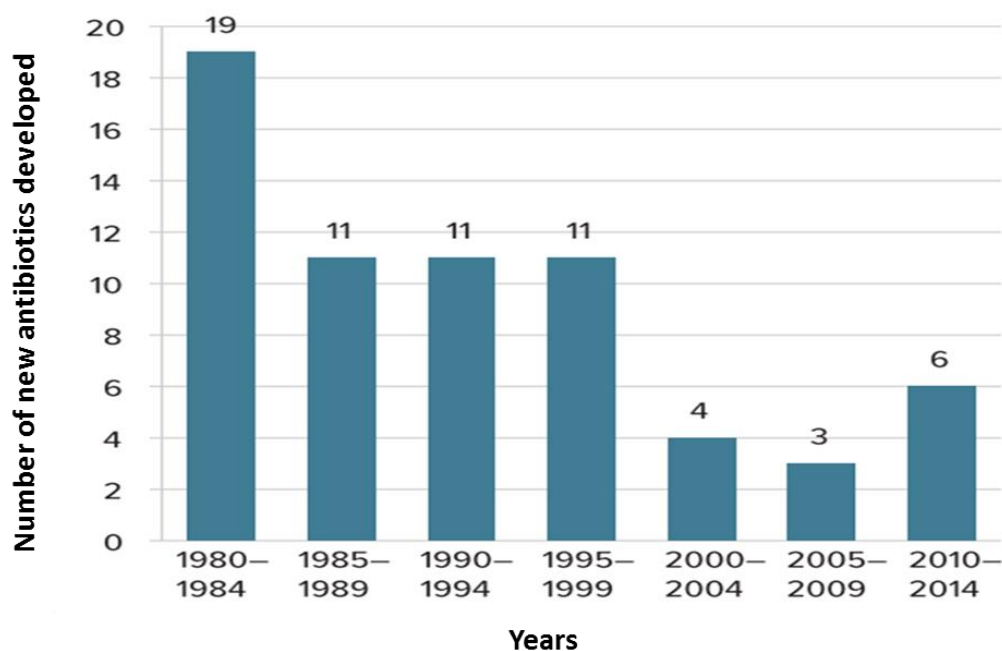


**Figure 1.5.** Therapeutic companies and academic institutions are investing less time and money into antibiotic research and development due to lack of funding and a significant return on development cost. A general decrease can be observed over the past four decades where fewer drugs are being developed to address the rise in drug resistant bacteria (Ventola, 2015). (Permission to reproduce this figure was granted by Elsevier Limited).

Another drawback for conventional antimicrobial agents is the development of multiple drug resistances and the consequent need to administer higher doses of antibiotics which may result in host toxicity. Therefore, finding new ways of drug administration is also being explored to increase the efficacy of drug therapy. One such way of increasing the efficacy of drugs is the use of antimicrobial nanoparticles (NP's) (Huh and Kwon, 2011). NP's offer distinctive advantages in diminishing acute toxicity, overcoming resistance and lowering cost when compared to conventional antibiotics. Antimicrobial NP's consists of metal and metal oxides, natural occurring antibacterial substances, and in conjunction with antibiotics have an increased antibacterial effect. Common metals used in NP's are silver, copper, zinc oxide, titanium oxide, gold and the use of carbon nanotubes. Metals increase the antimicrobial effects of antibiotics by disrupting the lipid bilayer (gold and zinc oxide), attacking the respiratory chain and cell division machinery (silver) and the production of ROS (titanium oxide and copper) (Huh and Kwon, 2011). Metals are well known for forming inhibitory complexes with enzymes (Louie and Meade, 1999) which together with antibiotics could prove to be successful in disrupting the redox defence networks within Mtb.

## **2. Threat of hydrogen peroxide on *M. tuberculosis* survival during infection**

Hydrogen peroxide is a major threat to pathogenic and non-pathogenic cells based on its ability to form highly reactive radicals and requires multiple systems working in conjunction to neutralize it when present at high concentrations. Hydrogen peroxide itself is generated in numerous biological processes, is involved in redox signalling (Netto and Antunes, 2016) and although it is a strong oxidant, hydrogen peroxide itself is relatively unreactive to most biological molecules and because of this can diffuse across larger distances than other ROS. The more favoured reactions with hydrogen peroxide involve metal centres, selenoproteins and thiol-based proteins (cysteine residues). Intracellular Fenton chemistry is one of the main processes involved in hydrogen peroxide reactive radical formation and involves the Fe<sup>2+</sup> ion reacting with hydrogen peroxide to release Fe<sup>3+</sup> and two OH<sup>·</sup> radicals. The OH<sup>·</sup> radicals can cause damage to DNA, lipids and proteins within the cells eventually resulting in cell death (Winterbourn, 2013).

## **3. Redoxin defence networks in *M. tuberculosis* cells**

The thiol-based redox defence mechanisms in Mtb cells are based on the thiol oxidation chemistry of cysteine (Cys). Sulfur occurs in major classes of biomolecules such as amino acids (methionine, cysteine, taurine, homocysteine and selenocysteine) and its reactivity is derived from its innate chemistry. In cysteine residues, sulfur is fully reduced with an oxidation state of -2 and its low redox potential ( $E_o = -0.27$  to  $-0.125$  V) allows the thiol side chain to undergo a range of oxidative modifications (Gupta and Carroll, 2014; Nauser et al., 2015). Interestingly, the fractional cysteine content of different species' proteins increases with an increase in apparent species complexity (Miseta and Csutora, 2000; Gupta and Carroll, 2014). The increase in cysteine content with higher complexity organisms could reflect the various redox states that the thiol/sulfhydryl group undergoes leading to increased redox functionality (Poole, 2015). For example, during eukaryote signalling processes, oxidized peroxiredoxins transmit information about the environmental oxidative stress conditions by transferring oxidizing equivalents to thiol groups of regulatory proteins who themselves are understood to be less reactive with oxidants such as hydrogen peroxide (H<sub>2</sub>O<sub>2</sub>) (Winterbourn and Hampton, 2008; Winterbourn and Hampton, 2014).

Reactive cysteines arranged into an active site -CXXC- motif are considered crucial in redox signal sensing and antioxidant defence. Those cysteine residues can either coordinate a metal ion or cofactor cluster, or remain metal-free to readily participate in thiol-disulfide

exchange reactions (Botello-Morte and Fillat, 2014). Thiolate radicals of cysteine residues (R-S<sup>-</sup>) can participate in free radical chain reactions to form a range of oxidized species generated by two electron chemistry. These cysteine residue modifications allow a range of biomolecules, including low-molecular-weight thiols and oxidoreductases, to undergo reversible redox reactions to maintain a reduced environment within the cellular cytoplasm and help protect the cellular components from oxidative damage.

### **3.1 The low-molecular-weight thiol mycothiol (MSH) sustains a reduced intracellular environment**

The class of *Actinobacteria* is a very large and diverse group of gram-positive, high GC content bacteria with members of varying morphology found in an extensive range of habitats from soil to seawater and even on the skin, lungs and in the gastrointestinal tract of humans. They cause multiple diseases such as leprosy, tuberculosis and diphtheria but have also been utilized in bioremediation projects. Inhabiting a diverse range of habitats, *Actinobacteria* have to deal with a wide range of organic compounds and cellular redox threats and therefore utilize mycothiol (MSH, also known in literature as AcCys-GlcN-Ins), rather than glutathione, to maintain redox balance within the cell (Newton et al., 2006).

Mycothiol is the major low-molecular-weight thiol present in *Mtb*, often present in millimolar amounts with analogous functions to the glutathione (GSH) system which is referred to as its cousin system (Newton et al., 2006). Promising work on mycothiol biosynthesis was conducted by Bornemann et al., 1997, who started working with synthetic GlcN-Ins to assay extracts of *Mycobacterium smegmatis* for enzyme activity. The work on mycothiol biosynthesis has since progressed with researchers now able to elucidate the entire biosynthesis pathway. Mycothiol biosynthesis is a multistep pathway and is carried out by what was originally thought to be only four proteins: MshA, MshB, MshC and MshD (Newton and Fahey, 2002). However, precursors utilized by MshA were not clear and it was later determined that another enzyme encoded by *ino1* (*myo*-Inositol-1-phosphate synthase) was responsible for converting Glc-6-P into Ins-P (Newton et al., 2008). The Ins-P is converted to GlcNAc-Ins-P by MshA1 (MSH glycosyltransferase) by the addition of UDP-GlcNAc and the subsequent release of UDP. The phosphate is then removed by MshA2 (MSH phosphatase) releasing GlcNAc-Ins. MshB (MSH deacetylase) then removes the acetyl group releasing CH<sub>3</sub>COOH and GlcN-Ins. The GlcN-Ins is then acted upon by MshC (MSH ligase) which links a cysteine residue to the compound, creating Cys-GlcN-Ins at the expense of ATP. Lastly MshD (MSH

acetyltransferase) adds on an acetyl group from AcetylCoA creating AcCys-GlcN-Ins (mycothiol, MSH) and releasing coenzyme A (CoA).

Mycothiol acts upon a range of alkylating compounds including formaldehyde and nitric oxide, by reacting and creating a mixed compound/disulfide (MSR, where R is the toxin). These mixed compounds/disulfides (MSR) are then cleaved by a mycothiol conjugate amidase, Mca, to release AcCysR (mercapturic acid, where R is the toxic compound) that is eventually transported out of the cell and GlcN-Ins which is recycled back into the mycothiol biosynthesis pathway (Newton and Fahey, 2002). Mycothiol is also involved in protein *S*-mycothionylation, a process in which mycothiol binds to cytosolic protein cysteine residues (R-SOH) protecting them from hyperoxidation, a process analogous to *S*-glutathionylation which is characteristic of the glutathione system (Figure 1.6) (Gallogly and Mieyal, 2007).

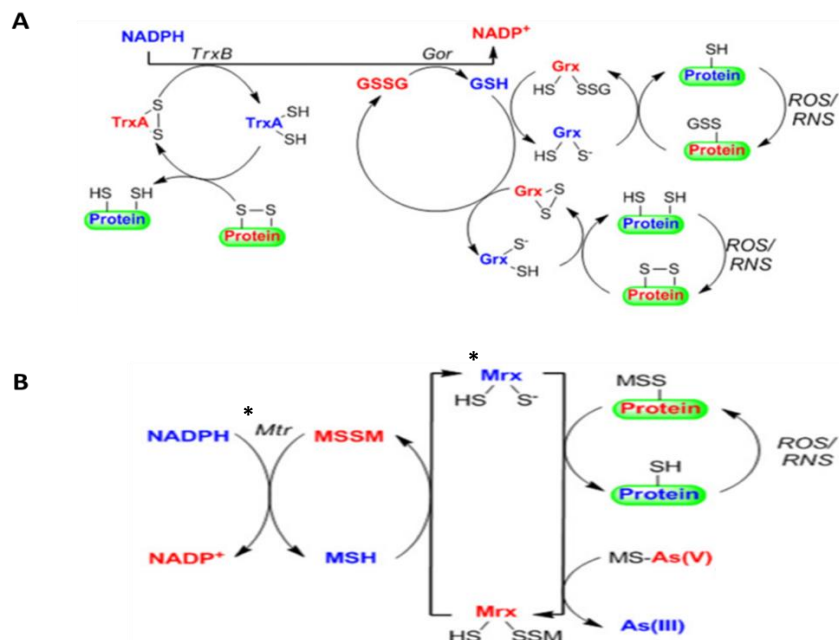


**Figure 1.6.** Summary of the *E. coli* glutathione *S*-glutathionylation (A) and the *Actinomycetes* mycothiol *S*-mycothionylation processes (B). (A) Protein disulfides are reduced by thioredoxin A (TrxA) while *S*-glutathionylated proteins are reduced by glutaredoxins (Grx). TrxB represents thioredoxin reductase and oxidized Grx is reduced by GSH to give GSSG which is recycled back to GSH by glutathione reductase (Gor). (B) *S*-mycothionylated proteins are reduced by Mrx resulting in an active protein-SH and the Mrx-SSM intermediate. The Mrx-SSM intermediate is thereafter reduced by MSH, leading to MSSM formation which is then recycled by Mtr at the expense of NADPH (Antelmann and Hamilton, 2012). \* Mtr/MR

(referred to in text) represents mycothione reductase and Mrx represents mycoredoxin in this figure. (Permission to use this figure was obtained from RightsLink).

Reduced mycoredoxin-1 (Mrx-1) rescues the mycothionylated proteins by forming a mixed disulfide with the mycothiol molecule and releasing the active protein. The mixed disulfide between mycothiol and mycoredoxin-1 is thereafter cleaved by the addition of a second mycothiol molecule, creating mycothione (MSSM) and releasing the reduced form of mycoredoxin-1 (Figure 1.6 B). Mycothione is thereafter reduced, releasing two mycothiol residues at the expense of NADPH via mycothione reductase (MR) (Van Laer et al., 2012).

### **3.2 Central hub of the Mtb redox defence: the thioredoxin (Trx) system**

The biologically active thioredoxin system comprising NADPH, thioredoxin (TrxB and TrxC) and thioredoxin reductase (TR) is a central disulfide reductase system (Figure 1.7) that provides electrons to a large range of proteins making it one of the major hubs for distributing reducing equivalents through the Mtb cell. For example, the thioredoxin system is critical for DNA synthesis by reducing ribonucleotide reductase and plays a critical role in defence against oxidative stress in the cell by extension of its disulfide bond reduction capabilities (Powis et al., 2000 and Zhao et al., 2006). Thioredoxin is a relatively small reductase protein of 12 kDa, contains a conserved -WCGPC- active site motif (Olson et al., 2013) and is ubiquitously present in archaea, bacteria and eukaryotes. It is made up of five  $\beta$ -strands (core of the protein) surrounded by four  $\alpha$ -helices with the active site being found after the  $\beta$ 2-sheet. Many other critical enzymes in thiol-dependent antioxidant systems such as glutaredoxin, peroxiredoxin and glutathione peroxidase also share the thioredoxin fold structure but differ in catalytic mechanisms (Lu and Holmgren, 2014).

The genome of Mtb encodes three thioredoxins (TrxA, TrxB and TrxC encoded by *trxA*, *trxB1* and *trxC* respectively) and bears a single copy of the thioredoxin reductase gene, (TrxR, encoded by *trxB2*). Of the three thioredoxins, TrxB and TrxC are involved in reduction of peroxides, dinitrobenzene and hydroperoxides *in vitro*. The central involvement of the thioredoxin system in antioxidant defence makes it an ideal drug target towards inhibiting one of the major redox hub systems in Mtb (Akif et al., 2008). However, TrxA of Mtb was found to be cryptic and inactive, unable to receive electrons from thioredoxin reductase (Akif *et al.*, 2008).

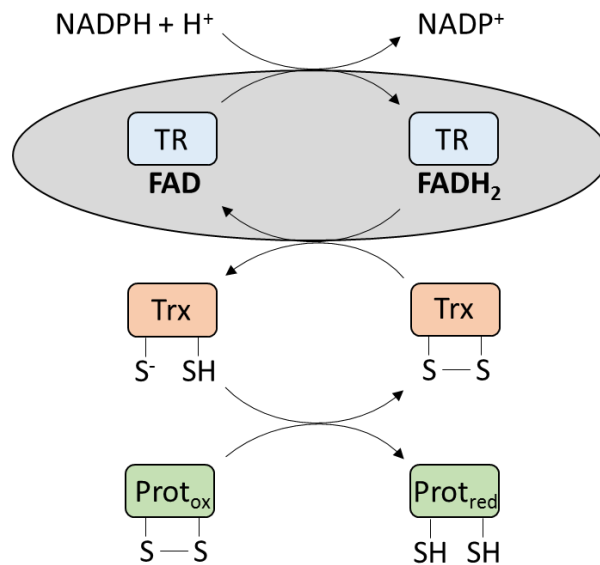


**Figure 1.7.** Electron flow from NADPH to thioredoxin (Trx) allows reduction of oxidized proteins (Prot<sub>ox</sub>) to the reduced protein state (Prot<sub>red</sub>) by thiol/S-S exchange. The grey oval shows the thioredoxin reductase (TR) enzyme and the flavin adenine dinucleotide redox cofactor (FAD/FADH<sub>2</sub>) that allows electrons to pass to thioredoxin (Trx) shifting the balance between the oxidized (TrxSS) and reduced forms (TrxSH). (This figure was adapted from Collet and Messens, 2010).

A knock-out mutant study conducted on the thioredoxin reductase (*trxB2* gene) of Mtb shows that when the bacterium lacks sufficient amounts of thioredoxin reductase other cellular processes are also impeded. It was found that the thioredoxin reductase mutant displayed stunted growth when cultured in rich medium, failed to establish and maintain infection in mice models, was prone to lytic cell death, displayed increased cytoplasmic thiol oxidation levels and increased susceptibility to antimicrobial compounds except for auranofin, a gold-containing thioredoxin reductase inhibitor (Lin et al., 2016). The numerous detrimental effects outlined when inhibiting the thioredoxin system supports the claim that this system is the central reducing hub of the antioxidant defence systems within Mtb. Thioredoxins have two key responsibilities within the cell by acting as electron carriers to supply reducing equivalents to pathways involved in biosynthesis and to protect cytosolic proteins from inactivation or aggregation under oxidative conditions (Arnér and Holmgren, 2000b). Under hypoxic and oxidative conditions, such as those Mtb is exposed to in the granuloma microenvironment, the protection of cytosolic proteins from oxidative damage becomes particularly important (Van Laer et al., 2012).

Thioredoxins' role in the antioxidant response depends on a cascade of electrons from NADPH to thioredoxin reductase and from thioredoxin reductase to thioredoxin B and C (Figure 1.7) (Cumming et al., 2014). Thioredoxins B and C are both able to consequently pass the electrons from thioredoxin reductase onto other proteins including thiol peroxidase (Tpx) which completes the electron cascade by reducing oxidants such as hydrogen peroxide into water (Jaeger et al., 2004; Lu and Holmgren, 2014). The thioredoxin system is also active on a wide range of oxidizable protein molecules, capable of reducing alkyl hydroperoxidase sub-unit C (AhpC) (Lu and Holmgren, 2014), mycothiol disulfides (mycothione, MSSM) (Attarian et al., 2009) and the bacterioferritin comigratory protein (BCP) peroxiredoxin by either TrxB or TrxC (Comtois et al., 2003). Tpx, BCP and AhpE belong to a large family of proteins known as peroxiredoxins (Prx) which reduce oxidants and are recycled by thioredoxin and low-molecular-weight thiols of the cell. Interestingly, from a eukaryotic perspective peroxiredoxins are also known to coordinate cell stress response via their role in peroxide signalling (Perkins et al., 2015).

### **3.3 Vastly abundant redox defence proteins of Mtb: the Mtb peroxiredoxins**

Peroxiredoxins are ubiquitously distributed through all living kingdoms and cellular compartments (Hugo et al., 2012) with peroxiredoxins constituting 0.1 – 0.8% of the total protein in mammalian cells, amongst the top ten most abundant proteins in *E. coli* and are the second or third most abundant in erythrocytes (Wood et al., 2003). The genome of Mtb encodes four different thiol-dependent peroxidases of the peroxiredoxin family: Tpx, AhpC, AhpE and BCP. In the presence of hydrogen peroxide, organic hydroperoxides, hypohalous acids (HOX), peroxy nitrates and trace metals, the peroxidatic cysteine (Cp) of peroxiredoxins is oxidized to sulfenic acid (Cys-SOH) and in the case of prokaryotes, rapidly forms a disulfide bond (S-S) with the resolving cysteine (Cr) whereas eukaryotic disulfide bond formation is much slower (Figure 1.8) (Klomsiri et al., 2011). In large or excess concentrations of oxidizing agents, the Cys-SOH can be further oxidized to cysteine sulfinic (Cys-SO<sub>2</sub>H) and sulfonic (Cys-SO<sub>3</sub>H) acids in a process known as hyperoxidation which ultimately renders the antioxidant proteins inactive (Chung et al., 2013). In bacterial cells hyperoxidation is an irreversible process as they, unlike eukaryotic cells, lack the protein sulfiredoxin which can reverse the hyperoxidized proteins in the sulfinic acid form back to the active Cys-SOH form (Biteau et al., 2003; Loi et al., 2015).

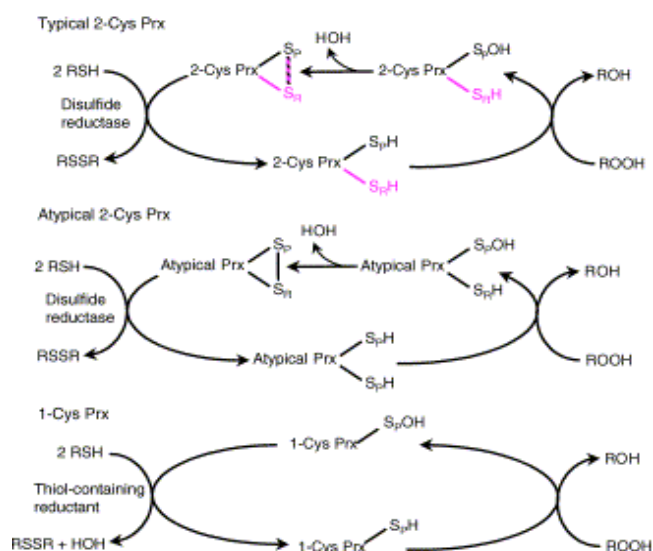


**Figure 1.8:** Overview of the three peroxiredoxin mechanisms namely typical 2-Cys, atypical 2-Cys and the 1-Cys peroxiredoxins. The pink in the diagram represents the resolving cysteine from another subunit whereas black represents the peroxidatic cysteine of the same subunit (Wood et al., 2003). (Permission to reproduce this figure was granted by Elsevier Limited)

Reduction of the disulfide bond between the peroxidatic and resolving cysteine residues, is mediated by thioredoxin or other related oxidoreductase proteins at the expense of NADPH or NADH, releasing both thiols on the peroxidatic and resolving cysteines in the reduced forms Cys-S<sup>-</sup> and Cys-SH respectively, to undergo the oxidative process once more (Gupta and Carroll, 2014). This simple reversible reaction is one of the central antioxidant mechanistic schemes present in Mtb, allowing various proteins to cycle through the oxidized and reduced states (Winyard et al., 2005).

The peroxiredoxin family can be further categorized into three mechanistic classes, namely the typical 2-Cys, atypical 2-Cys and the 1-Cys peroxiredoxins classes (Figure 1.8). The general catalytic mechanism of peroxiredoxins remains the same for all three classes in which a peroxide is reduced to a less toxic form (ROH, either its corresponding alcohol or water) and the peroxidatic cysteine is converted to the sulfenic acid intermediate (Cys-SOH) (Wood et al., 2003). Although natively occurring as obligate homodimers, the typical 2-Cys and the atypical 2-Cys peroxiredoxins have differing resolving steps for oxidized cysteine residues. In the case of the typical 2-Cys peroxiredoxin, the oxidized peroxidatic cysteine forms an intersubunit disulfide with the resolving cysteine residue of another molecule. Atypical 2-Cys residues follow a similar mechanism except the resolving cysteine is found on the same subunit therefore an intrasubunit disulfide bond is formed. The 1-Cys peroxiredoxin has only

the peroxidatic cysteine which is converted to Cp-SOH and thus requires a thiol-containing reductant to reduce the Cp-SOH back to Cp-S<sup>-</sup> (Wood et al., 2003).

### **3.3.1. Thioredoxin-dependent thiol peroxidase (Tpx) of Mtb**

Proteome analysis has shown that thiol peroxidase (Tpx) is more abundant than catalase/peroxidase (KatG) and AhpC and can be considered to be the leading antioxidant defence system in Mtb (Rao and Li, 2009). Thiol peroxidase is regarded as one of the most efficient peroxidases of Mtb in terms of its rate constants (Yuniastuti, 2012) for the reactions with hydroperoxides ( $3.3 \times 10^5 \text{ M}^{-1} \cdot \text{s}^{-1}$  with TrxB as reductant and  $0.9 \times 10^5 \text{ M}^{-1} \cdot \text{s}^{-1}$  with TrxC as a reductant) and peroxyntrites ( $1.5 \times 10^7 \text{ M}^{-1} \cdot \text{s}^{-1}$ ) (Jaeger et al., 2004). It is able to reduce a wide spectrum of hydroperoxides including hydrogen peroxide which is one of the main threats to Mtb cells within the hypoxic granuloma microenvironment. The reduced state is regenerated by either TrxB or TrxC of the Mtb thioredoxin system (Jaeger et al., 2004). While thioredoxin peroxidase is classified as an atypical 2-Cys peroxiredoxin (Hugo et al., 2012), it behaves as a 1-Cys peroxiredoxin during peroxyntrite reduction (Trujillo et al., 2006).

### **3.3.2. The alkyl hydroperoxidase reductase subunits C, D and E (AhpC, AhpD and AhpE)**

Alkyl hydroperoxide reductases, namely AhpC and AhpE all belong to the peroxiredoxin family. AhpC is the largest and most distributed peroxidatic protein with members found in archaea, bacteria and eukaryotes and utilize the mode of action of the typical 2-Cys peroxiredoxins (Figure 1.8). Mycobacterial AhpC can not only detoxify hydroperoxides but also displays reductive capabilities against reactive nitrogen species (RNS) (Guimarães et al., 2005). Although, functioning as a typical 2-Cys peroxiredoxin, AhpC does in fact have three cysteine residues with cysteine 61 being the peroxidatic cysteine, cysteine 174 the resolving cysteine and cysteine 176 whose role is unknown but could provide an alternate route for the disulfide formation between cysteine residues (Hillas et al., 2000). In enterobacteria, the AhpC system consists of alkyl hydroperoxidase sub-unit F (AhpF) as a reductant, but in Mtb the AhpF protein is absent and AhpD reductase acts in a comparable role. The AhpC system of Mtb is also very malleable in the sense that if AhpD is not available, it can employ TrxC but not TrxA or TrxB as reductants (Hugo et al., 2012).

The final alkyl hydroperoxide reductase to be discussed is alkyl hydroperoxidase sub-unit E (AhpE), which is found in aerobic gram-positive bacteria such as *Actinomycetes* and utilizes a 1-Cys peroxiredoxin mechanism (Hugo et al., 2012). AhpE is a highly conserved

hydroperoxide reductase amongst many mycobacterial species and interestingly it has been observed that AhpE expression increased during the dormant phase of the tuberculosis disease, denoting its role in Mtb latency. Initially the reductant of AhpE was unknown but it was later found to utilize the mycothiol pathway in its reduction (Hugo et al., 2014). In this mechanism, the active site cysteine residue is oxidized to Cys-SOH by a peroxide or peroxyxynitrite and thereafter a mycothiol molecule reacts with the AhpE-SOH to create a mixed mycothiol disulfide AhpE-SS-M. The mixed disulfide is then reduced by Mrx-1 which itself becomes mycothionylated, releasing the reduced reactive AhpE. AhpE shows a high specificity towards peroxyxynitrite which it reduces three orders of magnitude faster than hydrogen peroxide ( $1.9 \times 10^7$  vs  $8.2 \times 10^4 \text{ M}^{-1}\text{s}^{-1}$  respectively), indicating that it is capable of a broad role in redox defence in Mtb survival (Hugo et al., 2012).

### **3.3.3. The Bacterioferritin Comigratory Protein (BCP) of Mtb**

The remaining member of the Mtb peroxiredoxin family is the Bacterioferritin Comigratory Protein (BCP). A key feature of this protein is that it is a target for modification by a small protein named Pup. Pupylation is a post-translational modification that targets proteins for degradation by the proteasome itself and plays a role in virulence by mechanisms not fully understood (Hugo et al., 2012). BCP is also associated with the membrane fraction of Mtb, indicating its role as a possible primary defence able to neutralize threats before they even enter the cell (Reyes et al., 2016) and shows structural similarity in its primary structure with the yeast peroxiredoxin thiol specific antioxidant protein (TSA) and AhpC indicating it could be a novel member of the family. BCP is an atypical 2-Cys peroxiredoxin and exists as a monomer under native conditions (Jeong et al., 2000). In Mtb it is a general thioredoxin-dependent peroxidase whilst in other organisms has been shown to be more efficiently reduced by the glutathione system (Reyes et al., 2016). Mtb BCP, being a general peroxidase, shows reductive capabilities towards hydrogen peroxide, *t*-butyl hydroperoxide and linoleic acid hydroperoxide (Clarke et al., 2010; Jeong et al., 2000).

### **3.4. KatG, a system dedicated to the neutralization of hydrogen peroxide**

Catalase-peroxidase (KatG) is not a thiol-based antioxidant protein as the previously discussed systems, but it is a heme-protein containing a core with an iron center whose main role is hydrogen peroxide reduction in Mtb cells (Figure 1.9). It uses the same catalytic mechanism as other known catalases in which a hydrogen peroxide molecule is reduced and oxidizes the KatG to compound I. A second hydrogen peroxide molecule is used to reduce the

compound I effectively removing two hydrogen peroxide molecules with one catalytic cycle (Chouchane et al., 2000). KatG therefore has an increased efficiency at higher hydrogen peroxide concentrations.

One of the more notable characteristics of KatG in Mtb is that it activates the first line drug isoniazid (isonicotinic acid hydrazide, INH) which kills drug-susceptible Mtb cells. The process of INH activation involves KatG acting upon the INH compound creating the isonicotinoyl-acyl-radical which then reacts with  $\text{NAD}^+$  to create the INH-NADH complex which is the active form of the drug. The INH-NADH complex inhibits InhA, an enoyl acyl-carrier-protein reductase involved in Mtb cell wall biosynthesis, ultimately leading to loss of cell rigidity and leaking of intracellular components (Ghiladi et al., 2005).

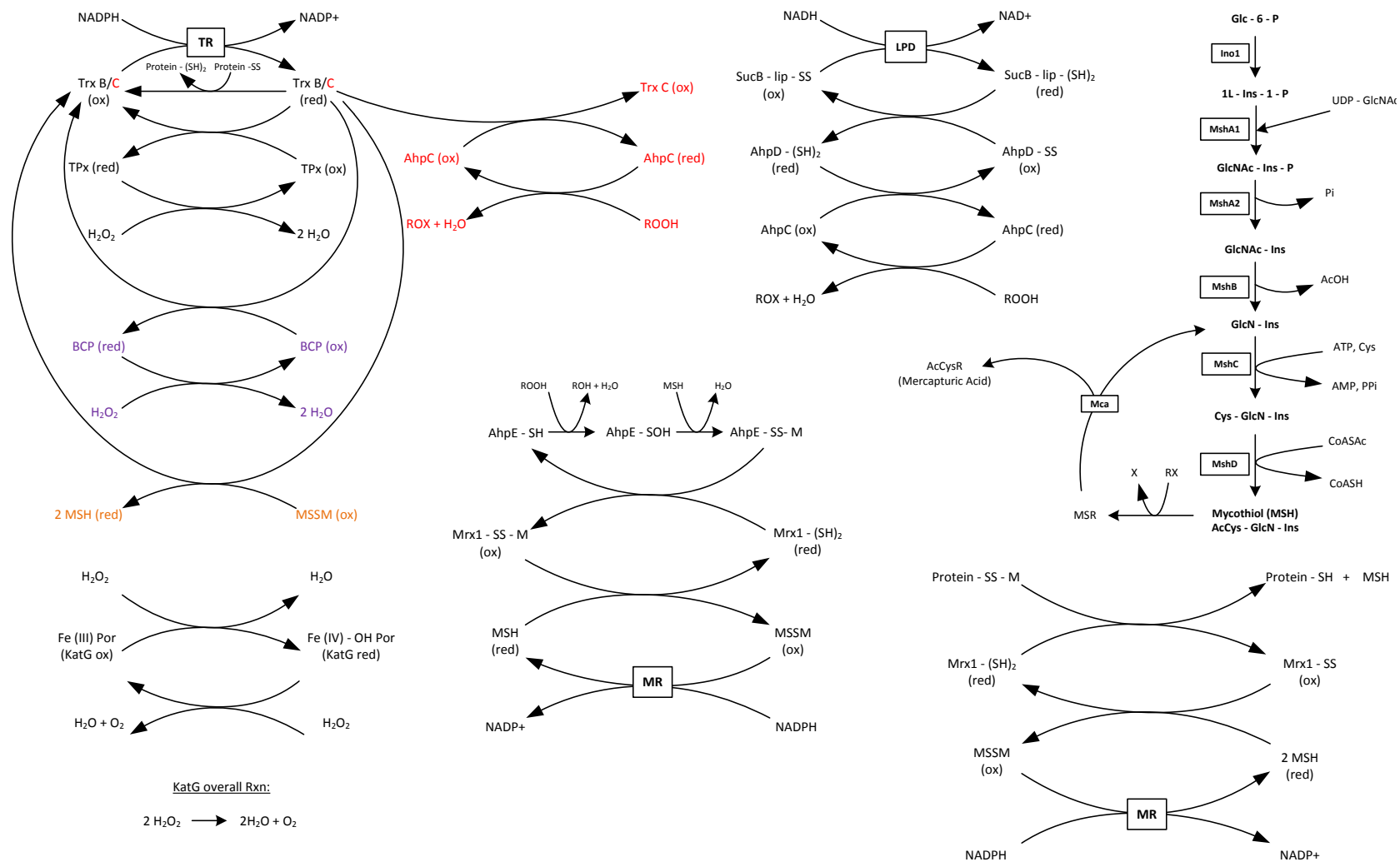


**Figure 1.9.** Arrow diagram representation of the redox defence mechanisms within the Mtb cell. These defences include the thioredoxin (Trx) system which links to the thiol peroxidase (Tpx, black), alkyl hydroperoxidase subunit C (AhpC, red), bacterioferritin comigratory protein (BCP, purple) and the disulfide between two mycothiol known as mycothione (MSSH, orange). Other systems include the catalase/peroxidase system (KatG), AhpE, mycothiol/mycoredoxin-1 system, the AhpC system with AhpD as the reductant and lastly the MSH biosynthesis pathway (including activity and mechanism of Mca).

#### **4. Computational modelling of the *Mycobacterium tuberculosis* redox defence systems**

The redox defence systems in the Mtb cell that focus on defending against hydrogen peroxide were summarized in Figure 1.9. The figure shows the interlinking nature of the systems and the central role played by the thioredoxin system which is able to reduce the thiol peroxidase, alkyl hydroperoxidase subunit C, bacterioferritin comigratory protein, mycothiol/mycothione systems and disulfides in other cellular proteins. It is likely that these systems work in conjunction to create a robust defence against hydrogen peroxide with each system known to possess varying reaction rates and affinities for this oxidant. The interlinked nature of this network argues that computational systems biology could be used to analyse the Mtb redox defence network to understand the synergy between these systems. Studying such biological networks relies on data generated from three techniques namely genomics, proteomics and kinetic modelling.

##### **4.1. Genomics and its possible applications in Mtb network biology**

Genomics is the study of the molecular organization of genomes, their information content and the gene products they encode. Researchers were able to sequence the entire Mtb genome (Pagel and Pomiankowski, 2002) and with the aid of bioinformatics tools, more than 3920 genes were uncovered that encode proteins with a length greater than 80 amino acids with additional genes identified for further study and classification. Following sequence analysis, roughly 40% of the Mtb genes were assigned precise function and 16% resembled genes with no known function (Pagel and Pomiankowski, 2002). Moving forward, various clinical strains were isolated from patients and their genomes sequenced. To mention a few, the PR08 (Jaafar et al., 2016) and KT-0184 (Kwon et al., 2016) Mtb strains were recently isolated, sequenced and analysed. Genome sizes were confirmed around approximately 4.4 Mb in both Mtb strains suggesting consistency amongst Mtb's genetic lineage, now with accurate descriptions being given to sub-systems, genes, coding sequences and RNA content of these cells.

The ability to sequence the entire genome also meant that the genomes of the XDR-TB and MDR-TB clinical strains could also be sequenced allowing the identification of biomarkers for these strains. Specifically within MDR-TB, an 81 base pair region within the *rpoB* gene enabled the development of a diagnostic test known as Xpert MTB/RIF for the rapid identification of clinical specimens along with the detection of rifampicin resistance consistent with MDR-TB isolates. The sequences obtained were also sample-specific denoting that the same information would not necessarily apply to a different strain. Differences in the

transcriptome were also observed during the different stages of the diseases lifecycle (including dormant and active stages) (Warner and Mizrahi, 2014).

Spoligotyping, a PCR based technique relies on the amplification of highly polymorphic repeats in the Mtb genome. This makes it a rapid diagnostic test outperforming those such as culturing/culture confirmation, susceptibility testing and restriction fragment length polymorphism (RFLP) in terms of accuracy, speed and use in quick diagnosis of newly afflicted individuals (Gori et al., 2005). Genomics will continue to drive the understanding of evolutionary processes and determination of genes of interest in Mtb. Improvement on existing software tools will further increase the significance of using genomics in finding new drugs to combat diseases by understanding genome network structure (Brazhnik et al., 2002; Warner and Mizrahi, 2014).

#### **4.2. Proteomic analysis and its role in studying Mtb cellular systems**

With the development of proteomics, many new avenues have been opened for TB research allowing the study of Mtb proteins along with proteins involved in Mtb-host interactions which help the pathogen influence the host immune response and ultimately remain viable in a microenvironment designed to be bactericidal. Applications of proteomics include searching for potential biomarkers for diagnosis of the disease within the host (in combination with genomics), identifying and confirming virulence factors, studying the response of both the host and pathogen during the infection process and clarifying the mechanisms of action with regard to virulence factors as they interface with host cells (Zhang, 2011).

With Mtb proteomics research, the two main technologies used were two-dimensional electrophoresis combined with mass spectrophotometry (2DE-MS) or western blotting (2DE-WB) and isotope labelling followed with multiple dimensional liquid chromatography combined with mass spectrophotometry (LC-MS) analysis (Schubert et al., 2015). The development of a label-free method based on one dimensional separation was achieved by LC-MS identification followed by exponentially modified protein abundance index (emPAI) quantification which was used to identify differentially abundant proteins in closely related hypo- and hyper-virulent clinical Mtb strains (Zhang, 2011).

These methods along with characterization of multiple proteins allowed the identification of potential drug targets within the Mtb cell, inspiring the creation of the Mtb drugome

(Kinnings et al., 2010). The drugome was created with the purpose of identifying possible drug targets within molecular interaction networks based on binding sites and biochemical interactions between cellular components. It includes not only the primary targets of the drug but also potential off-targets in the network, successfully providing opportunities for mapping a comprehensive drug-target space to aid in understanding drug efficacy, side-effects and drug resistance possibilities on a molecular basis (Kinnings et al., 2010; Mehaffy et al., 2012).

A challenge for proteomic studies is that the analysis of low-abundance proteins remains a major problem. In addition, most of the methods used for proteomics studies are not considered high-throughput and for this reason cannot be studied on the same scale as nucleic acids, making it time consuming (Graves and Haystead, 2002). There additionally exists a trade-off between throughput and accuracy and while many samples can be analysed in an automated fashion using MALDI-TOF for example, the quality is sacrificed and many proteins are not identified. Alternatively, fewer samples could be analysed using tandem mass spectrometry (MS/MS) but this method requires considerable time in data interpretation. Despite these shortcomings, proteomic studies, when combined with molecular biology, still have the potential to provide enormous insight into the biology of many organisms' intra- and extra-cellular protein networks (Graves and Haystead, 2002).

#### **4.3. Systems biology computational modelling approaches**

Genomics, proteomics and traditional biochemistry techniques provide data about gene and protein networks and their interactions which can be compiled to create kinetic models for use in computational systems biology. Researchers can use high throughput technologies and utilize data generated to cover the entire system for a 'top-down' approach whilst others can work from molecules to functional modules in a 'bottom-up' approach. A newer method named the 'middle-out' strategy involves starting from tissue models and working up to the organ and higher levels as well as down to the molecular details. In general, systems biology could be considered the application of dynamic systems theory in biology (Mendoza, 2009). The systems biology computational modelling approach can be further broken down into genome-scale modelling as well as specific kinetic modelling which involves smaller systems.

### 4.3.1. Genome-scale modelling vs kinetic modelling approaches

Genome scale models take into account the interconnected nature of metabolites, enzymes and regulatory factors creating a model, usually focusing on the metabolic pathways of a cell. This technique allows the creation of a mathematical model that links cellular aspects of the same time scale and simulates the reactions as they would occur *in vivo*. It provides an access point for precisely analysing cellular phenotype by simulating changes in genetic, regulatory, enzymatic and small molecule levels which are practically impossible to do *in vivo* due to the enormous amount of variables within a genome scale model. Hence, these models are broken into their sub-systems and studied further to get a more detailed understanding of the interactions taking place within the bigger superstructure of the metabolic and / or regulatory networks (Blazeck and Alper, 2011).

Genome scale models include information from previously conducted experiments pertaining to the study (genomics and proteomics) and obtain additional or missing parameters and validation of said parameters and reactions from literature sources as well as pre-existing models. Pre-existing models refer to those models previously used to understand and analyse the system in question. This could also be a model which is incomplete or has components that are present in the system within the current study. From this information a ‘draft’ model is constructed which is then simulated and manually curated to alter the model to a realistic result. There are also a wide range of external resources that aid in genome-scale model construction such as AUTOGRAPH (semi-automated approach to accelerate the curation process), BiGG (biochemical, genetic and genomically structured genome-scale metabolic network reconstructions), BioCyc (collection of >1000 pathway/genome databases), BRENDA (collection of enzyme functional data) and KEGG (Kyoto Encyclopaedia of Genes and Genomes, bioinformatics resource links genomes to pathways) to mention a few (Santos et al., 2011). Genome models are not without disadvantages, as they do not cover the total metabolic pool found within the cell. Further, these models share the structure and stoichiometry characteristics of reactions with kinetic models but leave out almost all of the kinetic details. They also provide a “context for content” explanation implying they give a general overview of the system by providing details of the major fluxes within a system as opposed to a bottom-up kinetic model which can provide detailed flux information for all reactions within a model. Genome-scale models have however been proved to be useful in large data integration (reconstruction of transcription regulation networks, signal transduction networks and the translation machinery) (Santos et al., 2011). Genome-scale models can be found for

*Mycobacterium tuberculosis* H37Rv on the various databases outlined below. For example, a comprehensive and detailed model describing Mtb H37Rv metabolism can be found on the Biochemical, Genetic and Genomic knowledge (BiGG) database describing 825 metabolites, 1025 reactions and 661 genes of interest within this model (<http://bigg.ucsd.edu>).

Kinetic models on the other hand are similar to genome scale models in the context that they are set up similarly (similar reaction schemes). Kinetic models (bottom-up strategy) take into account majority of the details of the system and rarely include a genome-scale survey of information as is the case with genome-scale models. The details of a kinetic model allows for the dynamics of the system to be explored as well as control the structure of the pathway. Once a model is created or made available for use, parameters and conditions can be altered to study biologically relevant properties such as homeostasis. This characteristic of the kinetic models allows a researcher to manipulate pathways *in silico* and ultimately study the changes in behaviour of that system (Santos et al., 2011). Top-down systems biology starts from the bird's eye view of the behaviour of the system by measuring genome-wide experimental data and aims to characterize the sub-systems comprising the larger superstructure and their respective interactions (Bruggeman and Westerhoff, 2007). Top-down kinetic modeling therefore takes into account the various components of the larger network and searches for correlations between the different variables of the system. Examples of this approach include predicting a particular limitation or stress during the fermentation process or to predicting the likely outcomes of therapeutic agents used in disease studies (Santos et al., 2011).

Kinetic models have been used successfully but also face a number of serious limitations (Materi and Wishart, 2007). First, kinetic parameters of all enzymes in a pathway are not always available, even with databases like BRENDA and Sabio-RK. The available parameters are also frequently determined at experimental optimum conditions instead of the physiological conditions of the organism. Second, these models represent relatively small and isolated metabolic pathways which are themselves embedded in a larger metabolic network. Boundary conditions are thus needed (the exchange of information with the rest of the larger system) and becomes important in the prediction of the models results. It has been shown that including the boundary information, even uncertain values, can drastically improve the predictive power of the kinetic models (Santos et al., 2011).

The various approaches (genome-scale modelling, bottom-up and top-down kinetic modelling) makes it difficult to select the best approach for a particular study. The choices are

often dependent on the expertise of user (software choice), the type of desired output, the knowledge of the model parameters (complete or incomplete sets of values) and the complexity of the system to be modelled. This gives the user freedom in terms of research but warrants caution as the type of results obtained are entirely dependent on the values used to construct the computational models. Consequently, utmost care needs to be exercised in extracting information from various sources so that the most accurate kinetic computational model can be constructed with the most realistic and comprehensive results possible (Materi and Wishart, 2007).

## **5. Conclusion**

Despite having vast amounts of literature and data regarding the individual redox defence proteins of Mtb, a comprehensive and holistic understanding of the redox network is still lacking. There currently exist no kinetic models to describe the Mtb redox defence system particularly in the hyperoxic microenvironment of the lung. The aim of this research was to therefore accurately data mine literature, create an accurate and comprehensive wire diagram of the Mtb redox defence network, with focus on hydrogen peroxide, and subject the network to structural motif detection and kinetic model analysis so that this systems' behaviour could be analysed to determine the roles played by the various redox proteins with regard to Mtb latency within the host and if any of these proteins could be possible druggable targets.

## **Chapter 2: Structural analysis of the *Mycobacterium tuberculosis* redox defence network reveals a unique bi-fan motif design in hydrogen peroxide defence**

### **2.1 Introduction**

Biological reductionism has allowed the cellular components of complex networks to be analyzed individually, providing a vast amount of information on their intra- and extra-cellular function (Barabási and Oltvai, 2004). The networks created by these cellular components coordinate cell growth, replication, defence strategies and mobility to name a few. The redox defence networks of cells consists of peroxiredoxins, thioredoxins, catalases and low-molecular-weight thiols such as mycothiol (with respect to mycobacteria) or glutathione. The interactions between these molecules creates a cascade of electron flow originating at either NADPH or NADH which ultimately provides electrons to reduce toxic compounds like hydrogen peroxide and recycle oxidized proteins (Rustad et al., 2008; Nelson and Parsonage, 2013). For pathogens such as *M. tuberculosis*, the redox network allows its survival for up to decades in its latent form within its host (Kumar et al., 2011). Dissection of this network could reveal topological patterns, referred to as motif designs that can shed light on various network/system functions based on the multiple protein interactions within the network (Wong et al., 2012).

In this chapter, the set of network motifs in the redox defence networks of *M. tuberculosis*, *E. coli* and *S. cerevisiae* were compared. Network motifs are statistically significant, over-represented sub-graphs contained in the larger superstructure of the network (Tran et al., 2015). In practice, network motifs are detected by comparing test networks against randomized networks and therefore motifs that are detected represent a specific function within the cell and will provide more information towards system organization (Yeager-Lotem et al., 2004). The idea of motifs was originally introduced by Uri Alon and co-workers who studied them in biological and non-biological networks (Milo et al., 2002). Motifs can be detected in numerous cellular networks and can be used to classify these individual networks (Dobrin et al., 2004). Motifs themselves consist of unique sets of nodes or vertices, representing the individual entities within the network (e.g. proteins), connected by edges (e.g. reactions) which themselves can be either directed or undirected. The connections between the edges and nodes within each of the motifs can be used to characterize a particular motif. Motif sizes range from two nodes and upward, with the three and four node motifs being the most studied. Three node

motifs come from a set of 13 different sub-graphs while four node motifs come from a set of 199 (Milo et al., 2002). These connections can be further classified into specific categories: cycles (flow from one node to the next, closing in on itself), feed-forward loops (FFL, contains one direct path to the target node and a path involving an intermediate node leading to the same target node), single (one node linking to various other target nodes) and multiple (multiple nodes linking to various other target nodes) input modules (SIM and MIM respectively). For example, a bi-fan motif which is a type of multiple input module, contains exactly two start (parent) nodes and two end (child) nodes (for examples see Milo et al., 2002; Konagurthu and Lesk, 2008).

Motif detection has been applied to numerous networks including protein-protein interactions of *S. cerevisiae* (Yeger-Lotem et al., 2004), the transcription network of *E. coli* (Konagurthu and Lesk, 2008), the *Caenorhabditis elegans* neural network (Tran et al., 2015), the World Wide Web, electronic circuits, food webs and social networks (Milo et al., 2002). This chapter focuses on the application of motif detection on the *M. tuberculosis* redox defence network to further understand how its defence system proteins are functionally organized with the goal of finding new drug targets. To aid in this analysis, the *M. tuberculosis* redox defence network was compared to the canonical *E. coli* and *S. cerevisiae* redox defence networks.

## 2.2 Methods

### 2.2.1 Wire diagram construction and motif detection within the Mtb redox network

Wire diagrams were constructed for hydrogen peroxide ( $H_2O_2$ ) reduction redoxin networks in all three organisms using information from literature. To simplify analysis, the redox couples and their respective reductase enzymes were each described as individual nodes (see also Rohwer et al., 2016). The wire diagrams were focused on the hydrogen peroxide reduction network in the cell and included all known redox defence proteins specific to this task. Text files (extension .txt) were created in SciTE (Scintella Text Editor) converting the wire diagram information into a text file format for use in the motif detection programs. The files followed the format:

<Node 1> <Node2>,

where Node 1 represents the parent node and Node 2 represents the child node which indicated to the respective program that the first node leads to or acts upon the second.

The text files contained NADPH, NADH and hydrogen peroxide as individual nodes as these are the boundaries of the systems. The text files were then loaded and analyzed using two programs, MAVisto (Version 2.7.0) (Schreiber and Schwöbbermeyer, 2005) and FANMOD (Fast Network Motif Detection) (Wernicke and Rasche, 2006).

For MAVisto, the file was uploaded and allowed to run using the default motif search settings for both three and four node motif detections and each case 2000 randomizations were used. The program allowed for immediate visualization of results and network motifs were detected, displayed and then exported for later analysis. MAVisto and FANMOD name the motifs detected based on their own predesigned library. For example in MAVisto, the motif ID 2F represents the common two node motif, parent node leading to child node. For each motif, a *Z*-score, *P*-value, mean frequency and standard deviation was determined (Appendix).

FANMOD (Rasche and Wernicke, 2006) was used to confirm the results obtained from MAVisto. The program was used in a similar fashion and sub-graph sizes of three and four were once again detected for each individual organism with the option ‘full enumeration’ selected along with the ‘directed’ sub-graph option. To keep analysis consistent, 2000 randomizations were used with 3 ‘exchanges per edge’ and ‘exchange attempts’. The option to ‘re-estimate sub-graph number’ was selected for greater accuracy (Rasche and Wernicke, 2006). Results were visualized using the ‘HTML-export’ function, opening a web browser to view the FANMOD predesignated motif ID, frequency (original network), mean-frequency of the random networks, standard deviation, *Z*-score, *P*-value and the sub-graph image (Appendix).

For the purpose of this study, although the *Z*-scores and *P*-values are obtained (Appendix) for the motif designs detected within the three networks, they have not been looked at further due to the small size of the networks. Motif detection was carried out to simply identify the different 3 and 4 node motif designs within the networks to identify unique motifs that could be attributed to *Mtb* latency and survivability within the host granuloma microenvironment.

### **2.2.2 Analytical solutions and kinetic model simulations for unique bi-fan motif in *M. tuberculosis***

Analytical solutions were derived for the bi-fan and control bi-parallel motif designs. In all cases, mass action kinetic expressions were used to derive these analytical solutions (Pillay et al., 2011). All model simulations were done using the Python Simulator for Cellular Systems (PySCeS, <http://pysces.sourceforge.net/>) (Olivier et al., 2005). Scripts were constructed





**Figure 2.2.** A proposed reaction scheme for Mtb BCP. The red sulfur residues indicate oxidized species, which are in turn reduced by the NADPH/thioredoxin reductase/thioredoxin system.

### 2.3.1.2 Which of the three thioredoxins of Mtb would be able to reduce Mtb BCP?

The genome of Mtb encodes for three thioredoxin proteins i.e. TrxA, TrxB and TrxC. Sequence alignment amongst these three thioredoxin proteins reveals that TrxA deviates from the conserved thioredoxin catalytic motif, which is -WCXXC-, whilst TrxB and TrxC both contain the conserved motif (Figure 2.3, outlined in red). This is supported by other studies showing that Mtb TrxA is cryptic and not biologically active (Akif et al., 2008). In TrxA, the substitutions of tryptophan (W) to leucine (L) and glycine (G) to alanine (A) could explain loss of protein function as glycine and tryptophan are specifically linked to conservation of catalytic protein function such as thioredoxins (Holmgren, 1995; Parrini et al., 2005; Barnes, 2007).

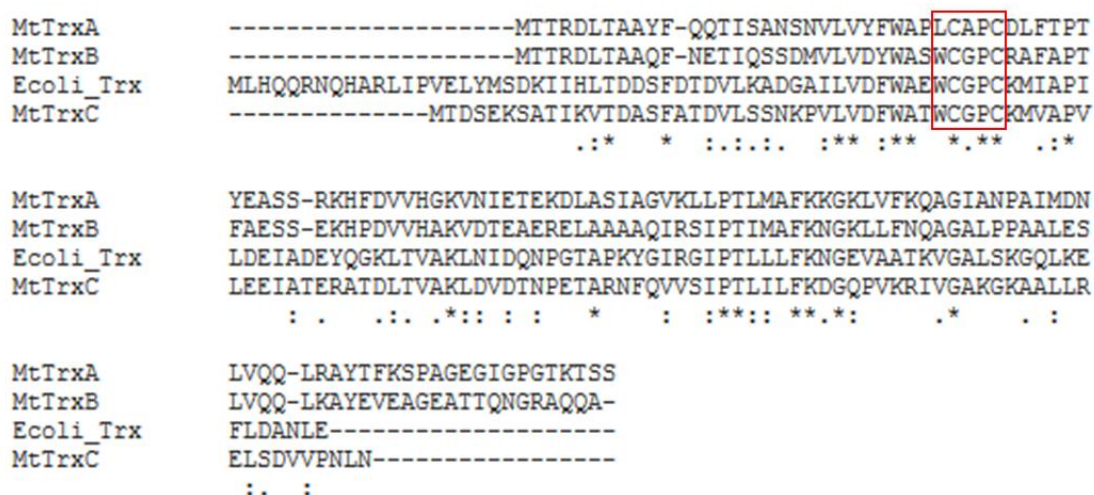


**Figure 2.3.** Multiple amino acid sequence alignment between the three Mtb thioredoxins (TrxA, TrxB and TrxC) and the *E. coli* thioredoxin reveals the conserved -WCXXC- catalytic motif amongst Mtb TrxB, TrxC and *E. coli* Trx (outlined in red). Mtb TrxA deviates from the conserved -WCXXC- catalytic motif suggesting loss of activity *in vivo* is a result of amino acid substitutions around the protein active site.

In the wire diagram constructed for Mtb, TrxB and TrxC are both possible sources of reducing equivalents for the Mtb BCP peroxiredoxin (Figure 2.4).

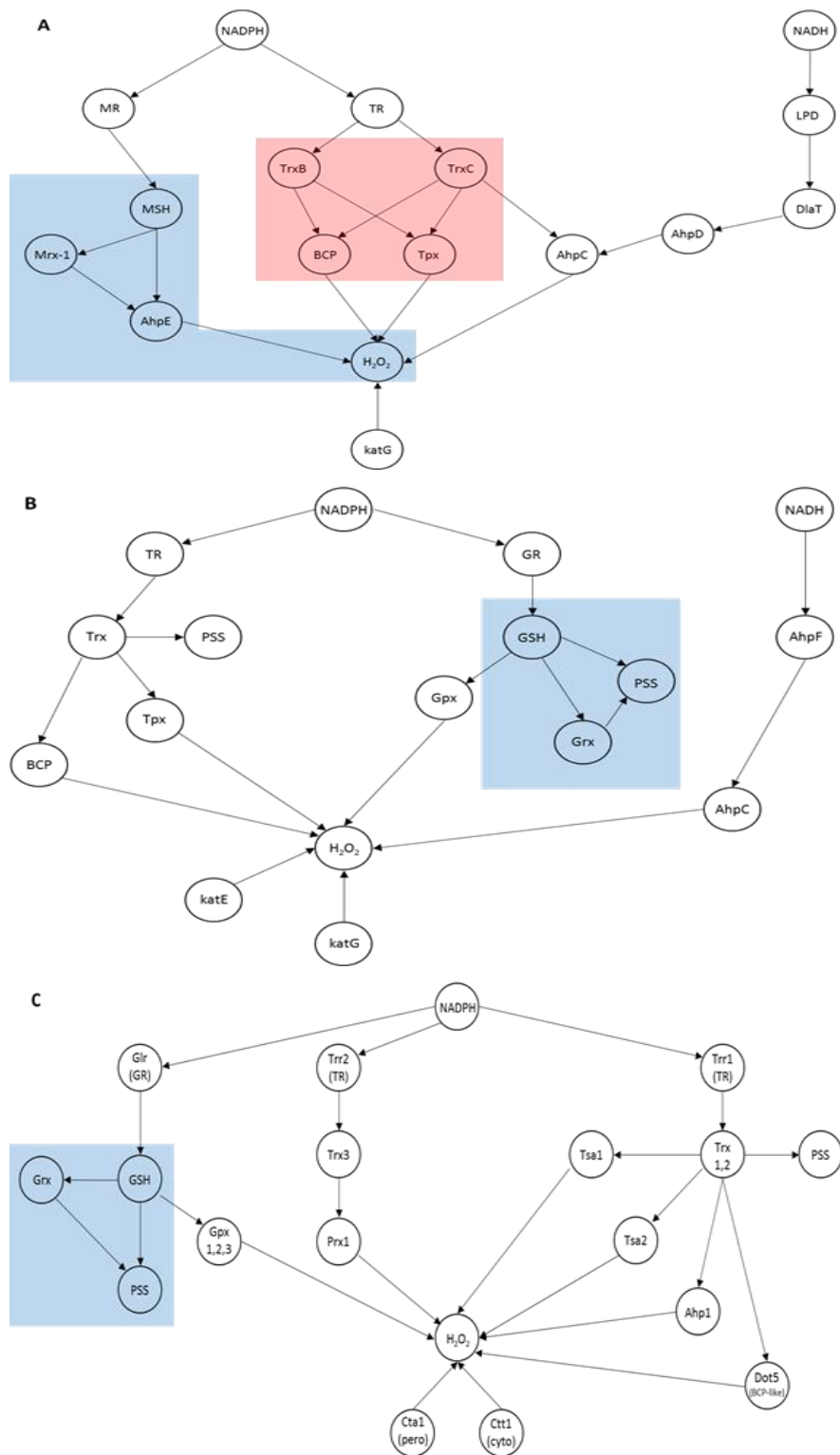


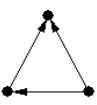
**Figure 2.4.** Construction of the redox defence networks of (A) *M. tuberculosis*, (B) *E. coli* and (C) *S. cerevisiae* for use in the motif detection programs MAVisto and FANMOD. Networks

were constructed to represent interactions between proteins and to analyze similarities and differences amongst redox defence networks of the model organisms against *M. tuberculosis*. Red shading (A) indicates the bi-fan motif of *M. tuberculosis* whilst the blue (A, B and C) indicates the presence of a feed-forward loop. Key: NADPH, nicotinamide adenine dinucleotide phosphate; NADH, nicotinamide adenine dinucleotide; H<sub>2</sub>O<sub>2</sub>, hydrogen peroxide; MR, mycothiol disulfide reductase; MSH, mycothiol; Mrx1, mycoredoxin-1; AhpE, alkyl hydroperoxidase sub-unit E; katG, catalase-peroxidase; TR, thioredoxin reductase; TrxB/C, thioredoxin B and C; BCP, bacterioferritin comigratory protein; Tpx, thiol peroxidase; LPD, lipoamide dehydrogenase (Rajashankar et al., 2005); DlaT, dihydrolipoamide acyltransferase (Voskuil et al., 2011); AhpD, alkyl hydroperoxidase sub-unit D; AhpC, alkyl hydroperoxidase sub-unit C; GSH, glutathione (Jothivasan and Hamilton, 2008; Rawat and Av-Gay, 2007); Gpx, glutathione peroxidase (Arenas et al., 2011 and Inoue et al., 1999); Grx, glutaredoxin (Arenas et al., 2011 and Inoue et al., 1999); AhpF, alkyl hydroperoxidase sub-unit F (Brandes et al., 2007); PSS, protein disulfide; Prx1, peroxiredoxin-1 (Greetham and Grant, 2009); Tsa1/2, thiol-specific antioxidant protein 1 and 2 (Herrero et al., 2008); Ahp1, alkyl hydroperoxidase 1 (Lee et al., 1999); Dot5, nuclear Tpx-BCP like (Herrero et al., 2008); Cta1, peroxisome catalase (Jamieson, 1998); Ctt1, cytoplasmic catalase (Jamieson, 1998).

### **2.3.2 Motifs detected in the *M. tuberculosis* H<sub>2</sub>O<sub>2</sub> reduction defence network**

The three wire diagrams for *M. tuberculosis*, *E. coli* and *S. cerevisiae* (Figure 2.4 A-C) were analyzed by motif detection analysis for three and four node connections. As mentioned above, the different connections within a system contribute to the properties of that particular system which could shed light on the individual roles of isolated pathways in the network superstructure. Using MAVisto and FANMOD motif detection programs, a number of common three node motifs were detected (Table 2.1) with the Z-score, P-value and frequency also determined (Tables S1 to S12, Appendix).

**Table 2.1.** Common three node motifs in the hydrogen peroxide reduction networks of *M. tuberculosis*, *E. coli* and *S. cerevisiae* generated by both FANMOD and MAVisto motif detection programs.

Canonical Motif ID		Motif connections	Absence/Presence in species		
FANMOD	MAVisto		Mtb	<i>E. coli</i>	<i>S. cerevisiae</i>
6	F7F		✓	✓	✓
12	F8R		✓	✓	✓
36	GCR		✓	✓	✓
38	FKX		✓	✓	✓

For the three node sub-graphs, all three organisms had a similar set of motifs (Table 2.1). Generally, the presence of the same set of motifs suggests positive selection for these interaction patterns because of their functional and structural properties (Tran et al., 2015). The simplified single input module (motif ID: 6/F7F); a uni-directional pathway with one node leading to another which in turn leads to the next (motif ID: 12/F8R); simplified multiple input module (two nodes leading to one, motif ID: 36/GCR) and the feed-forward loop (motif ID: 38/FKX) were detected in the redox defence systems of all three organisms albeit with varying frequencies (see Figure 2.5, 2.6 and Appendix). This suggests that these motif designs are favored for hydrogen peroxide reduction compared to other three node motif designs.

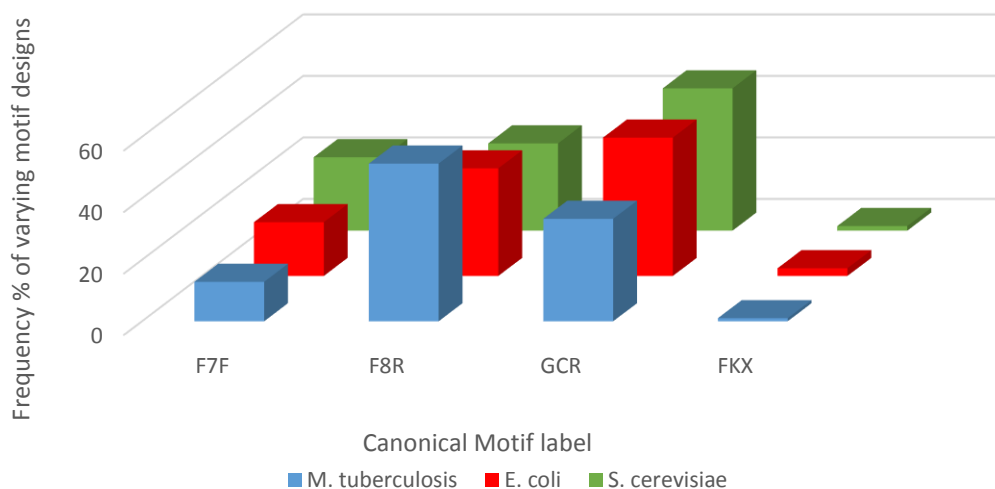


**Figure 2.5.** Frequencies of the common three node motifs detected for *M. tuberculosis*, *E. coli* and *S. cerevisiae* detected using MAVisto.

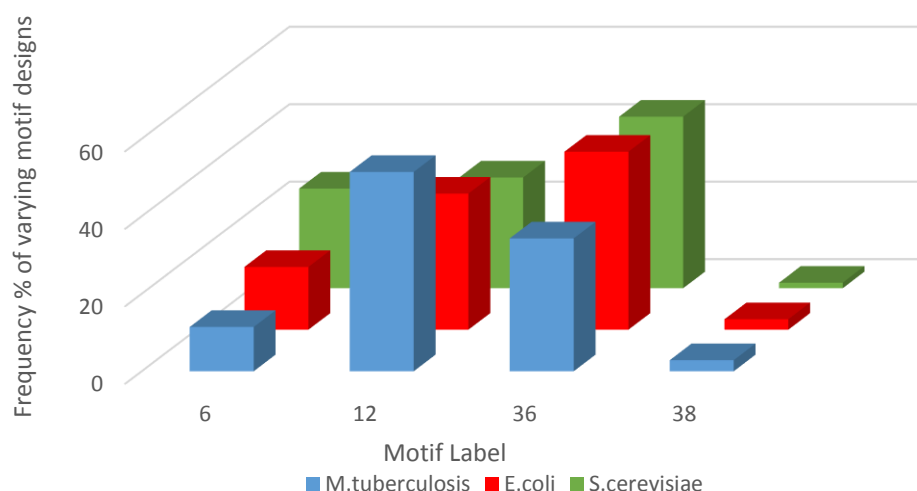


**Figure 2.6.** Frequencies of the common three node motifs detected for *M. tuberculosis*, *E. coli* and *S. cerevisiae* detected using FANMOD.

By contrast, the analysis of the four node sub-graphs showed both common and unique motif designs suggesting variation in these systems' capacities to reduce hydrogen peroxide. The 14 four node motifs detected once again included single input modules (e.g. motif ID: 14/PMN4F); multiple input modules (e.g. motif ID: 2184/Q9PFR); simple pathways with nodes leading to one another (e.g. motif ID: 392/RJ9KF) and adaptations of the feed-forward loop (e.g. motif ID's: 2076/Q9GBX and 2188/Q9QK9) (Table 2.2) with varying frequencies across the three redox networks (Figure 2.7 and 2.8). Most of the motif designs were shared across all three species, again suggesting that these motif designs are sufficient in redox networks centered on hydrogen peroxide reduction (Table 2.2).

However, with respect to *M. tuberculosis*, two unique motif patterns were observed i.e. motif ID: 204/PMRM9 and 2118/PMYH9 (Table 2.2, shaded red and blue respectively). The latter motif is present due to connections between AhpE, MSH and Mrx-1 for reducing hydrogen peroxide, with AhpE being the node leading to and responsible for hydrogen peroxide reduction (Figure 2.4 A, blue highlight). Motif ID: 204/PMRM9 (known as the bi-fan motif), was particularly intriguing because this motif design arises from the wiring or connecting of the thioredoxins TrxB and TrxC with the peroxiredoxins Tpx and BCP (Figure 2.4 A, red highlight). As the *M. tuberculosis* thioredoxin system reduces two of the four peroxiredoxins present in the redox network, the properties of this motif design were further analyzed.

**Table 2.2.** Common and unique four node motifs in the hydrogen peroxide reduction networks of *M. tuberculosis*, *E. coli* and *S. cerevisiae* generated by both FANMOD and MAVisto motif detection programs.

Canonical Motif ID		Motif connections	Absence/Presence in species		
FANMOD	MAVisto		Mtb	E. coli	S. cerevisiae
14	PMN4F		x	✓	✓
28	PMN8R		✓	✓	✓
74	PMQGF		x	✓	✓
140	PNHHF		x	✓	✓
142	PMO8X		✓	✓	✓
204	PMRM9		✓	x	x
392	RJ9KF		✓	✓	✓
536	PNOKF		✓	✓	✓
2076	Q9GBX		✓	✓	✓
2116	PMXCR		✓	x	✓
2118	PMYH9		✓	x	x
2182	PUBTX		✓	✓	✓
2184	Q9PFR		✓	✓	✓
2188	Q9QK9		x	✓	✓

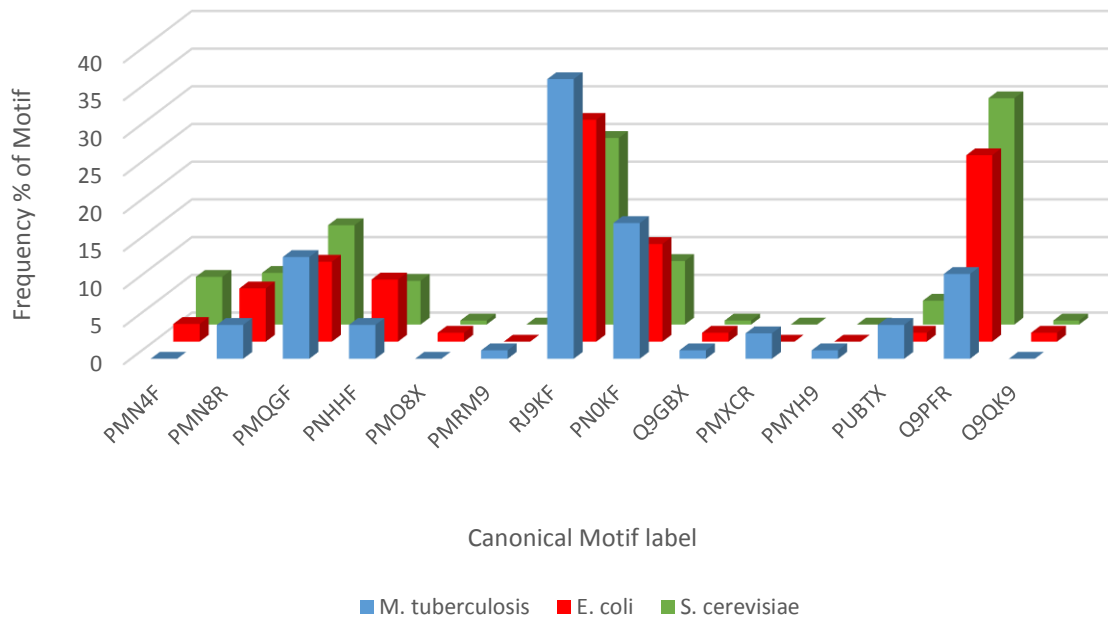


**Figure 2.7.** Frequencies of the common and unique four node motifs detected for *M. tuberculosis*, *E. coli* and *S. cerevisiae* detected using MAVisto.

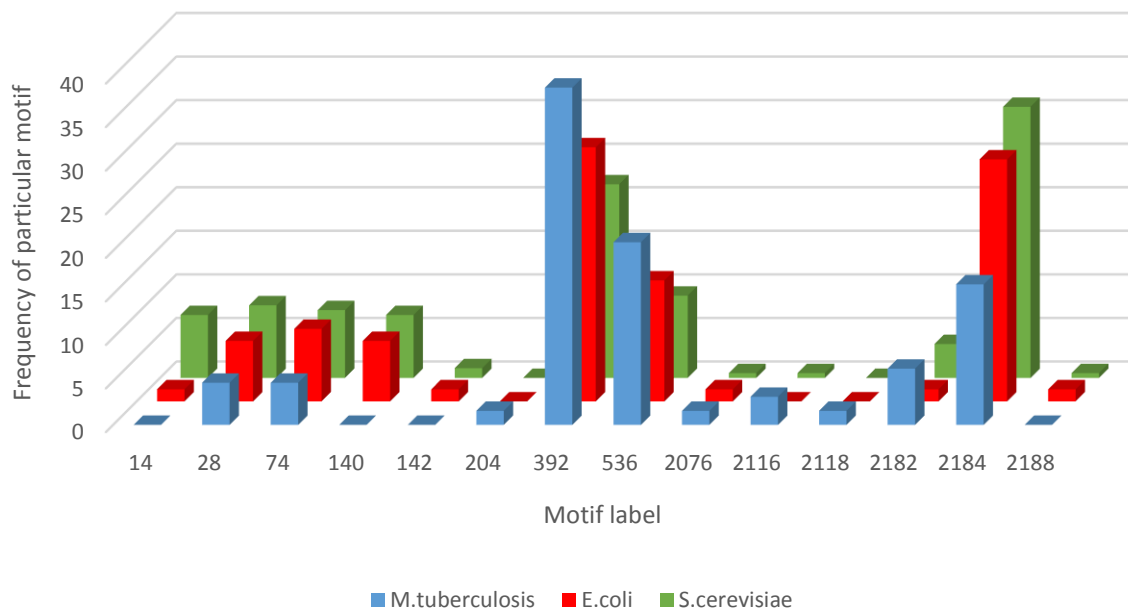


**Figure 2.8.** Frequencies of the common and unique four node motifs detected for *M. tuberculosis*, *E. coli* and *S. cerevisiae* detected using FANMOD.

### 2.3.3 Analytical solutions solved for the bi-parallel and unique bi-fan motif of Mtb

To understand the role of the unique bi-fan motif in the *M. tuberculosis* redox network, the properties of the bi-fan motif were compared to a bi-parallel motif (Figure 2.9) which served as the control for this analysis and is not present in any of the current redox networks being studied. The bi-fan motif comprising TrxB, TrxC, Tpx and BCP were connected to NADPH and hydrogen peroxide which were treated as fixed boundaries of the system.

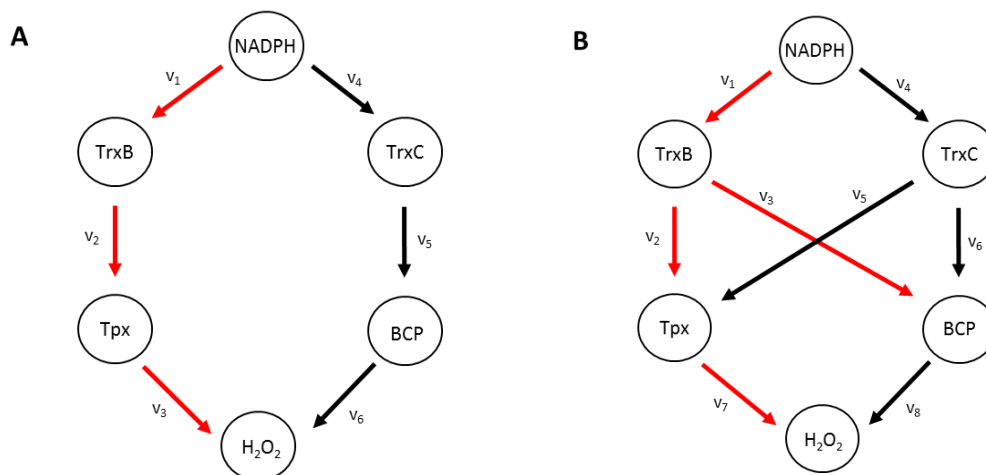


**Figure 2.9.** Diagrammatic representation of the bi-parallel motif (A) and the bi-fan motif (B). Each of the nodes represents a moiety couple, i.e. the coupling of the reduced and oxidized forms into a single node. The crossing of the black (TrxC arm of the motif) and red (TrxB arm of the motif) arrows in (B) shows that two thioredoxins are responsible for the simultaneous reduction of two peroxiredoxins.

Analytical solutions for the bi-fan and bi-parallel motifs were evaluated using mass action kinetics as described previously (see Pillay et al., 2011). Scheme I below describes the reactions pertaining to the TrxB-dependent reactions of the bi-parallel motif. For the analytical solutions, the nodes were described by their reduced (SH) and oxidized forms (SS). The rates of the TrxB-dependent reactions of the bi-parallel motif can be described by rate equations 1-3 while the sum of the TrxB moiety couple is described by equation (4).

*Scheme I: the bi-parallel motif (Figure 2.9A)*

$$v_1 = k_1 \cdot NADPH \cdot TrxBSS \quad (1)$$

$$v_2 = k_2 \cdot TrxBSH \cdot TpxSS \quad (2)$$

$$v_3 = k_{c1} \cdot TpxSH \cdot H_2O_2 \quad (3)$$

$$TrxB_{total} = TrxBSH + TrxBSS \quad (4)$$

The rates of the TrxC-dependent reactions of the bi-parallel motif can similarly be described by the following rate equations (equations 5-7). The sum of the TrxC moiety couple is described by equation (8).

$$v_4 = k_4 \cdot NADPH \cdot TrxCSS \quad (5)$$

$$v_5 = k_5 \cdot TrxC SH \cdot BcpSS \quad (6)$$

$$v_6 = k_{c2} \cdot BcpSH \cdot H_2O_2 \quad (7)$$

$$TrxC_{total} = TrxC SH + TrxCSS \quad (8)$$

where  $v_1, v_2, v_3, v_4, v_5$  and  $v_6$  are the rates of reactions;  $k_1, k_2, k_4, k_5, k_{c1}$  and  $k_{c2}$  are the rate constants and capitalized species names are the concentrations of the reactants. At steady-state,  $v_1 = v_2$  and therefore:

$$k_1 \cdot NADPH \cdot (TrxB_{total} - TrxB SH) = k_2 \cdot TrxB SH \cdot TpxSS \quad (9)$$

This expression can be rearranged to yield:

$$TrxB SH = \frac{k_1 \cdot NADPH \cdot TrxB_{total}}{k_2 \cdot TpxSS + k_1 \cdot NADPH} \quad (10)$$

Substituting equation (10) into equation (2) gives equation (11) which has the same form as the Michaelis-Menten equation:

$$\begin{aligned} v_2 &= k_2 \cdot TrxB SH \cdot TpxSS \\ v_2 &= k_2 \cdot \left( \frac{k_1 \cdot NADPH \cdot TrxB_{total}}{k_2 \cdot TpxSS + k_1 \cdot NADPH} \right) \cdot TpxSS \\ &= \frac{(k_1 \cdot NADPH \cdot TrxB_{total}) \cdot TpxSS}{\frac{k_1 \cdot NADPH}{k_2} + TpxSS} \end{aligned} \quad (11)$$

where  $k_1 \cdot NADPH \cdot TrxB_{total}$  is the apparent  $V_{max}$ ,  $\frac{k_1}{k_2} \cdot NADPH$  is the apparent  $K_m$  and  $TpxSS$  is the oxidized peroxiredoxin substrate in question. The TrxC mediated reduction of BCP (Figure 2.9 A right, black arrows) follows a similar solution with the  $TpxSS$  being substituted for  $BcpSS$ .

This result shows that reduction of single peroxiredoxin is limited to its respective cognate thioredoxin, i.e. Tpx is reduced by TrxB and BCP is reduced by TrxC and these reactions have no direct effect on each other. Ordinary differential equations were then used to determine the effect of thioredoxin on the  $TpxSS$  concentration.  $TpxSS$  is produced and consumed by the reactions (3) and (2) respectively, therefore:

$$\begin{aligned}\frac{dTpxSS}{dt} &= v_3 - v_2 \\ &= k_{c1} \cdot TpxSH \cdot H_2O_2 - \left( \frac{(k_1 \cdot NADPH \cdot TrxB_{total}) \cdot TpxSS}{\frac{k_1}{k_2} \cdot NADPH + TpxSS} \right)\end{aligned}\quad (12)$$

Solving for  $TpxSH$  at steady-state yields:

$$TpxSH = \frac{(k_1 \cdot k_2 \cdot TrxB_{total} \cdot NADPH) \cdot (TpxSS)}{k_{c1} \cdot H_2O_2 \cdot (k_1 \cdot NADPH + k_2 \cdot TpxSS)} \quad (13)$$

Similarly, the steady-state BCP concentration can be determined by equation (14):

$$BcpSH = \frac{(k_4 \cdot k_6 \cdot TrxC_{total} \cdot NADPH) \cdot (BcpSS)}{k_{c2} \cdot H_2O_2 \cdot (k_4 \cdot NADPH + k_6 \cdot BcpSS)} \quad (14)$$

These results further demonstrate that the activities of both BCP and Tpx are only affected by their cognate thioredoxin and not the thioredoxin of the parallel arm. However, these steady-state concentrations depend on the NADPH, thioredoxin reductase ( $v_4$  and  $v_1$ ) and hydrogen peroxide concentrations and therefore BCP and Tpx can indirectly affect each other's steady-state concentrations and activity. This result implies that if the NADPH and thioredoxin reductase concentrations were not limiting, the two arms of the bi-parallel motif will reduce hydrogen peroxide independently of one another. Further, if either TrxB or TrxC, or Tpx or BCP were inactive, the reductive flux of hydrogen peroxide could continue through the active arm of the motif.

A similar approach was taken in solving the equations for the bi-fan motif (Figure 2.9 B), although the bi-fan motif contains two additional reactions, i.e. TrxB reducing BCP and TrxC reducing Tpx (Figure 2.9 B). The system of reactions can be described with the following rate equations (15-22):

Scheme II: the bi-fan motif (Figure 2.9B):

$$v_1 = k_1 \cdot TrxBSS \cdot NADPH \quad (15)$$

$$v_2 = k_2 \cdot TrxBSH \cdot TpxSS \quad (16)$$

$$v_3 = k_3 \cdot TrxBSH \cdot BcpSS \quad (17)$$

$$v_4 = k_4 \cdot TrxCSS \cdot NADPH \quad (18)$$

$$v_5 = k_5 \cdot TrxCSS \cdot TpxSS \quad (19)$$

$$v_6 = k_6 \cdot TrxCSS \cdot BcpSS \quad (20)$$

$$v_7 = k_{c1} \cdot TpxSH \cdot H_2O_2 \quad (21)$$

$$v_8 = k_{c2} \cdot BcpSH \cdot H_2O_2 \quad (22)$$

At steady-state,  $v_1 = v_2 + v_3$  and can be expressed as follows:

$$k_1.TrxBSS.NADPH = k_2.TpxSS.TrxBSH + k_3.BcpSS.TrxBSH \quad (23)$$

Rearranging and solving for  $TrxBSH$  yields the following equation:

$$TrxBSH = \frac{k_1.TrxB_{total}.NADPH}{k_1.NADPH+k_3.BcpSS+k_2.TpxSS} \quad (24)$$

Substituting equation (24) into equation (16) yields:

$$\begin{aligned} v_2 &= k_2.TrxBSH.TpxSS \\ &= \frac{(k_1.TrxB_{total}.NADPH).(TpxSS)}{\frac{k_1.NADPH+k_3.BcpSS}{k_2}+TpxSS} \end{aligned} \quad (25)$$

When compared to the bi-parallel motif (equation 11), the rate of Tpx reduction (equation 25) now incorporates the term  $k_3.BcpSS$  into the denominator showing that the rate of reaction  $v_2$  is dependent on the rate of reduction of  $BcpSS$  by  $TrxBSH$ . The solution for  $TrxCSS$  and  $v_5$  can be similarly analyzed to yield the following expression:

$$v_5 = \frac{(k_4.TrxC_{total}.NADPH).(TpxSS)}{\frac{k_4.NADPH+k_6.BcpSS}{k_5}+TpxSS} \quad (26)$$

The ordinary differential equation for reduced Tpx can be obtained as follows:

$$\begin{aligned} \frac{dTpxSS}{dt} &= v_7 - v_2 - v_5 \\ &= k_{c1}.H_2O_2.TpxSH - v_2 - v_5 \end{aligned} \quad (27)$$

where  $v_2$  and  $v_5$  are equations (25) and (26) respectively, showing the utilization or removal of  $TpxSS$ , and the expression  $k_{c1}.H_2O_2.TpxSH$  is the production of  $TpxSS$ .

However, the steady-state solution for equation (27) was extremely complex and did not shed any insights into this system's configuration (Appendix, equation S1). In summary, unlike the bi-parallel solution (equation 11), the bi-fan analytical solution (equations 25-26) includes both peroxiredoxins in both rate expressions showing that the rate of  $TpxSS$  reduction is affected by the reduction of  $BcpSS$  and *vice versa*. Further, a single thioredoxin, TrxB or TrxC, is sufficient for hydrogen peroxide reduction via either arm of the motif. The bi-fan analytical solution (equations 25-26) also implied that Tpx and BCP affect each because they directly share a reductive source, i.e. either TrxB or TrxC. However, this trade-off in the system means that this particular system is not reliant on a single thioredoxin for the peroxiredoxins to remain

active. The complexity of the differential equations for the bi-fan motif prompted kinetic model simulations to be carried out to further understand the trade-offs within the bi-fan motif system.

### 2.3.4 Core model simulations to determine dynamics of the bi -parallel and –fan motifs

Core models of the bi-parallel and bi-fan motifs were developed in Jupyter Notebook using PySCeS, with model parameters set to one (Tables 2.3 and 2.4) so that the steady-state properties of these differing connectivities could be explored. The behavior of these models was analyzed to determine if the systems behaved as predicted by their analytical solutions.

**Table 2.3.** Species concentrations used for the core computational models of the bi-parallel and bi-fan motif designs.

Motif Model	Species	Initial Concentration ( $\mu\text{M}$ )	
All	NADPH	5 <sup>b</sup>	
	NADP <sup>+</sup>	1 <sup>b</sup>	
	Thioredoxin reductase (TR)	5 <sup>b</sup>	
	Thioredoxin B <sub>red</sub> (TrxB <sub>SH</sub> )	0.5 <sup>a</sup>	
	Thioredoxin B <sub>ox</sub> (TrxB <sub>SS</sub> )	0.5 <sup>a</sup>	
	Thioredoxin C <sub>red</sub> (TrxC <sub>SH</sub> )	0.5 <sup>a</sup>	
	Thioredoxin C <sub>ox</sub> (TrxC <sub>SS</sub> )	0.5 <sup>a</sup>	
	Thiol peroxidase <sub>red</sub> (Tpx <sub>SH</sub> )	0.5 <sup>a</sup>	
	Thiol peroxidase <sub>ox</sub> (Tpx <sub>SS</sub> )	0.5 <sup>a</sup>	
	Bacterioferritin comigratory protein <sub>red</sub> (Bcp <sub>SH</sub> )	0.5 <sup>a</sup>	
	Bacterioferritin comigratory protein <sub>ox</sub> (Bcp <sub>SS</sub> )	0.5 <sup>a</sup>	
		H <sub>2</sub> O <sub>2</sub>	1 <sup>b</sup>

<sup>a</sup> Note that the concentrations of moiety conserved couples together equal 1.

<sup>b</sup> Fixed species in the computational models.

**Table 2.4.** Reactions and reaction parameters for core computational modeling of both the bi-parallel and bi-fan motif.

Reaction	Parameter	Value
<b>Both models (thioredoxin reductase reaction scheme)</b>		
R1: NADPH + TrxBSS $\rightarrow$ NADP + TrxBSH	$k_{cat1}$	1 s <sup>-1</sup>
	$K_{1nadph}$	1 $\mu$ M
	$K_{1trxbss}$	1 $\mu$ M
R2: NADPH + TrxCSS $\rightarrow$ NADP + TrxCSH	$k_{cat2}$	1 s <sup>-1</sup>
	$K_{1nadph}$	1 $\mu$ M
	$K_{2trxcss}$	1 $\mu$ M
<b>Bi-parallel motif script</b>		
R3: TrxBSH + TpxSS $\rightarrow$ TrxBSS + TpxSH	$k_3$	1 $\mu$ M <sup>-1</sup> .s <sup>-1</sup>
R4: TpxSH + H <sub>2</sub> O <sub>2</sub> $\rightarrow$ TpxSS + 2 H <sub>2</sub> O	$k_4$	1 $\mu$ M <sup>-1</sup> .s <sup>-1</sup>
R5: TrxCSH + BcpSS $\rightarrow$ TrxCSS + BcpSH	$k_5$	1 $\mu$ M <sup>-1</sup> .s <sup>-1</sup>
R6: BcpSH + H <sub>2</sub> O <sub>2</sub> $\rightarrow$ BcpSS + 2 H <sub>2</sub> O	$k_6$	1 $\mu$ M <sup>-1</sup> .s <sup>-1</sup>
<b>Bi-Fan motif script</b>		
R3: TrxBSH + TpxSS $\rightarrow$ TrxBSS + TpxSH	$k_3$	1 $\mu$ M <sup>-1</sup> .s <sup>-1</sup>
R4: TrxBSH + BcpSS $\rightarrow$ TrxBSS + BcpSH	$k_4$	1 $\mu$ M <sup>-1</sup> .s <sup>-1</sup>
R5: TrxCSH + TpxSS $\rightarrow$ TrxCSS + TpxSH	$k_5$	1 $\mu$ M <sup>-1</sup> .s <sup>-1</sup>
R6: TrxCSH + BcpSS $\rightarrow$ TrxCSS + BcpSH	$k_6$	1 $\mu$ M <sup>-1</sup> .s <sup>-1</sup>
R7: TpxSH + H <sub>2</sub> O <sub>2</sub> $\rightarrow$ TpxSS + 2 H <sub>2</sub> O	$k_7$	1 $\mu$ M <sup>-1</sup> .s <sup>-1</sup>
R8: BcpSH + H <sub>2</sub> O <sub>2</sub> $\rightarrow$ BcpSS + 2 H <sub>2</sub> O	$k_8$	1 $\mu$ M <sup>-1</sup> .s <sup>-1</sup>

Although the thioredoxin reductase concentration was similar between models, the flux through the bi-fan system was higher over a range of hydrogen peroxide concentrations when compared to the bi-parallel motif (Figure 2.10) suggesting that the saturation in both models may have resulted from a saturation of the moiety couples in the system (Pillay et al., 2009; Padayachee and Pillay, 2016). Therefore, the oxidized and reduced forms of Tpx and BCP were examined and it was found a higher hydrogen peroxide concentration was required to distribute Tpx and BCP into their oxidized forms for the bi-fan motif (Figure 2.10 B, black arrow). The result suggested that the bi-fan motif offered a greater hydrogen peroxide reduction capacity when compared to the bi-parallel motif which may be significant for redox defence systems in persistent pathogens.

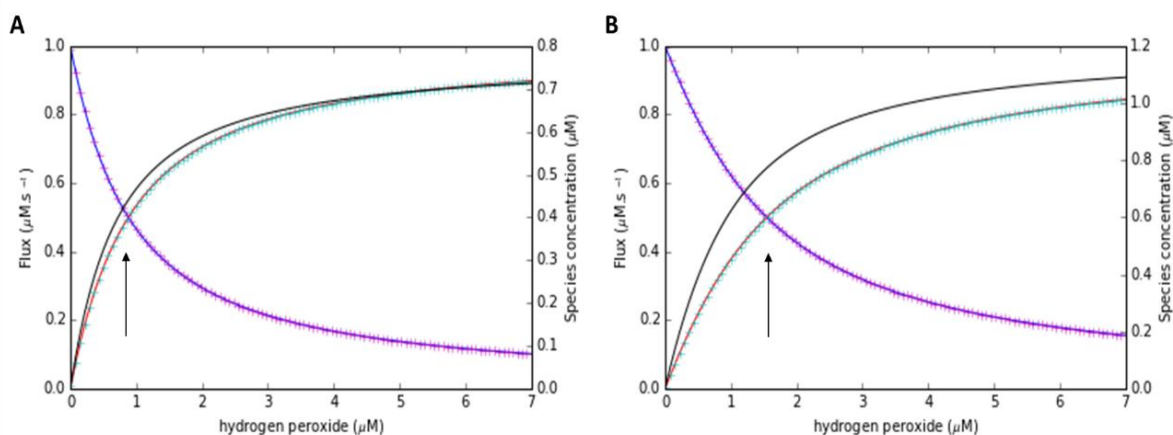


**Figure 2.10.** Core model simulations of the bi-parallel (A) and bi-fan (B) motif designs show that the bi-fan connectivities allow for the system to handle higher hydrogen peroxide concentrations. The thioredoxin reductase flux ( — ) and the steady-state concentrations of the reduced ( + + + + ) and oxidized ( — ) forms of Tpx and the reduced ( — ) and oxidized ( + + + + ) forms of BCP are shown. The black arrow in each of the figures indicates the crossing point of the reduced and oxidized peroxiredoxin species concentrations, where oxidized species begin to accumulate in the system.

Another critical factor in the activity of the systems lay in their dependence on reduced thioredoxin concentrations. A low thioredoxin concentration could result from a high thioredoxin demand for other reductive reactions as explained earlier in this thesis (Chapter 1, section 3.2). The effect of a changing thioredoxin demand for both TrxB and TrxC sub-systems was evaluated (Figure 2.11). With regard to the bi-parallel motif, the peroxiredoxins' flux remained constant if their cognate thioredoxin concentration was not varied, i.e. when the concentration of the thioredoxin C pool (TrxC<sub>SH</sub>) was varied, Tpxs' flux remained constant and *vice versa*. However, both peroxiredoxins were sensitive to changes in the demand of their cognate thioredoxin concentration (Figure 2.11 A-B). This result supported the analytical solution of the system (section 2.3.3) which showed that a thioredoxin in one arm of the motif had no effect on the opposite arms' peroxiredoxin flux provided that NADPH and thioredoxin reductase were not limiting in the system.

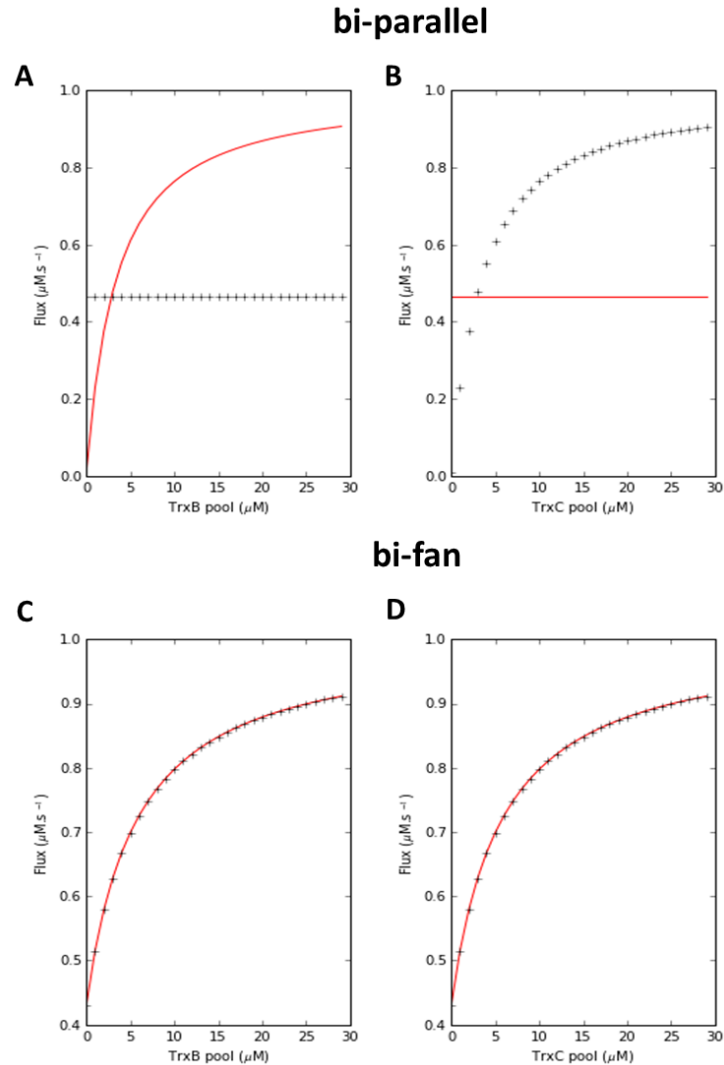


**Figure 2.11.** Steady-state flux analysis of the bi-parallel (A-B) and bi-fan (C-D) systems showing the effect of increasing the respective total thioredoxin B and C moiety pools on peroxidase mediated hydrogen peroxide reduction fluxes in these systems. Fluxes of the reactions pertaining to hydrogen peroxide reduction for the peroxidases Tpx ( — ) and BCP ( + + + + ) are shown for both the bi-fan and bi-parallel motif models as the availability of reduced thioredoxin B and C increases.

In contrast to the bi-parallel motif, the rates of hydrogen peroxide reduction by Tpx and BCP were consistent regardless of changes in either thioredoxin concentration (Figure 2.11 C-D). Interestingly, this result shows that this systems' configuration allows for the activity of both peroxidases when a single thioredoxin is inactive, partially active or present at low concentrations within the system. The fluxes of both Tpx and BCP mediated hydrogen peroxide reduction were therefore robust with respect to changes in TrxB and TrxC concentrations.

To determine whether changes in the reduced thioredoxin B and C moiety concentrations also resulted in different behaviors by the bi-parallel and bi-fan systems, two additional reactions ( $\text{PSS} + \text{TrxBSH} \rightarrow \text{PSH} + \text{TrxBSS}$  and  $\text{PSS} + \text{TrxC SH} \rightarrow \text{PSH} + \text{TrxCSS}$ , where PSS and PSH represent oxidized and reduced proteins respectively) were added to both motif reaction schemes to simulate the increased demand for thioredoxins within these systems (Figure 2.12).

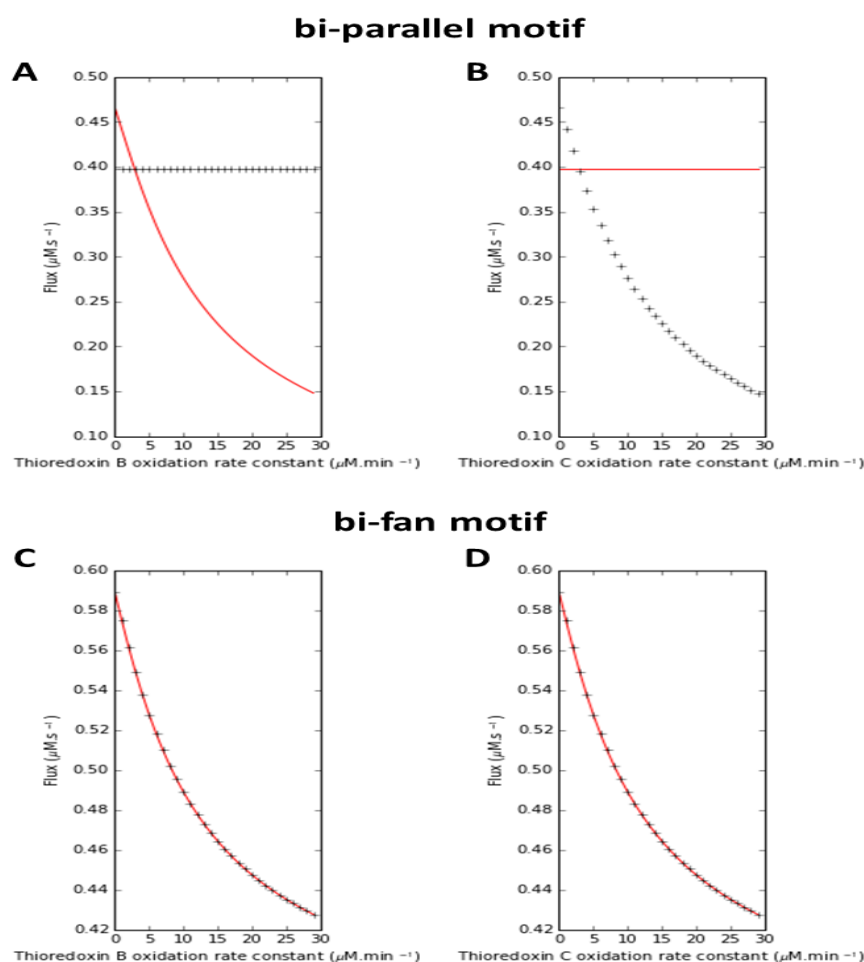


**Figure 2.12.** Steady-state flux analysis of the bi-parallel (A-B) and bi-fan (C-D) systems showing the effects of keeping constant thioredoxin B and C moiety pools respectively and the impact on the fluxes of peroxidase mediated hydrogen peroxide reduction when thioredoxin B and C demands increase respectively. Fluxes of the Tpx ( — ) and BCP ( +++ ) mediated reduction of hydrogen peroxide are shown as the rate of thioredoxin B and C consumption is increased. Note: the y-axis scales vary between the bi-parallel and bi-fan motif designs due to differences in their fluxes.

When using constant thioredoxin B and C moiety pools respectively, increasing the rate of thioredoxin consumption by PSS meant less thioredoxin was available to reduce the peroxiredoxins, Tpx and BCP. Thus, there was a decrease in fluxes associated with hydrogen peroxide reduction when their cognate steady-state reduced thioredoxin concentrations were reduced (Figure 2.12). In agreement with Figure 2.11, the bi-parallel motif design (Figure 2.12 A-B) showed that when thioredoxin B was depleted (Figure 2.12 A), the Tpx-mediated hydrogen peroxide reduction flux decreased while BCP's reductive flux remained unaffected and *vice versa* (Figure 2.12 B). On the other hand, for the bi-fan motif (Figure 2.12 C-D), when either reduced thioredoxin concentration was decreased then both the fluxes of Tpx and BCP mediated hydrogen peroxide reduction decreased but the system did display a greater tolerance towards reductant concentration fluctuations. For example, the Tpx and BCP hydrogen peroxide reduction fluxes decreased from  $0.59 \mu\text{M}\cdot\text{s}^{-1}$  to  $0.41 \mu\text{M}\cdot\text{s}^{-1}$  in the bi-fan motif (Figure 2.12 C-D) whereas in the bi-parallel motif, peroxiredoxin reductive fluxes decreased from  $0.46 \mu\text{M}\cdot\text{s}^{-1}$  to  $0.15 \mu\text{M}\cdot\text{s}^{-1}$  over the same range (Figure 2.12 A-B). This result supports the hypothesis that reductive redundancy could contribute towards *M. tuberculosis* persistent latency within the host.

## 2.4 Discussion

Protein-protein interaction maps provide an insightful and valuable framework for understanding the functional organization of a cells' proteome (Stelzl et al., 2005). Here the redox defence networks of *M. tuberculosis*, *E. coli* and *S. cerevisiae* were analyzed with focus on the redox couples crucial in hydrogen peroxide defence. This analysis was carried out with the aim of identifying key motifs which support Mtb cell viability within host granuloma during the course of infection (Pieters, 2008).

Motifs containing three nodes were present across all three organisms, suggesting conservation of these connection designs within redox defence networks. However, analysis of four node motifs showed differences between the systems' connections. Among the 14 motifs detected across all three redox networks (Table 2.2), *M. tuberculosis* had two unique configurations. One motif, ID: 2118/PMYH9, was found to be the connection of the peroxiredoxin AhpE with the MSH/Mrx-1 system, with the subsequent reduction of hydrogen peroxide by AhpE (Figure 2.4 A). The presence of such a motif in *M. tuberculosis* was attributed to the presence of the MSH/Mrx-1 system, which is absent in the *E. coli* and *S. cerevisiae* redox systems. The second unique motif, ID: 204/PMRM9, was a bi-fan motif

comprised of two thioredoxins, TrxB and TrxC, both reducing the two peroxiredoxins Tpx and BCP (Figure 2.4 A; Figure 2.9 A).

The bi-fan and control bi-parallel motif designs were compared using analytical solutions which revealed that the peroxiredoxin arms of the bi-parallel system were independent of one another. In contrast, the bi-fan motif showed dependence on both thioredoxins within the system and was further examined by analysis of ordinary differential equations, but these solutions were extremely complex (equation S1, Appendix) and core kinetic models were then opted for use in further analysis. It is also important to note that reaction and affinity constants within the reaction schemes outlined in this chapter were set to one for an easier interpretation of the behaviour of the system. With realistic values, the fluxes of these reactions are expected to change but the overall trends outlined by the two motif designs are still expected (described in Chapter 2, equations 11, 25 and 26).

Core kinetic models revealed important system properties when comparing the bi-parallel and bi-fan motif designs. The bi-fan motif design required a higher concentration of hydrogen peroxide before the peroxiredoxins' redox cycles became saturated (Figure 2.10) and the peroxiredoxin-mediated hydrogen peroxide reduction fluxes were relatively robust to a change in either thioredoxin concentration, showing that the reduction redundancy within the system may be beneficial to the cell. Thus, if a single thioredoxin is inactive or at low concentrations, both peroxiredoxins can still be able to substantially reduce hydrogen peroxide. By contrast, in the bi-parallel motif the hydrogen peroxide reduction system is reliant on both thioredoxins to be present at significant concentrations for their cognate peroxiredoxins to remain active (Figure 2.11). This result was further bolstered by carrying out simulations of the bi-fan and bi-parallel motif designs using a biologically realistic environment where the total pool of thioredoxin in the cell was kept constant and the thioredoxin B and C fluxes were split amongst the peroxiredoxin and other thioredoxin demands (Figure 2.12). The results show that in the bi-fan motif, both Tpx and BCP maintained their hydrogen peroxide reductive capabilities and remained more robust to thioredoxin concentration fluctuations when compared to that of the bi-parallel motif design (Figure 2.12 A-B).

Figure 2.12 shows the effects of keeping thioredoxin B and C moiety pools constant and the subsequent effects on the peroxiredoxin fluxes. When the thioredoxin oxidation rates were increased in the bi-parallel motif, the flux of hydrogen peroxide reduction for each of the cognate peroxiredoxins decreased from  $0.45 \mu\text{M}\cdot\text{s}^{-1}$  to  $0.15 \mu\text{M}\cdot\text{s}^{-1}$  while the unaffected

peroxiredoxin flux remained constant at  $0.40 \mu\text{M}\cdot\text{s}^{-1}$  (Figure 2.12 A-B). In contrast, when either of the thioredoxin oxidation rates were increased in the bi-fan motif, both peroxiredoxin fluxes decreased simultaneously from  $0.59 \mu\text{M}\cdot\text{s}^{-1}$  to  $0.43 \mu\text{M}\cdot\text{s}^{-1}$  (Figure 2.12 C-D). When compared to the bi-parallel motif design, this result still shows that the redundancy within the bi-fan motif allows the hydrogen peroxide reductive capacity of the cell to be maintained in the face of increasing thioredoxin oxidation. The redundancy of the thioredoxin-mediated reduction of peroxiredoxins in the bi-fan motif shows that this system may have evolved to ensure sustainable reduction of peroxiredoxins when thioredoxin concentrations fluctuate within the cell. This is supported by the fact that thioredoxin is known to be involved in various other cellular reactions including DNA replication, transcription factor regulation and a growth factor among many other roles (Powis et al., 2000). Thioredoxin also plays a role in helping cells recover from oxidative damage via methionine sulfoxide reductase (MsrA) (Gleason and Holmgren, 1988; Gladyshev, 2002) and could also be redistributed in this manner to aid in cell survival during hypoxic conditions. A study carried out where auranofin, an anti-rheumatic drug, was repurposed to be used as a potent thioredoxin reductase inhibitor in an Mtb study (Harbut et al., 2015) could further support the importance of the bi-fan motif embedded within the redox defence network. By inhibiting thioredoxin reductase, the bi-fan motif as well as other thioredoxin-dependent reactions would be essentially halted. The results shown in this chapter also serve as a rationale for the effectiveness of auranofin, ideally making the bi-fan motif and other central hub systems suitable candidates for future drug targets focusing on redox protein inhibition within the Mtb and other pathogenic cells sharing similar properties.

To our knowledge results presented here are the first such analysis for the hydrogen peroxide reduction network of *M. tuberculosis*. These findings needed to be confirmed using realistic parameters and consequently the components of the bi-fan motif were prime candidates for *in vitro* analysis.

## **Chapter 3: *In vitro* analysis of the thioredoxin reductase, thioredoxin C and the bacterioferritin comigratory protein components within the bi-fan motif**

### **3.1 Introduction**

In Chapter 2, structural analysis of the *M. tuberculosis* redox defence network revealed a novel bi-fan motif associated with hydrogen peroxide defence, which comprised the two biologically active thioredoxins (TrxB and TrxC) both reducing the two peroxiredoxins Tpx and BCP. The work presented in this chapter serves as a basis to show that the bi-fan motif could be assessed using *in vitro* analysis. As a first step it was necessary to obtain pure protein samples of the Mtb thioredoxin reductase, thioredoxin C and BCP proteins for the kinetic characterization of the interactions between these proteins.

### **3.2 Materials**

The GeneJET Plasmid Miniprep Kit was obtained from ThermoFisher Scientific (Johannesburg, South Africa) and the TGX Stain-Free™ FastCast™ Acrylamide Kit (12%) was obtained from BIO RAD Laboratories (Pty) Ltd (Johannesburg, South Africa). Dithiothreitol (DTT), bovine pancreas insulin, 5,5-dithio-bis-(2-nitrobenzoic acid) (DTNB), bovine serum albumin (BSA), isopropyl β-D-1-thiogalactopyranoside (IPTG), kanamycin antibiotic, β-nicotinamide adenine dinucleotide phosphate (NADPH), 4-(2-aminoethyl)benzenesulfonyl fluoride hydrochloride (AEBSF), phenylmethane sulfonyl fluoride (PMSF), Coomassie G-250 and R-250 and N,N,N',N'-tetramethylethylenediamine (TEMED) were obtained from Sigma (Capital Labs, South Africa). Ni-NTA agarose was obtained from Whitehead Scientific (Pty) Ltd (Cape Town, South Africa). Common reagents and chemicals were obtained from Saarchem (Merck, South Africa). *E. coli* BL21 cells were available in the lab. Gene synthesis of the thioredoxin reductase (TR, *rv3913*), thioredoxin C (TrxC, *rv3914*) and bacterioferritin comigratory protein (BCP, *rv2521*) clones in pET28a expression vectors was carried out by GenScript Ltd (Hong Kong). The DNA sequences were codon optimized for successful expression in *E. coli* BL21 host cells.

#### **3.2.1 Preparation of lyophilized plasmid DNA**

The lyophilized pET28a clone plasmid DNA was resuspended in 1× TE buffer by gentle finger tapping as per the protocol provided by GenScript. These DNA stock solutions were used when transforming *E. coli* BL21 cells for subsequent protein expression.

### **3.2.2 Preparation of common reagents**

#### **3.2.2.1 Kanamycin stock solution**

A stock solution (30 mg/mL) was prepared by dissolving kanamycin sulfate (0.3 g) in 10 mL of dH<sub>2</sub>O. The solution was filter sterilized (0.2 µm filter) and stored in 1 mL aliquots at -20°C.

#### **3.2.2.2 IPTG stock solution**

A stock solution (100 mM) was prepared by dissolving IPTG (0.238 g) in 10 mL of dH<sub>2</sub>O. The solution was filter sterilized (0.2 µm filter) and stored in 1 mL aliquots at -20°C.

#### **3.2.2.3 DTT stock solution**

A DTT stock solution (1 M) was made fresh daily. DTT powder (0.154 g) was dissolved in 1 mL of dH<sub>2</sub>O and stored at room temperature. 100 µL of this stock was made up to a final volume of 1 mL (final concentration 100 mM) for use in the thioredoxin specific activity assay.

#### **3.2.2.4 Bovine pancreas insulin stock solution**

A stock insulin solution (1.6 mM) was prepared by suspending bovine pancreas insulin (50 mg) in 500 µL 100 mM potassium phosphate buffer (pH 6.5). The pH of the solution was thereafter adjusted to 2-3 with 1 M HCl to completely dissolve the protein and was thereafter rapidly titrated back to the original pH 6.5 and made up to a final volume of 5 mL with ddH<sub>2</sub>O. The clear solution was stored at -20°C until use in the thioredoxin specific activity assay.

#### **3.2.2.5 DTNB stock solution**

A stock solution of DTNB (63.1 mM) was freshly prepared by dissolving DTNB powder (0.025 g) in 99% ethanol to a final volume of 1 mL. The resulting solution is light sensitive and was subsequently stored in the dark for use in the thioredoxin reductase specific activity assay.

#### **3.2.2.6 NADPH stock solution**

NADPH (stock solution and powder) is susceptible to oxidation by exposure to air. To avoid constant exposure to air, stock vials were prepared by keeping 10 mg portions of the powder in separate micro centrifuge tubes (-20°C, caps were further sealed with parafilm for longer periods of storage). At the time of use, the sub-aliquoted stock was resuspended in ddH<sub>2</sub>O (250 µL) resulting in a final concentration of 50 mM and stored at -20°C. NADPH

concentration was determined by direct spectroscopy at 340 nm using an extinction coefficient of  $6200 \text{ M}^{-1} \cdot \text{cm}^{-1}$  (Arnér and Holmgren, 2000a).

### **3.2.2.7 10% (w/v) ammonium persulfate solution**

A 10% (w/v) ammonium persulfate solution for use in the SDS-PAGE electrophoresis technique was prepared fresh at time of use by dissolving ammonium persulfate powder (0.2 g) in 2 mL of dH<sub>2</sub>O.

### **3.2.2.8 SDS-PAGE sample loading buffer (4×)**

The SDS-PAGE sample loading buffer was prepared by mixing 1 M Tris-HCl (pH 6.8, 1.5 mL), 1 M DTT (3 mL), SDS (0.6 g), bromophenol blue (0.03 g), glycerol (2.4 mL) and bringing up to a final volume of 7.5 mL. The solution was aliquoted and stored at 4°C.

### **3.2.2.9 SDS-PAGE tank buffer (10×)**

10× SDS-PAGE tank buffer was prepared by adding Tris (15.15 g), glycine (71.32 g) and SDS (5 g) to dH<sub>2</sub>O and brought up to a final volume of 500 mL. For SDS-PAGE electrophoresis, 100 mL (10X SDS-PAGE tank buffer) was brought up to a final volume of 1 L using dH<sub>2</sub>O.

### **3.2.2.10 Bovine serum albumin standard solution**

A 1 mg/mL of bovine serum albumin solution was made up in dH<sub>2</sub>O for further use in the Bradford protein concentration quantitation assay.

### **3.2.2.11 Bradford reagent**

Coomassie brilliant blue G-250 (50 mg) was dissolved in methanol (50 mL). Thereafter, 85% (w/v) phosphoric acid (100 mL) was added to the solution and the made up to a total volume of 1 L using dH<sub>2</sub>O. The solution was stirred for one hour and filtered through Whatman number 1 filter paper into a darkened amber bottle and stored at 4°C.

## **3.2.3 Bacterial growth media**

### **3.2.3.1 Luria Bertani (LB) broth**

Tryptone powder (1% (w/v)), yeast extract (0.5% (w/v)) and NaCl (0.5% (w/v)) were dissolved in dH<sub>2</sub>O while making up to the required volume of broth. The broth was then autoclaved, stored at room temperature and supplemented with the appropriate antibiotic when necessary (kanamycin, 50 µg/mL final concentration).

### **3.2.3.2 Luria Bertani (LB) agar**

Tryptone powder (1% (w/v)), yeast extract (0.5% (w/v)), NaCl (1% (w/v)) and bacteriological agar (2% (w/v)) were dissolved in dH<sub>2</sub>O and made up to the required volume. The solution was autoclaved and upon cooling, the solution was poured into petri dishes. The broth was also supplemented with the appropriate antibiotic when necessary (kanamycin, 50 µg/mL final concentration). The solidified petri plates were stored at 4°C when not in use.

### **3.2.3.3 Glucose stock solutions**

A glucose stock solution (1 M) was prepared by dissolving glucose powder (1.8 g) in 10 mL of ddH<sub>2</sub>O. The solution was filter sterilized (0.2 µm filter) and the solution stored at 4°C until use. A working glucose solution (10% (w/v)) was prepared by dissolving glucose powder (1 g) in 10 mL of ddH<sub>2</sub>O. The solution was filter sterilized (0.2 µm filter) and stored at 4°C until use.

### **3.2.3.4 SOC media recipe**

Tryptone powder (2% (w/v)), yeast extract (0.5% (w/v)), NaCl (10 mM), KCl (2.5 mM) and MgCl<sub>2</sub> (10 mM) were dissolved in dH<sub>2</sub>O and made up to the required volume. The resulting solution was autoclaved and upon cooling was supplemented with glucose (20 mM final concentration). SOC media was stored at 4°C when not in use.

## **3.3 Methods**

### **3.3.1 Transformation of pET28a plasmids into *E. coli* BL21 cells for expression**

*E. coli* BL21 cells were made competent using the calcium chloride (CaCl<sub>2</sub>) treatment method (Dagert and Ehrlich, 1979). An overnight *E. coli* BL21 culture (1 mL) was transferred into fresh LB broth (25 mL) and grown until an OD<sub>600</sub> of 0.3-0.4 was obtained (150 rpm, 37°C). Duplicate 10 mL samples were placed in ice-cold centrifuge tubes, chilled on ice (10 minutes) and thereafter centrifuged (4500 x g, 10 minutes, 4°C). The supernatant was discarded and the resulting cell pellet resuspended in ice-cold 0.1 M CaCl<sub>2</sub> (10 mL per pellet). The solution was then centrifuged once more (4500 x g, 10 minutes, 4°C), the supernatant discarded and the pellet resuspended in ice-cold 0.1 M CaCl<sub>2</sub> (2 mL per cell pellet). The suspension was incubated on ice for a further 30 minutes before transformation.

Stock solutions of pET28a clones were made up to 0.04 µg/µL. Competent cells (20 µL) were then incubated with the plasmid DNA (2.5 µL, final concentration of DNA 100 ng) on

ice (4°C, 30 minutes). The mixture was then heat shocked (42°C, 90 seconds) and immediately cooled on ice (4°C, 2 minutes). Pre-warmed SOC media (80 µL, 37°C) was added to the competent cells transformation mix and incubated at 37°C in a shaking water bath (1 hour). The transformation mix (50 µL) was spread plated on LB agar plates containing kanamycin (final concentration, 50 µg/mL) and grown overnight at 37°C.

Control LB agar plates were set up to check viability of *E. coli* BL21 cells (no kanamycin added, only competent cells plated) and test activity of kanamycin antibiotic (final concentration, 50 µg/mL, plated competent cells without plasmid). Controls were carried out for each of the three plasmid transformations and a single colony selected from successfully transformed plates and grown in LB broth containing kanamycin (final concentration, 50 µg/mL) overnight at 37°C. The GeneJET Plasmid Miniprep Kit was then used to isolate plasmid DNA from the three respective overnight cultures.

### **3.3.2 Sequencing of gene synthesis products**

Expression plasmids containing the *rv3913*, *rv3914* and *rv2521* genes respectively, were sequenced in both directions using the pET28a plasmid T7 promoter and terminator primers (Central Analytical Facility, Stellenbosch University, South Africa). Sequences were curated manually using the BioEdit Sequence Alignment Editor version 7.2.5 (Hall, 1999) and converted to amino sequences using the online ExPASy translate tool (<http://web.expasy.org/translate>). The amino acid sequences were then aligned to the corresponding sequences from the Tuberculosis Database (TBDB, <http://www.tbdb.org>) using the online Clustal Omega sequence alignment tool (<http://www.ebi.ac.uk/Tools/msa/clustalo>).

### **3.3.3 SDS-PAGE acrylamide gel electrophoresis**

Protein samples were visualized on a 12% acrylamide gel during SDS-PAGE run using the BIO RAD Mini-PROTEAN Tetra cell electrophoresis equipment (1.0 mm glass plates used). Stacker and resolver gels were prepared as per protocol provided with the TGX Stain-Free™ FastCast™ Acrylamide Kit (12%) and polymerization of the gel initiated with the addition of TEMED and 10% (w/v) ammonium persulfate. Samples were prepared by boiling them (5 minutes, 80-90°C) in 4× SDS-PAGE sample loading buffer before loading them onto the gels.

Gels were run for a total of 90 min (100V) and thereafter stained in Coomassie blue gel stain (Coomassie brilliant blue R-250 (0.125% (w/v)), methanol (50% (v/v)) and glacial acetic

acid (10% (v/v))) while on an orbital shaker (50 rpm) overnight. The following day, excess stain was removed and the gels de-stained with de-stain solution I (50% (v/v) methanol and 10% (v/v) glacial acetic acid) until the gel background became clear and was finally placed in de-stain II (5% (v/v) methanol and 7% (v/v) glacial acetic acid) until the gel returned to its original size. Gels were then photographed under white light using the DNR MiniBIS Pro Versadoc imaging system.

### **3.3.4 IPTG expression of the *rv3913*, *rv3914* and *rv2521* genes from *M. tuberculosis* in host *E. coli* BL21 cells**

A high cell density culturing method (Sivashanmugam et al., 2009) was used for the high yield expression of recombinant proteins in *E. coli* BL21 cells transformed with the pET28a expression vectors housing the Mtb TR, TrxC and BCP genes respectively. The transformed cells were cultured in three separate LB broth cultures containing kanamycin (final concentration, 50 µg/mL) overnight to obtain high cell density cultures (150 rpm, overnight, 37°C). Cells were then centrifuged (1500 x g, 5 minutes) and the pellet resuspended in high cell density media (LB broth, 50 mM Na<sub>2</sub>HPO<sub>4</sub>, 25mM KH<sub>2</sub>PO<sub>4</sub>, 5mM MgSO<sub>4</sub>, 0.2 mM CaCl<sub>2</sub>, 0.1% (w/v) NH<sub>4</sub>Cl, 1% (v/v) of 10% (w/v) glucose, pH 8) and grown for 1 hour (37°C, 150 rpm) before the addition of IPTG (0.5 mM) to begin induction of the recombinant proteins (37°C, 150 rpm). Hourly samples were taken following IPTG induction to determine the optimal time for each proteins' induction and the samples centrifuged (12 000 x g, 10 minutes, 4°C) and pellets stored at -20°C.

### **3.3.5 Nickel affinity protein (Ni-NTA) purification**

Cell pellets (after IPTG induced expression) were resuspended in refrigerated 1× phosphate-buffered saline (PBS) (500 mM NaCl, 2.7 mM KCl, 10 mM Na<sub>2</sub>HPO<sub>4</sub>, 1.8 mM KH<sub>2</sub>PO<sub>4</sub>, 20% (v/v) glycerol, 0.2 mM AEBSF, 1 mM PMSF (added to sonication tube separately as it is unstable in water), pH 7.2) equal to ten times the weight of cells and sonicated using the VirSonic 60 Ultrasonic Cell Disrupter (8W) for ten seconds followed by ten seconds on ice. This sonication procedure was repeated ten times for each sample. The cell suspension was thereafter centrifuged (12 000 x g, 30 minutes, 4°C) and the supernatant stored at -20°C for further use in the Ni-NTA purification columns.

Protein purification columns (total volume of 15 mL) were packed with Ni-NTA agarose beads (2 mL) and the ethanol from the Ni-NTA agarose allowed to flow through the column, always ensuring the resin bed never dried. The column was then equilibrated with one column

volume of equilibration buffer (20 mM imidazole, 0.5 M NaCl, 1mM  $\beta$ -mercaptoethanol, 20 mM Tris-HCl (pH 8)) and thereafter incubated with the appropriate crude extract (2 hours, 4°C) in a Revolver™ 360° Sample Mixer. Following incubation, the unbound fraction was eluted by gravity and the column washed twice with one column volume of 1× PBS buffer (500 mM NaCl, 2.7 mM KCl, 10 mM Na<sub>2</sub>HPO<sub>4</sub>, 1.8 mM KH<sub>2</sub>PO<sub>4</sub>, 20% (v/v) glycerol, pH 7.2) to remove unbound and loosely bound proteins from the column. The column was thereafter washed with one column volume each of 1× PBS buffer containing a gradient of imidazole concentrations (500 mM NaCl, 2.7 mM KCl, 10 mM Na<sub>2</sub>HPO<sub>4</sub>, 1.8 mM KH<sub>2</sub>PO<sub>4</sub>, 20% (v/v) glycerol, imidazole at 20, 40, 80, 150 and 250 mM respectively, pH 7.2) and samples collected and analyzed using SDS-PAGE (Section 3.3.3). The resin was then incubated with 0.5 M NaOH (30 minutes, room temperature), eluted by gravity and stored in 30% (v/v) ethanol (4°C).

### **3.3.6 Specific activity assays of the Mtb thioredoxin reductase and thioredoxin C proteins**

Crude protein samples were collected every hour following IPTG induction and the total protein concentration determined using the Bradford assay. This assay is based on the binding of Coomassie brilliant blue G-250 to protein residues, shifting the dye from the cationic form to the anionic form causing a shift in the maximum absorption from 365 nm to 595 nm (Bradford, 1976). A standard curve of varying concentrations of bovine serum albumin (0 - 100  $\mu$ g/mL) against the absorbance value at 595 nm was constructed. Measurements were all taken from the linear region of the standard curve (Appendix, Figure S1).

The DTNB reduction assay (Holmgren, 1977) was used to determine the activity of the Mtb thioredoxin reductase protein. The final assay contained 0.1 M Tris-HCl (pH 8), 0.5 mM DTNB, 0.24 mM NADPH, 0.1 mg/mL BSA, 0.5 M NaCl and crude extract containing thioredoxin reductase or pure protein in a final volume of 1 mL. NaCl (0.5 M) was included in the reaction mixture as the presence of a univalent cation allowed increased sensitivity of the reaction (Lim and Lim, 1995). The reaction was initiated with the addition of the protein sample and proceeded at 25°C. The change in absorbance at 412 nm was directly monitored and a cuvette without thioredoxin reductase was used as a reference. All absorbance measurements were carried out using the UV-1800 Shimadzu spectrophotometer.

For thioredoxin C, the insulin reduction assay was used to determine the activity of the protein (Holmgren, 1979). To fully reduce thioredoxin C before beginning the reaction, a method involving the pre-incubation of thioredoxin C (1 mL) containing crude extract or pure

protein (final concentration, 0.05 µg/mL) with 0.1 M DTT (10 µL) for 10 minutes (25°C) was used in this study (Padayachee and Pillay, 2016). A master mix solution containing 84 mM potassium phosphate buffer (pH 7), 2.67 mM EDTA and 0.21 mM insulin was made to a final volume of 9 mL. The master mix (750 µL) was placed in a 1 mL cuvette and the pre-reduced protein suspension (250 µL) was added to the cuvette to initiate the reaction. The final reaction mixture contained 63 mM potassium phosphate buffer (pH 7), 2 mM EDTA, 0.01 mM insulin and 1 mM DTT in a final volume of 1 mL. Absorbance values were directly monitored at 650 nm in the UV-1800 Shimadzu spectrophotometer and a cuvette with no protein was used as the reference cuvette.

### **3.4 Results**

#### **3.4.1 Successful gene synthesis and protein expression of the *rv3913*, *rv3914* and *rv2521* genes from *M. tuberculosis***

Gene synthesis was used in this study as the genomic DNA of *M. tuberculosis* was difficult to obtain due to the health risk involved with the culturing of the bacterium outside of a designated lab. Sequence information was readily available from the Tuberculosis Database (TBDB, <http://www.tbdb.org>) and the genes were synthesized in the pET28a expression plasmid. Codon optimization was also selected as *M. tuberculosis* and *E. coli* utilize and favor different codons for translation (Lin et al., 2002)

Once the expression plasmids housing the synthesized genes were sequenced and translated to amino acid sequences, they were aligned to the amino acid sequences of their respective proteins. The alignment showed that the three proteins were identical to the original protein sequences obtained from Tuberculosis Database (Figure 3.1).

```

A   TR_T7_promoter__1   MTAPPVHRAHHPVRDVIVIGSGPAGYTAALYAARAQLAPLVFEGTSFGGALMTTIDVEN
    Rv3913_TR           MTAPPVHRAHHPVRDVIVIGSGPAGYTAALYAARAQLAPLVFEGTSFGGALMTTIDVEN
    *****

    TR_T7_promoter__1   YPGFRNGITGPELMDREMQALRFGADLRMEDVESVSLHGPKLSVVIADGQTHRRAVIL
    Rv3913_TR           YPGFRNGITGPELMDREMQALRFGADLRMEDVESVSLHGPKLSVVIADGQTHRRAVIL
    *****

    TR_T7_promoter__1   AMGAAARYLQVPGEQELLGRGVSSCATCDGFFFRDQDIIVIGGGDSAMEEATFLTRFARS
    Rv3913_TR           AMGAAARYLQVPGEQELLGRGVSSCATCDGFFFRDQDIIVIGGGDSAMEEATFLTRFARS
    *****

    TR_T7_promoter__1   VTLVHRRDEFRAASKIMLDRARNNDKIRFLTNHTVVAVDGDTITVIGLRVRDNTIGAETTLF
    Rv3913_TR           VTLVHRRDEFRAASKIMLDRARNNDKIRFLTNHTVVAVDGDTITVIGLRVRDNTIGAETTLF
    *****

    TR_T7_promoter__1   VTGVFVAIGHEPRSGLVREAIDVDPDGYVLVQGRITTSISLPGVFAAGDLVDRTYRQAVIA
    Rv3913_TR           VTGVFVAIGHEPRSGLVREAIDVDPDGYVLVQGRITTSISLPGVFAAGDLVDRTYRQAVIA
    *****

    TR_T7_promoter__1   AGSGCAAIDAERWLAEHAATGEADSTDALIGAQR*
    Rv3913_TR           AGSGCAAIDAERWLAEHAATGEADSTDALIGAQR*
    *****

B   TrxC_I7_promoter__1   MTDSEKSATIKVTDASFATDVLSSNKPVLVDFWATWCGPCKMVAFLVEEITERATDLIV
    Rv3914_TrxC         MTDSEKSATIKVTDASFATDVLSSNKPVLVDFWATWCGPCKMVAFLVEEITERATDLIV
    *****

    TrxC_I7_promoter__1   AKLDVDTNPETARNFQVVSIPILILFKDQGQFVKRIVGAKGKAALLRELSDVVFNLN*
    Rv3914_TrxC         AKLDVDTNPETARNFQVVSIPILILFKDQGQFVKRIVGAKGKAALLRELSDVVFNLN*
    *****

C   BCP_I7_promoter__1   MKTIRLTPGDKAPAFITLPDADGNNVSLADYRGRRVIVYFYPAASTPGCTKQACDFRNL
    Rv2521_BCP         MKTIRLTPGDKAPAFITLPDADGNNVSLADYRGRRVIVYFYPAASTPGCTKQACDFRNL
    *****

    BCP_I7_promoter__1   GDFITAGLNVVGI SPDKPEKLATFRDAQGLTFPILLSDPDREVLTAWGAYGEKQMYGKTVQ
    Rv2521_BCP         GDFITAGLNVVGI SPDKPEKLATFRDAQGLTFPILLSDPDREVLTAWGAYGEKQMYGKTVQ
    *****

    BCP_I7_promoter__1   GVIRSTFVVDGKIVVAQYNVKATGHVAKLRRLDSV*
    Rv2521_BCP         GVIRSTFVVDGKIVVAQYNVKATGHVAKLRRLDSV*
    *****

```

**Figure 3.1.** Amino acid sequence alignments of the transcripts of the *Mtb* thioredoxin reductase (A), thioredoxin C (B) and BCP (C) genes housed in the pET28a expression plasmids reveal complete identity when compared to the transcripts of the *rv3913*, *rv3914* and *rv2521* genes from the Tuberculosis Database (TBDB) respectively.

Following sequence confirmation, *E. coli* BL21 cells transformed with the respective plasmids were induced with IPTG to express the proteins to determine whether they would successfully express under the conditions described, be degraded or stored in inclusion bodies (Thomas and Baney, 1996). Samples were taken hourly following IPTG induction to determine the optimal time points for expression for each of the three respective proteins using SDS-PAGE. *Mtb* thioredoxin reductase, thioredoxin C and BCP all ran at their expected sizes (35, 13 and 19 kDa respectively) indicating that the proteins were successfully expressed (Figure 3.2). The optimal induction time points for the expression of TR, TrxC and BCP were overnight (O/N), 5 hours and 6 hours respectively under the expression conditions described.

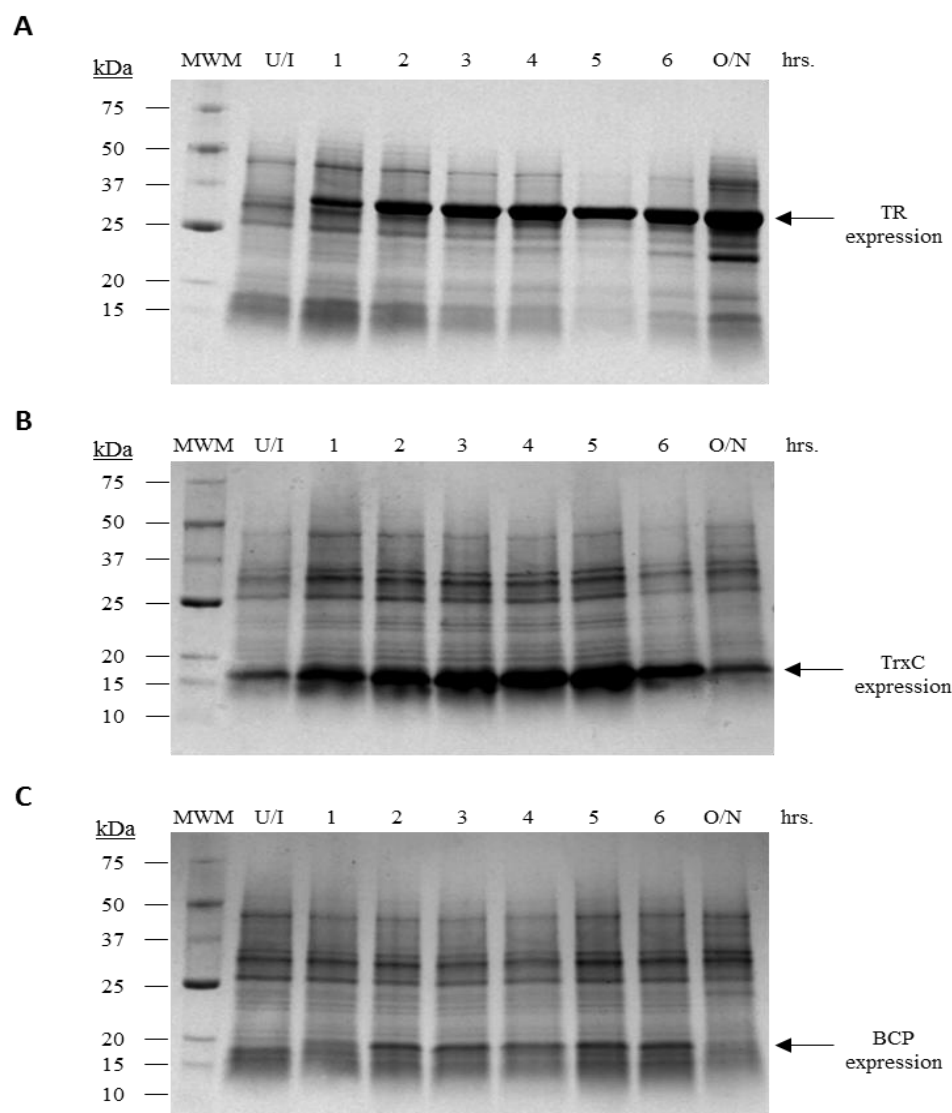


**Figure 3.2.** *E. coli* BL21 cells housing the three pET28a expression plasmids for the proteins thioredoxin reductase (A), thioredoxin C (B) and BCP (C) were induced with 0.5 mM IPTG under the control of the T7 promoter. Samples were taken every hour following induction (1-6 hrs. and an overnight sample, O/N) and run against an uninduced sample (U/I) and a BioRad precision plus unstained protein standard (MWM, 10-250 kDa range).

### 3.4.2 Successful purification of the thioredoxin reductase, thioredoxin C and BCP proteins using the Ni-NTA purification method and testing of their specific activities

To purify recombinant protein, transformed *E. coli* BL21 cells containing the expression plasmids were induced with IPTG (Section 3.3.4) and grown for the optimal times based on their respective expression profiles (Figure 3.2). The crude extracts were used in nickel affinity chromatography (Ni-NTA) purification and a modified wash step including 20% (v/v) glycerol (Section 3.3.5) allowed for purification of pure protein (Figure 3.3), indicating successful

purification of His-tagged recombinant protein from a crude extract starting sample. Glycerol (20% (v/v)) was added to prevent non-specific hydrophobic protein interactions which had resulted in co-purification of contaminating protein products (data not shown, Bornhorst and Falke, 2000). The sizes of protein products purified corresponded to the expected sizes for TR, TrxC and BCP respectively.

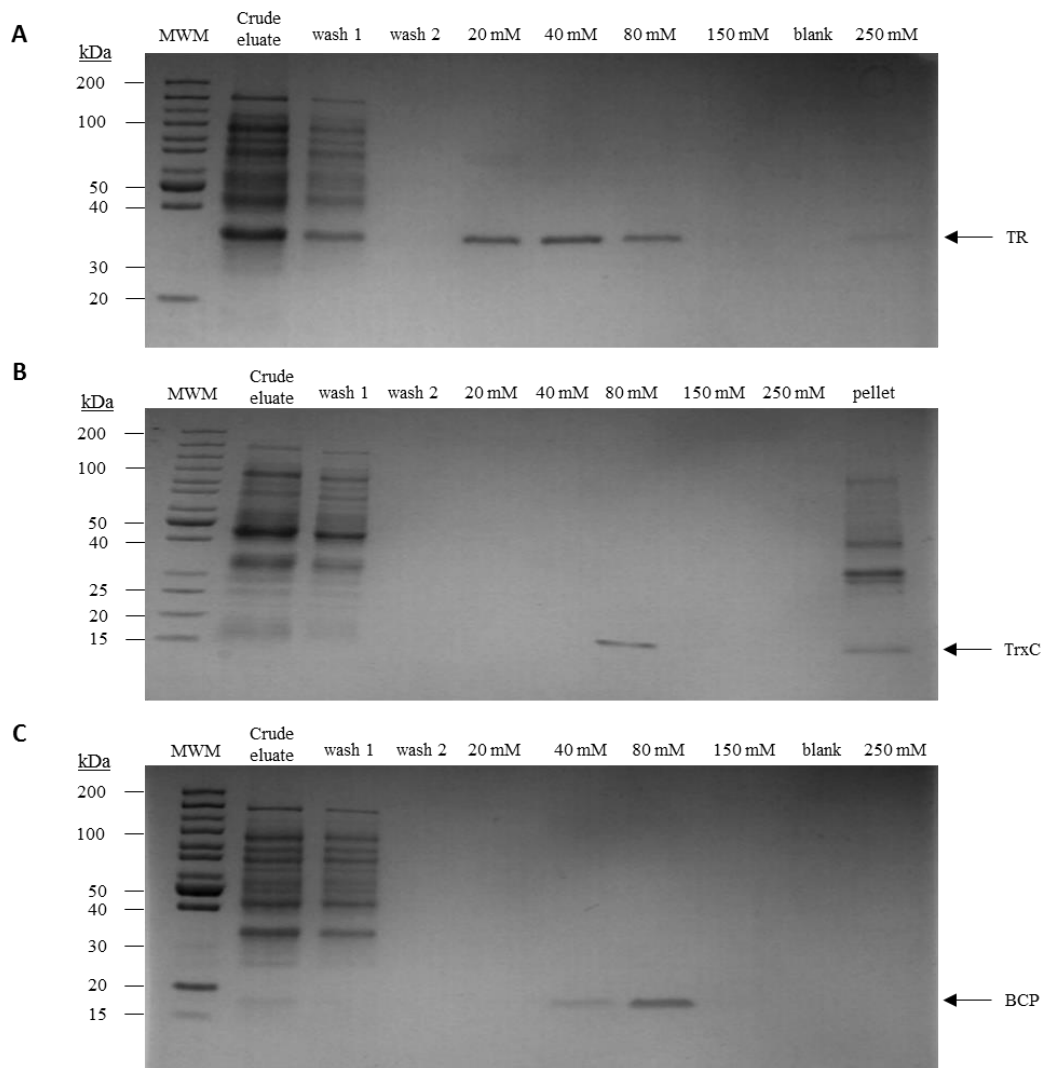


**Figure 3.3.** Nickel affinity chromatography (Ni-NTA) purification of the His-tagged thioredoxin reductase (A), thioredoxin C (B) and BCP (C) proteins to yield pure protein samples. Due to low expression of thioredoxin C, the cell debris pellet following sonication was run alongside pure protein (B) to determine if sonication was successfully releasing thioredoxin C. The samples were eluted over a range of imidazole concentrations (20-250 mM) and run against the PageRuler Unstained Protein ladder (MWM, 10-200 kDa range).

Problems were encountered when up-scaling the expression experiment for the recombinant protein TrxC as yields were considerably lower than that of the other two proteins.

It was assumed that insufficient sonication was performed and therefore the pellet was compared to the eluate (Figure 3.3 B) to determine if this was the case. Based on the gel image protein expression was much lower overall but when samples were pooled a sufficient amount of protein was obtained to carry out the insulin reduction assay (Section 3.3.6).

Once protein expression was optimized for the three proteins, specific activities of the Mtb thioredoxin reductase and thioredoxin C proteins were determined using the DTNB and insulin reduction assays respectively (Figure 3.4) across a number of time points (1-6 hours, overnight and pure protein samples). Pure protein was also tested to determine if the protein fractions purified by Ni-NTA chromatography maintained activity. The specific activities of the proteins corresponded to the SDS-PAGE data (Figure 3.2) and the pure proteins were active (Figure 3.4).

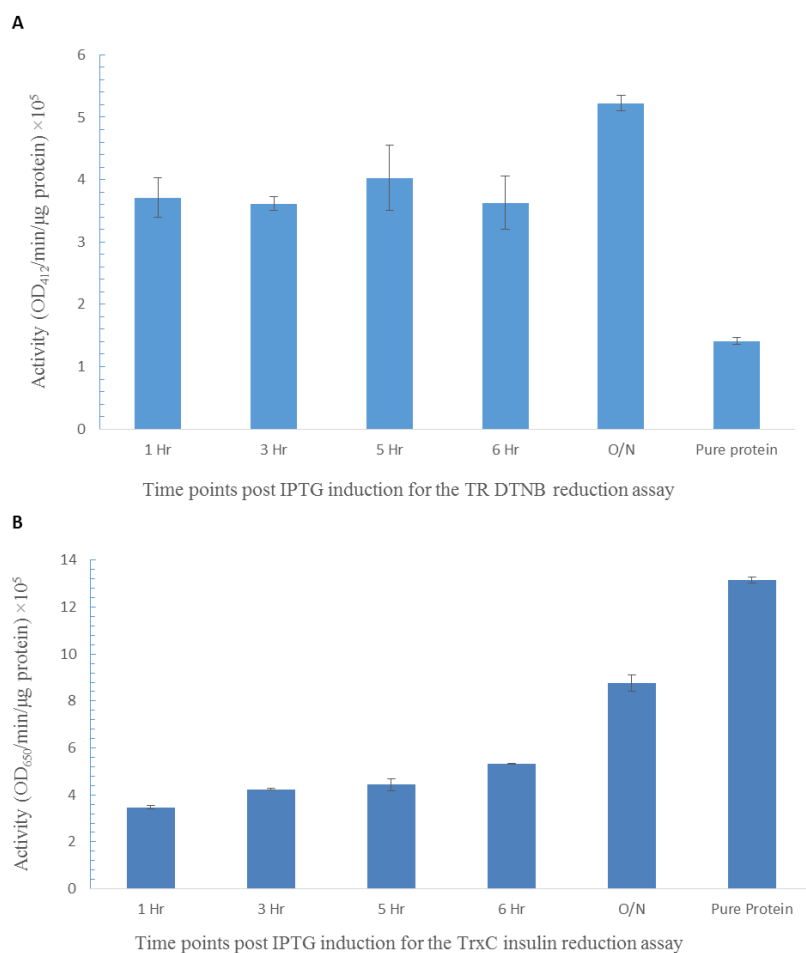


**Figure 3.4.** Specific activities of the thioredoxin reductase DTNB reduction assay (A) and thioredoxin C insulin reduction assay (B) of crude and pure protein fractions induced with 0.5 mM IPTG from one hour until a final overnight (O/N) sample was taken. Duplicate samples were used for each sample time-point and standard error bars are indicated.

### 3.5 Discussion

To study the *M. tuberculosis* thioredoxin reductase/thioredoxin C/BCP coupled system, NADPH oxidation can be monitored at 340 nm but pure protein samples were required. In this study three pET28a expression plasmids containing the genes for Mtb thioredoxin reductase, thioredoxin C and BCP respectively were acquired. Sequencing and alignment of translated amino acid sequences of the respective expression plasmids (Figure 3.1) revealed that the three genes were correctly synthesized and were under the control of the T7 promoter of the pET28a expression plasmid. The clones were IPTG induced (Figure 3.2) and Ni-NTA chromatography purification resulted in successful purification of the proteins in this study (Figure 3.3).

To test if the pure proteins samples could be used for future kinetic work, specific activity assays were used that were previously developed and optimized in our lab for the thioredoxin reductase and thioredoxin proteins. The thioredoxin assay based on the DTT-dependent reduction of insulin (Holmgren, 1979) was chosen. The assay involved pre-incubating thioredoxin C containing crude extract with DTT prior to the test reaction, which shortened the overall reaction time and removed the need for pure thioredoxin reductase protein when compared to previous assays (Padayachee and Pillay, 2016). The thioredoxin reductase specific activity assay involved the reduction of DTNB and directly monitoring absorbance at 412 nm (Arnér and Holmgren, 2000a) as opposed to the use of the thioredoxin protein, the natural substrate of thioredoxin reductase. Divalent cations were also included in the reaction (0.5 M NaCl) as they were found to greatly increase the sensitivity of the DTNB reduction assay by altering the thioredoxin reductase conformation resulting in an exposed active site which could readily react with DTNB (Lim and Lim, 1995).

The specific activity assays described above were used in conjunction with the expression profile (Figure 3.2 and 3.4 respectively) to determine the optimal time points for expression. It was concluded that overnight expression for thioredoxin reductase and 6 hours of expression for thioredoxin C yielded the highest specific activities. The hydrogen peroxide reduction activity of the BCP protein could also be measured using the horseradish peroxidase (HRP) competition assay (Nelson and Parsonage, 2011; Toledo et al., 2011). The assay takes advantage of the high reaction rate of HRP with hydrogen peroxide and its oxidation to compound I can be directly measured at an absorbance of 403 nm. The competition between the HRP and peroxiredoxin for hydrogen peroxide can therefore give an accurate second-order rate constant for the peroxiredoxins' reaction with hydrogen peroxide (Toledo et al., 2011).

However, due to time constraints, this assay was not carried out but future studies will involve using the HRP competition assay to determine the reactivity of BCP with hydrogen peroxide followed by an analysis of the entire bi-fan motif. The purified system will therefore serve as a comprehensive and experimentally tractable *in vitro* tool for studying the hydrogen peroxide reduction of the bi-fan motif within the redox defence network of *M. tuberculosis*.

## Chapter 4: General discussion

*M. tuberculosis* (Mtb), the causative agent of tuberculosis (TB), is a significant health concern claiming millions of lives per annum and with the rise in drug resistant strains, treatment regimens have become that much more complex. Able to evade the host immune system, *M. tuberculosis* can remain dormant and reactivate even after decades within the host. The strong defence exhibited by the *M. tuberculosis* bacterium along with the inability to curb infection using established treatment options has warranted the exploration of new avenues in search of alternative TB vaccines, drug therapies and intracellular druggable targets. Systems biology is one such avenue which takes into account the interacting nature of cellular components and the subsequent consequences of these interactions. Research presented in this dissertation was centered on using systems biology approaches to potentially elucidate new inhibitory targets within the redox defence network of *M. tuberculosis* by using mathematical and computational modeling techniques and *in vitro* analyses. A further aim was to create a broad yet comprehensive understanding of the interactions between the redox defence proteins partially responsible for the viability of *M. tuberculosis* in the host for decades despite the constant bactericidal microenvironment it inhabits during the course of infection.

The complete detailed reconstruction of the Mtb redox defence network has not, to our knowledge, been previously presented in literature and this step allowed the development of wire diagrams that mapped out the interactions of the hydrogen peroxide reduction network. Using the canonical *E. coli* and *S. cerevisiae* redox defence networks as comparison, the hydrogen peroxide reduction network of *M. tuberculosis* was analyzed using motif detection programs to detect both common and unique motifs. A unique bi-fan motif was uncovered within the *M. tuberculosis* redox defence network and the properties of this motif design were further explored using mathematical as well as core computational modeling to simulate steady-state behavior of the bi-fan motif.

Both the analytical solutions and core computational modeling showed that the reductive redundancy found within the bi-fan system makes it particularly robust to changes in either thioredoxin concentration with the rates of hydrogen peroxide reduction mediated by Tpx and BCP being unaffected when either thioredoxin concentration was varied. Computational modeling of the bi-fan system further showed that the bi-fan motif design required a higher hydrogen peroxide concentration, when compared to a control bi-parallel motif, to saturate the

Tpx and BCP redox cycles. Considering the granuloma microenvironment in which *M. tuberculosis* resides over the course of infection, the presence of the bi-fan motif embedded in the redox defence network could be important for the cells' survival by allowing their hydrogen peroxide reductive capacity to remain robust to changes in thioredoxin demand throughout the cell and to tolerate higher oxidative stress. Analysis of the bi-fan and bi-parallel systems in a biologically realistic environment where the thioredoxin B and C concentrations are expected to fluctuate in the cell based on the varying thioredoxin demand, showed that the bi-fan motif displayed greater robustness with regard to the availability of thioredoxin when compared to the bi-parallel motif. Intriguingly, thioredoxin reductase is crucial for maintaining the thioredoxin redox poise in this motif and its inhibition via auranofin dramatically affects cell viability (Harbut et al., 2015). The thioredoxin reductase inhibition study exemplifies the possible importance of the bi-fan motif within the *M. tuberculosis* redox defence network and its role in *M. tuberculosis*' persistence once within the host. The description of this motif is the first such analysis regarding the complete hydrogen peroxide reduction network of *M. tuberculosis*. Moreover, this method could also be applied to other pathogenic bacteria and help in future characterization studies of various cellular networks. Due to a lack of kinetic information regarding the proteins comprising the bi-fan motif, the components were consequently selected for *in vitro* kinetic analysis.

The genes for thioredoxin reductase (*rv3913*), thioredoxin C (*rv3914*) and BCP (*rv2521*) were synthesized on pET28a expression plasmids under the control of the T7 promoter. Expression of the genes were IPTG-induced and crude samples containing the three respective proteins were Ni-NTA purified to obtain pure protein samples. The thioredoxin reductase and thioredoxin C proteins were then assayed using DTNB and insulin reduction assays respectively to determine their specific activities. The activity of BCP was going to be tested using a HRP competition assay to determine its second-order rate constant with regard to hydrogen peroxide reduction, but due to time constraints, this was not carried out. The *in vitro* characterization of the system will be tested in future studies.

Overall, novel insights into the *M. tuberculosis* redox defence network were obtained through a combination of systems biology techniques. This work serves as a good starting point for further adoption of such approaches in the study of cellular network structures of pathogens to clearly understand the interactions between proteins tasked with specific roles within their cellular redox networks.

## Reference List

- Akif, M., Khare, G., Tyagi, A. K., Mande, S. C. and Sardesai, A. A. (2008). 'Functional studies of multiple thioredoxins from *Mycobacterium tuberculosis*.', *Journal of Bacteriology*, 190(21), pp. 7087–7095.
- Antelmann, H. and Hamilton, C. J. (2012). 'Bacterial mechanisms of reversible protein S-thiolation: Structural and mechanistic insights into mycoredoxins.', *Molecular Microbiology*, 86(4), pp. 759–764.
- Arenas, F. A., Diaz, W. A., Leal, C. A., Perez-Donoso, J. M., Imlay, J. A. and Vasquez, C. C. (2011). 'The *Escherichia coli* *btuE* gene, encodes a glutathione peroxidase that is induced under oxidative stress conditions.', *Biochemical and Biophysical Research Communications*, 1(2), pp. 93–106.
- Arnér, E. S. J. and Holmgren, A. (2000a). 'Measurement of Thioredoxin and Thioredoxin Reductase.', *Current Protocols in Toxicology*.
- Arnér, E. S. J. and Holmgren, A. (2000b). 'Physiological functions of thioredoxin and thioredoxin reductase.', *European Journal of Biochemistry*, 267(20), pp. 6102–6109.
- Asif, M. (2013). 'Rifampin and Their Analogs: A Development of Antitubercular Drugs.', *World Journal of Organic Chemistry*, 1(2), pp. 14–19.
- Attarian, R., Bennie, C., Bach, H. and Av-Gay, Y. (2009). 'Glutathione disulfide and S-nitrosoglutathione detoxification by *Mycobacterium tuberculosis* thioredoxin system.', *Federation of European Biochemical Societies Letters*, 583(19), pp. 3215–3220.
- Barabási, A. and Oltvai, Z. N. (2004). 'Network Biology: Understanding the cell's functional organization.', *Nature Reviews*, 5, pp. 101–113.
- Barnes, M. R. (2007). *Bioinformatics for Geneticists: A bioinformatics primer for the analysis of genetic data, Second Edition*.
- Biteau, B., Labarre, J. and Toledano, M. B. (2003). 'ATP-dependent reduction of cysteine-sulphinic acid by *S. cerevisiae* sulphiredoxin.', *Nature*, 425(6961), pp. 980–984.
- Blazeck, J. and Alper, H. (2011). 'Systems metabolic engineering: Genome-scale models and beyond.', *Biotechnology Journal*, 5(7), pp. 647–659.
- Bornemann, C., Jardine, M. A., Spies, H. S. C. and Steenkamp, D. J. (1997).

‘Biosynthesis of mycothiol: elucidation of the sequence of steps in *Mycobacterium smegmatis*.’, *Biochemical Journal*, 325, pp. 623–629.

Bornhorst, J. A. and Falke, J. J. (2000). ‘Purification of proteins using polyhistidine affinity tags.’, *Methods in Enzymology*, 326, pp. 245–254.

Botello-Morte, I. and Fillat, M. F. (2014). ‘Thiol-based redox regulators in prokaryotes : The relevance of the CXXC motifs.’, *OA Biochemistry*, 2(18), pp. 1–8.

Bradford, M. M. (1976). ‘A Rapid and Sensitive Method for the Quantitation of Microgram Quantities of Protein Utilizing the Principle of Protein-Dye Binding.’, *Analytical Biochemistry*, 72, pp. 248–254.

Brandes, N., Rinck, A., Leichert, L. I. and Jakob, U. (2007). ‘Nitrosative stress treatment of *E. coli* targets distinct set of thiol-containing proteins.’, *Molecular Microbiology*, 66(4), pp. 901–914.

Brazhnik, P., De La Fuente, A. and Mendes, P. (2002). ‘Gene networks: How to put the function in genomics.’, *Trends in Biotechnology*, 20(11), pp. 467–472.

Bruggeman, F. J. and Westerhoff, H. (2007). ‘The nature of systems biology.’, *Trends in Microbiology*, 15(1), pp. 45–50.

Campos, P. E., Suarez, P. G., Sanchez, J., Zavala, D., Arevalo, J., Ticona, E., Nolan, C. M., Hooton, T. M. and Holmes, K. K. (2003). ‘Multidrug-resistant *Mycobacterium tuberculosis* in HIV-Infected Persons, Peru.’, *Emerging Infectious Diseases*, 9(12), pp. 1571–1578.

Chouchane, S., Lippai, I. and Magliozzo, R. S. (2000). ‘Catalase-peroxidase (*Mycobacterium tuberculosis* KatG) catalysis and isoniazid activation.’, *Biochemistry*, 39, pp. 9975–9983.

Chung, H. S., Wang, S. B., Venkatraman, V., Murray, C. I. and Van Eyk, J. E. (2013). ‘Cysteine oxidative posttranslational modifications: Emerging regulation in the cardiovascular system.’, *Circulation Research*, 112(2), pp. 382–392.

Clarke, D. J., Ortega, X. P., Mackay, C. L., Valvano, M. A., Govan, J. R. W., Campopiano, D. J., Langridge-Smith, P. and Brown, A. R. (2010). ‘Subdivision of the bacterioferritin comigratory protein family of bacterial peroxiredoxins based on catalytic activity.’, *Biochemistry*, 49, pp. 1319–1330.

Collet, J. F. and Messens, J. (2010). 'Structure, function, and mechanism of thioredoxin proteins.', *Antioxidants & Redox Signaling*, 13(8), pp. 1205–1216.

Comtois, S. L., Gidley, M. D. and Kelly, D. J. (2003). 'Role of the thioredoxin system and the thiol-peroxidases Tpx and Bcp in mediating resistance to oxidative and nitrosative stress in *Helicobacter pylori*.' , *Microbiology*, 149, pp. 121–129.

Cumming, B. M., Lamprecht, D. A., Wells, R. M., Saini, V., Mazorodze, J. H. and Steyn, A. J. C. (2014) 'The Physiology and Genetics of Oxidative Stress in Mycobacteria.' , *Microbiology Spectrum*, 2(3), pp. 1–22.

D'Ambrosio, K., Limauro, D., Pedone, E., Galdi, I., Pedone, C., Bartolucci, S. and De Simone, G. (2009). 'Insights into the catalytic mechanism of the Bcp family: Functional and structural analysis of Bcp1 from *Sulfolobus solfataricus*.' , *Proteins: Structure, Function and Bioinformatics*, 76(4), pp. 995–1006.

Dagert, M. and Ehrlich, S. (1979). 'Prolonged incubation in calcium chloride improves the competence of *Escherichia coli* cells.' , *Genetics*, 6, pp. 23–28.

Dobrin, R., Beg, Q. K., Barabási, A. L. and Oltvai, Z. N. (2004). 'Aggregation of topological motifs in the *Escherichia coli* transcriptional regulatory network.' , *BMC Bioinformatics*, 5(1), pp. 1–10.

Ducati, R. G., Ruffino-Netto, A., Basso, L. A. and Santos, D. S. (2006). 'The resumption of consumption - A review on tuberculosis.' , *Memorias do Instituto Oswaldo Cruz*, 101, pp. 697–714.

Fattorini, L., Migliori, G. B. and Cassone, A. (2007). 'Extensively drug-resistant (XDR) tuberculosis: An old and new threat.' , *Annali dell'Istituto Superiore di Sanita*, 43, pp. 317–319.

Forrellad, M. a, Klepp, L. I., Gioffré, A., Sabio, Y., García, J., Morbidoni, H. R., de la Paz Santangelo, M., Cataldi, A. A. and Bigi, F. (2013). 'Virulence factors of the *Mycobacterium tuberculosis* complex.' , *Virulence*, 4(1), pp. 3–66.

Gallogly, M. M. and Mieyal, J. J. (2007). 'Mechanisms of reversible protein glutathionylation in redox signaling and oxidative stress.' , *Current Opinion in Pharmacology*, 7(4), pp. 381–391.

Ghiladi, R. A., Medzihradzky, K. F., Rusnak, F. M. and Ortiz De Montellano, P. R. (2005). 'Correlation between isoniazid resistance and superoxide reactivity in *Mycobacterium*

tuberculosis KatG.’, *Journal of the American Chemical Society*, 127(3), pp. 13428–13442.

Gladyshev, V. N. (2002). ‘Thioredoxin and peptide methionine sulfoxide reductase: convergence of similar structure and function in distinct structural folds.’, *Proteins: Structure, Function and Genetics*, (46), pp. 149–152.

Gleason, F. K. and Holmgren, A. (1988). ‘Thioredoxin and related proteins in procaryotes.’, *Federation of European Microbiological Societies Microbiology Letters*, 54(4), pp. 271–297.

Gomes, M., Correia, A., Mendonça, D. and Duarte, R. (2014). ‘Risk factors for drug-resistant tuberculosis.’, *Journal of Tuberculosis Research*, 2, pp. 111–118.

Gori, A., Bandera, A., Marchetti, G., Esposti, A. D., Catozzi, L., Nardi, G. P., Gazzola, L., Ferrario, G., Van Embden, J. D. A., Van Soolingen, D., Moroni, M. and Franzetti, F. (2005). ‘Spoligotyping and Mycobacterium tuberculosis.’, *Emerging Infectious Diseases*, 11(8), pp. 1242–1248.

Grange, J. M. and Zumla, A. I. (2008). ‘Tuberculosis.’, in *Bacterial Infections, Section 8, Chapter 56*, pp. 1–57. doi: 10.1016/B978-0-443-06691-7.50061-3.

Graves, P. R. and Haystead, T. A. J. (2002). ‘Molecular biologist’s guide to proteomics.’, *Microbiology and Molecular Biology Reviews*, 66(1), pp. 39–63.

Greetham, D. and Grant, C. M. (2009). ‘Antioxidant activity of the yeast mitochondrial one-Cys peroxiredoxin is dependent on thioredoxin reductase and glutathione in vivo.’, *Molecular and Cellular Biology*, 29(11), pp. 3229–3240.

Guimarães, B. G., Souchon, H., Honoré, N., Saint-Joanis, B., Brosch, R., Shepard, W., Cole, S. T. and Alzari, P. M. (2005). ‘Structure and mechanism of the alkyl hydroperoxidase AhpC, a key element of the Mycobacterium tuberculosis defense system against Oxidative Stress.’, *Journal of Biological Chemistry*, 280(27), pp. 25735–25742.

Gupta, V. and Carroll, K. S. (2014). ‘Sulfenic acid chemistry, detection and cellular lifetime.’, *Biochimica et Biophysica Acta*, 1840, pp. 847–875.

Hall, T. A. (1999). ‘BioEdit: a user-friendly biological sequence alignment editor and analysis program for Windows 95/98/NT.’, *Nucleic Acids Symposium Series*, 41, pp. 95–98.

Harbut, M. B., Vilchèze, C., Luo, X., Hensler, M. E., Guo, H., Yang, B., Chatterjee, A.

K., Nizet, V., Jacobs, W. R., Schultz, P. G. and Wang, F. (2015). 'Auranofin exerts broad-spectrum bactericidal activities by targeting thiol-redox homeostasis.', *Proceedings of the National Academy of Sciences*, 112(14), pp. 4453–4458.

Hatzios, S. K. and Bertozzi, C. R. (2011). 'The regulation of sulfur metabolism in mycobacterium tuberculosis.', *PLoS Pathogens*, 7(7), pp. e1002036.

Hemnani, T., and Parihar, M. S. (1998). 'Reactive oxygen species and oxidative DNA damage.', *Indian Journal of Physiology and Pharmacology*, 42(4), pp. 440–452.

Herrero, E., Ros, J., Bellí, G. and Cabiscol, E. (2008). 'Redox control and oxidative stress in yeast cells.', *Biochimica et biophysica acta*, 1780(11), pp. 1217–1235.

Hillas, P. J., Soto Del Alba, F., Oyarzabal, J., Wilks, A. and Ortiz De Montellano, P. R. (2000). 'The AhpC and AhpD antioxidant defense system of Mycobacterium tuberculosis.', *Journal of Biological Chemistry*, 275(25), pp. 18801–18809.

Holmgren, A. (1977). 'Bovine Thioredoxin System: purification of thioredoxin reductase from calf liver and thymus and studies of its function in disulfide reduction.', *The Journal of Biological Chemistry*, 252(13), pp. 4600–4606.

Holmgren, A. (1979). 'Thioredoxin catalyzes the reduction of insulin disulfides by dithiothreitol and dihydrolipoamide.', *The Journal of Biological Chemistry*, 254(19), pp. 9627–9632.

Holmgren, A. (1995). 'Thioredoxin structure and mechanism: conformational changes on oxidation of the active-site sulfhydryls to a disulfide.', *Structure*, 3(3), pp. 239–243.

Hugo, M., Van Laer, K., Reyes, A. M., Vertommen, D., Messens, J., Radi, R. and Trujillo, M. (2014). 'Mycothioli/mycoredoxin 1-dependent reduction of the peroxiredoxin AhpE from mycobacterium tuberculosis', *Journal of Biological Chemistry*, 289, pp. 5228–5239.

Hugo, M., Radi, R. and Trujillo, M. (2012). 'Thiol-Dependent peroxidases in Mycobacterium tuberculosis antioxidant defense.', in *Understanding Tuberculosis- Deciphering the Secret Life of the Bacilli*, pp. 334.

Huh, A. J. and Kwon, Y. J. (2011). "Nanoantibiotics": A new paradigm for treating infectious diseases using nanomaterials in the antibiotics resistant era.', *Journal of Controlled Release*, 156(2), pp. 128–145.

Huppert, L. A., Ramsdell, T. L., Chase, M. R., Sarracino, D. A., Fortune, S. M. and Burton, B. M. (2014). 'The ESX system in *Bacillus subtilis* mediates protein secretion.', *PLoS One*, 9(5), pp. e96267.

Inoue, Y., Matsuda, T., Sugiyama, K., Izawa, S. and Kimura, A. (1999). 'Genetic analysis of glutathione peroxidase in oxidative stress response of *Saccharomyces cerevisiae*.', *The Journal of Biological Chemistry*, 274(38), pp. 27002–27009.

Jaafar, M. M., Halim, M. Z. A., Ismail, M. I., Shien, L. L., Kek, T. L., Fong, N. Y., Nor, N. M., Zainuddin, Z. F., Hock, T. T., Najimudin, M. N. M. and Salleh, M. Z. (2016). 'Genome sequencing and annotation of *Mycobacterium tuberculosis* PR08 strain', *Genomics Data*, 7, pp. 119–120.

Jaeger, T., Budde, H., Flohé, L., Menge, U., Singh, M., Trujillo, M. and Radi, R. (2004). 'Multiple thioredoxin-mediated routes to detoxify hydroperoxides in *Mycobacterium tuberculosis*.', *Archives of Biochemistry and Biophysics*, 423(1), pp. 182–191.

Jaeger, T. and Flohé, L. (2006). 'The thiol-based redox networks of pathogens: unexploited targets in the search for new drugs.', *BioFactors*, 27, pp. 109–120.

Jamieson, D. J. (1998). 'Oxidative stress responses of the yeast *Saccharomyces cerevisiae*.', *Yeast*, 14(16), pp. 1511–1527.

Jeong, W., Cha, M. and Kim, I. (2000). 'Thioredoxin-dependent hydroperoxide peroxidase activity of Bacterioferritin Comigratory Protein (BCP) as a new member of the Thiol-specific Antioxidant Protein (TSA)/Alkyl Hydroperoxide Peroxidase C (AhpC) family.', *The Journal of Biological Chemistry*, 275(4), pp. 2924–2930.

Jothivasan, V. K. and Hamilton, C. J. (2008). 'Mycothiols: synthesis, biosynthesis and biological functions of the major low molecular weight thiol in actinomycetes.', *Natural Product Reports*, 25, pp. 1091–1117.

Karakousis, P. C., Bishai, W. R. and Dorman, S. E. (2004). 'Mycobacterium tuberculosis cell envelope lipids and the host immune response.', *Cellular Microbiology*, 6(2), pp. 105–116.

Kashmiri, Z. N. and Mankar, S. A. (2014). 'Free radicals and oxidative stress in bacteria.', *International Journal of Current Microbiology and Applied Sciences*, 3(9), pp. 34–40.

Kinnings, S. L., Xie, L., Fung, K. H., Jackson, R. M., Xie, L. and Bourne, P. E. (2010).

‘The Mycobacterium tuberculosis drugome and its polypharmacological implications.’, *PLoS Computational Biology*, 6(11), pp. e1000976.

Klomsiri, C., Karplus, P. A. and Poole, L. B. (2011). ‘Cysteine-based redox switches in enzymes.’, *Antioxidants & Redox Signaling*, 14(6), pp. 1065–1077.

Konagurthu, A. S. and Lesk, A. M. (2008). ‘On the origin of distribution patterns of motifs in biological networks.’, *BMC Systems Biology*, 2(73), pp. 1–8.

Korbel, D. S., Schneider, B. E. and Schaible, U. E. (2008). ‘Innate immunity in tuberculosis: myths and truth.’, *Microbes and Infection*, 10(9), pp. 995–1004.

Kumar, A., Farhana, A., Guidry, L., Saini, V., Hondalus, M. and Steyn, A. J. C. (2011). ‘Redox homeostasis in mycobacteria: the key to tuberculosis control?’, *Expert Reviews in Molecular Medicine*, 13, pp. 1–25.

Kwon, T., Han, S. J., Yoo, W. G., Yun, M. R., Lee, S., Lee, J. S. and Kim, D. W. (2016). ‘Draft genome sequence of Mycobacterium tuberculosis KT-0133, isolated in South Korea.’, *Genome Announcements*, 4(1), pp. 3–4.

Lee, J., Spector, D., Godon, C., Labarre, J. and Toledano, M. B. (1999). ‘A new antioxidant with alkyl hydroperoxide defense properties in yeast.’, *Journal of Biological Chemistry*, 274(8), pp. 4537–4544.

Lim, H. W. and Lim, C. J. (1995). ‘Direct reduction of DTNB by E.coli thioredoxin reductase’, *Journal of Biochemistry and Molecular Biology*, pp. 17–20.

Lin, K., Kuang, Y., Joseph, J. S. and Kolatkar, P. R. (2002). ‘Conserved codon composition of ribosomal protein coding genes in Escherichia coli, Mycobacterium tuberculosis and Saccharomyces cerevisiae: lessons from supervised machine learning in functional genomics.’, *Nucleic Acids Research*, 30(11), pp. 2599–2607.

Lin, K., O’Brien, K. M., Trujillo, C., Wang, R., Wallach, J. B., Schnappinger, D. and Ehrt, S. (2016). ‘Mycobacterium tuberculosis thioredoxin reductase is essential for thiol redox homeostasis but plays a minor role in antioxidant defense.’, *PLOS Pathogens*, 12(6), pp. e1005675.

Loi, V. V., Rossius, M. and Antelmann, H. (2015). ‘Redox regulation by reversible protein S-thiolation in bacteria.’, *Frontiers in Microbiology*, 6(187), pp. 1–22.

Louie, A. Y. and Meade, T. J. (1999). 'Metal complexes as enzyme inhibitors.', *Chemical Reviews*, 99(9), pp. 2711–2734.

Lu, J. and Holmgren, A. (2014). 'The thioredoxin antioxidant system.', *Free Radical Biology & Medicine*, 66, pp. 75–87.

Marzano, C., Gandin, V., Folda, A., Scutari, G., Bindoli, A. and Pia, M. (2007). 'Inhibition of thioredoxin reductase by auranofin induces apoptosis in cisplatin-resistant human ovarian cancer cells.', *Free Radical Biology & Medicine*, 42, pp. 872–881.

Materi, W. and Wishart, D. S. (2007). 'Computational systems biology in drug discovery and development: methods and applications.', *Drug Discovery Today*, 12(7), pp. 295–303.

Mehaffy, M. C., Kruh-Garcia, N. A. and Dobos, K. M. (2012). 'Prospective on Mycobacterium tuberculosis proteomics.', *Journal of Proteome Research*, 11(1), pp. 17–25.

Mendoza, E. R. (2009). 'Systems Biology: Its Past, Present and Potential.', *Philippine Science Letters*, 2(1), pp. 16–34.

Milo, R., Shen-Orr, S., Itzkovits, S., Kashtan, N., Chklovskii, D. and Alon, U. (2002). 'Network motifs: simple building blocks of complex networks.', *Science*, 298(5594), pp. 824–827.

Miseta, A. and Csutora, P. (2000). 'Relationship between the occurrence of cysteine in proteins and the complexity of organisms.', *Molecular Biology and Evolution*, 17(8), pp. 1232–1239.

Nausser, T., Koppenol, W. H. and Schöneich, C. (2015). 'Protein thiyl radical reactions and product formation: A kinetic simulation.', *Free Radical Biology & Medicine*, 80, pp. 158–163.

Nelson, K. J. and Parsonage, D. (2011). 'Measurement of peroxiredoxin activity.', *Current Protocol Toxicology*, 7(7), pp. 1–33.

Netto, L. E. S. and Antunes, F. (2016). 'The roles of peroxiredoxin and thioredoxin in hydrogen peroxide sensing and in signal transduction.', *Molecules and Cells*, 39(1), pp. 65–71.

Newton, G. L., Buchmeier, N. and Fahey, R. C. (2008). 'Biosynthesis and functions of mycothiol, the unique protective thiol of Actinobacteria.', *Microbiology and Molecular Biology reviews*, 72(3), pp. 471–494.

Newton, G. L. and Fahey, R. C. (2002). 'Mycothioliol biochemistry.', *Archives of Microbiology*, 178, pp. 388–394.

Newton, G. L., Ta, P., Bzymek, K. P. and Fahey, R. C. (2006). 'Biochemistry of the initial steps of mycothiol biosynthesis.', *Journal of Biological Chemistry*, 281, pp. 33910–33920.

Ohno, H., Zhu, G., Mohan, V. P., Chu, D., Kohno, S., Jacobs, W. R. and Chan, J. (2003). 'The effects of reactive nitrogen intermediates on gene expression in *Mycobacterium tuberculosis*.' , *Cellular Microbiology*, 5, pp. 637–648.

Olivier, B. G., Rohwer, J. M. and Hofmeyr, J. H. S. (2005). 'Modelling cellular systems with PySCeS.' , *Bioinformatics*, 21(4), pp. 560–561.

Olson, A. L., Neumann, T. S., Cai, S. and Sem, D. S. (2013). 'Solution structures of *Mycobacterium tuberculosis* thioredoxin C and models of the intact thioredoxin system suggest new approaches to inhibitor and drug design.' , *National Institutes of Health*, 81(4), pp. 675–689.

Padayachee, L. and Pillay, C. S. (2016). 'The thioredoxin system and not the Michaelis-Menten equation should be fitted to substrate saturation datasets from the thioredoxin insulin assay.' , *Redox report: Communications in Free Radical Research*, 2.

Pagel, M. and Pomiankowski, A. (2002). 'Genomics and Tuberculosis.' , *Indian Journal of Chest Disease and Allied Sciences*, 44, pp. 221–223.

Parrini, C., Taddei, N., Ramazzotti, M., Degl'Innocenti, D., Ramponi, G., Dobson, C. M. and Chiti, F. (2005). 'Glycine residues appear to be evolutionarily conserved for their ability to inhibit aggregation.' , *Structure*, 13(8), pp. 1143–1151.

Perkins, A., Nelson, K. J., Parsonage, D., Poole, L. B. and Karplus, P. A. (2015). 'Peroxiredoxins: guardians against oxidative stress and modulators of peroxide signaling.' , *Trends in Biochemical Sciences*, 40(8), pp. 435–445.

Pieters, J. (2008). 'Mycobacterium tuberculosis and the macrophage: maintaining a balance' , *Cell Host and Microbe*, 3, pp. 399–407.

Pillay, C. S., Hofmeyr, J. H. S., Olivier, B. G., Snoep, J. L. and Rohwer, J. M. (2009). 'Enzymes or redox couples? The kinetics of thioredoxin and glutaredoxin reactions in a systems biology context.' , *The Biochemical Journal*, 417(1), pp. 269–275.

Pillay, C. S., Hofmeyr, J. H. S. and Rohwer, J. M. (2011). 'The logic of kinetic regulation in the thioredoxin system.', *BMC Systems Biology*, 5(15).

Poole, L. B. (2015). 'The basics of thiols and cysteines in redox biology and chemistry.', *Free Radical Biology & Medicine*, 80, pp. 148–157.

Powis, G., Mustacich, D. and Coon, A. (2000). 'The role of the redox protein thioredoxin in cell growth and cancer.', *Free Radical Biology & Medicine*, 29(3–4), pp. 312–322.

Rajashankar, K. R., Bryk, R., Kniewel, R., Buglino, J. A., Nathan, C. F. and Lima, C. D. (2005). 'Crystal structure and functional analysis of lipoamide dehydrogenase from *Mycobacterium tuberculosis*.' *The Journal of Biological Chemistry*, 280(40), pp. 33977–33983.

Rao, P. K. and Li, Q. (2009). 'Protein turnover in mycobacterial proteomics.', *Molecules*, 14, pp. 3237–3258.

Rasche, F. and Wernicke, S. (2006). 'Fast Network Motif Detection–Manual.', *Bioinformatics*, 22(9).

Rawat, M. and Av-Gay, Y. (2007). 'Mycothiols-dependent proteins in actinomycetes.', *Federation of European Microbiological Societies Reviews*, 31(3), pp. 278–292.

Reyes, A. M., Vazquez, D. S., Zeida, A., Hugo, M., Piñeyro, M. D., De Armas, M. I., Estrin, D., Radi, R., Santos, J. and Trujillo, M. (2016). 'PrxQ B from *Mycobacterium tuberculosis* is a monomeric, thioredoxin-dependent and highly efficient fatty acid hydroperoxide reductase.', *Free Radical Biology & Medicine*, 101, pp. 249–260.

Rohwer, J. M., Viljoen, C., Christensen, C. D. and Mashamaite, L. N. (2016). 'Using kinetic modelling to reveal the nature of the ultrasensitive response in cellular redoxin networks.', *Perspectives in Science*.

Rustad, T. R., Harrell, M. I., Liao, R. and Sherman, D. R. (2008). 'The enduring hypoxic response of *Mycobacterium tuberculosis*.' *PloS One*, 3(1), pp. e1502.

Santos, F., Boele, J. and Teusink, B. (2011). *A practical guide to genome-scale metabolic models and their analysis*. 1st edn, *Methods in Enzymology*. 1st edn. Elsevier Inc. doi: 10.1016/B978-0-12-385118-5.00024-4.

Schreiber, F. and Schwöbbermeyer, H. (2005). 'MAVisto: A tool for the exploration of

network motifs.’, *Bioinformatics*, 21(17), pp. 3572–3574.

Schubert, O. T., Ludwig, C., Kogadeeva, M., Zimmermann, M., Rosenberger, G., Gengenbacher, M., Gillet, L. C., Collins, B. C., Röst, H. L., Kaufmann, S. H. E., Sauer, U. and Aebbersold, R. (2015). ‘Absolute proteome composition and dynamics during dormancy and resuscitation of *Mycobacterium tuberculosis*.’, *Cell Host & Microbe*, pp. 1–13.

Sharma, M., Bose, M., Abhimanyu, Sharma, L., Diwakar, A., Kumar, S., Gaur, S. N. and Banavalikar, J. N. (2012). ‘Intracellular survival of *Mycobacterium tuberculosis* in macrophages is modulated by phenotype of the pathogen and immune status of the host.’, *International Journal of Mycobacteriology*, 1(2), pp. 65–74.

Sivashanmugam, A., Murray, V., Cui, C., Zhang, Y., Wang, J. and Li, Q. (2009). ‘Practical protocols for production of very high yields of recombinant proteins using *Escherichia coli*.’, *Protein Science*, 18(5), pp. 936–948.

Smith, I. (2003). ‘*Mycobacterium tuberculosis* pathogenesis and molecular determinants of virulence.’, *Clinical Microbiology Reviews*, 16(3), pp. 463–496.

Stelzl, U., Worm, U., Lalowski, M., Haenig, C., Brembeck, F. H., Goehler, H., Stroedicke, M., Zenkner, M., Schoenherr, A., Koeppen, S., Timm, J., Mintzlaff, S., Abraham, C., Bock, N., Kietzmann, S., Goedde, A., Toksöz, E., Droege, A., Krobitsch, S., Korn, B., Birchmeier, W., Lehrach, H. and Wanker, E. E. (2005). ‘A human protein-protein interaction network: A resource for annotating the proteome.’, *Cell*, 122(6), pp. 957–968.

Takayama, K., Wang, C. and Besra, G. S. (2005). ‘Pathway to synthesis and processing of mycolic acids in *Mycobacterium tuberculosis*.’, *Clinical Microbiology Reviews*, 18(1), pp. 81–101.

Thomas, J. G. and Baney, F. (1996). ‘Protein misfolding and inclusion body formation in recombinant *Escherichia coli* cells overexpressing heat-shock proteins.’, *The Journal of Biological Chemistry*, 271(19), pp. 11141–11147.

Toledo, J. C., Audi, R., Oiguscu, R., Monteiro, G., Netto, L. E. S. and Augusto, O. (2011). ‘Horseradish peroxidase compound I as a tool to investigate reactive protein-cysteine residues: From quantification to kinetics.’, *Free Radical Biology & Medicine*, 50(9), pp. 1032–1038.

Tran, N. T. L., Deluccia, L., McDonald, A. F. and Huang, C. (2015). ‘Cross-disciplinary

detection and analysis of network motifs.’, *Libertas Academica*, 9, pp. 49–60.

Trujillo, M., Mauri, P., Benazzi, L., Comini, M., De Palma, A., Flohé, L., Radi, R., Stehr, M., Singh, M., Ursini, F. and Jaeger, T. (2006). ‘The mycobacterial thioredoxin peroxidase can act as a one-cysteine peroxiredoxin.’, *Journal of Biological Chemistry*, 281(29), pp. 20555–20566.

Tufariello, J. M., Chan, J. and Flynn, J. L. (2003). ‘Latent tuberculosis: mechanisms of host and bacillus that contribute to persistent infection.’, *The Lancet Infectious Diseases*, 3(9), pp. 578–590.

Ung, K. S. E. and Av-Gay, Y. (2006). ‘Mycothiol-dependent mycobacterial response to oxidative stress.’, *Federation of European Biochemical Societies Letters*, 580, pp. 2712–2716.

Van Laer, K., Buts, L., Foloppe, N., Vertommen, D., Van Belle, K., Wahni, K., Roos, G., Nilsson, L., Mateos, L. M., Rawat, M., Van Nuland, N. A. J. and Messens, J. (2012). ‘Mycoredoxin-1 is one of the missing links in the oxidative stress defence mechanism of Mycobacteria.’, *Molecular Microbiology*, 86(4), pp. 787–804.

Ventola, C. L. (2015). ‘The antibiotic resistance crisis-part 1: causes and threats.’, *Pharmacy and Therapeutics*, 40(4), pp. 277–283.

Voskuil, M. I., Bartek, I. L., Visconti, K. and Schoolnik, G. K. (2011). ‘The response of Mycobacterium tuberculosis to reactive oxygen and nitrogen species.’, *Frontiers in Microbiology*, 2(105), pp. 1–12.

Warner, D. F. and Mizrahi, V. (2014). ‘Translating genomics research into control of tuberculosis: lessons learned and future prospects.’, *Genome Biology*, 15, pp. 1–12.

Wernicke, S. and Rasche, F. (2006). ‘FANMOD: a tool for fast network motif detection.’, *Bioinformatics*, 22(9), pp. 1152–1153.

Winterbourn, C. C. (2013). *The biological chemistry of hydrogen peroxide*. 1st edn, *Methods in Enzymology*. 1st edn. Elsevier Inc. doi: 10.1016/B978-0-12-405881-1.00001-X.

Winterbourn, C. C. and Hampton, M. B. (2008). ‘Thiol chemistry and specificity in redox signaling.’, *Free Radical Biology & Medicine*, 45, pp. 549–561.

Winterbourn, C. C. and Hampton, M. B. (2014). ‘Redox biology: Signaling via a peroxiredoxin sensor.’, *Nature Chemical Biology*, 11(1), pp. 5–6.

Winyard, P. G., Moody, C. J. and Jacob, C. (2005). 'Oxidative activation of antioxidant defence.', *Trends in Biochemical Sciences*, 30(8), pp. 453–461.

Wong, E., Baur, B., Quader, S. and Huang, C. H. (2012). 'Biological network motif detection: Principles and practice.', *Briefings in Bioinformatics*, 13(2), pp. 202–215.

Wood, Z. A., Schroder, E., Harris, R. J. and Poole, L. B. (2003). 'Structure, mechanism and regulation of peroxiredoxins.', *Trends in Biochemical Sciences*, 28(1), pp. 32–40.

World Health Organization (2012). 'Global tuberculosis report 2012', *WHO report*, doi: 978 92 4 156450 2.

World Health Organization (2015). 'Global Tuberculosis Report 2015', *WHO report*, doi: 10.1017/CBO9781107415324.004.

Yeger-Lotem, E., Sattath, S., Kashtan, N., Itzkovitz, S., Milo, R., Pinter, R. Y., Alon, U. and Margalit, H. (2004). 'Network motifs in integrated cellular networks of transcription-regulation and protein-protein interaction.', *Proceedings of the National Academy of Sciences of the United States of America*, 101(16), pp. 5934–5939.

Yuniastuti, A. (2012). 'The role and characteristic of antioxidant for redox homeostasis control system in Mycobacterium tuberculosis.', *International Research Journal of Microbiology*, 3(13), pp. 416–422.

Zar, H. J., Eley, B., Nicol, M. P., Figaji, A. and Hawkrigde, A. (2012). 'Advances in childhood tuberculosis—contributions from the University of Cape Town.', *South African Medical Journal*, pp. 518–521.

Zhang, L. (2011). 'Proteomic progress in studying tuberculosis from 2010 to 2011.', *Journal of Biophysical Chemistry*, 2(4), pp. 395–400.

Zhao, F., Yan, J., Deng, S., Lan, L., He, F., Kuang, B. and Zeng, H. (2006). 'A thioredoxin reductase inhibitor induces growth inhibition and apoptosis in five cultured human carcinoma cell lines.', *Cancer Letters*, 236, pp. 46–53.

Zumla, A., Raviglione, M., Hafner, R. and von Reyn, C. F. (2013). 'Tuberculosis.', *The New England Journal of Medicine*, 368, pp. 745–55.

# Appendix

## Computational model script S1: *M. tuberculosis* unique Bi-Fan motif

```
#Core model of the Bi-Fan motif in M. tuberculosis
#####
#Reactions with rate expressions#
#####

FIX: NADPH NADP H2O2 H2O

# TR, Thioredoxin reductase reaction:

R1: NADPH + TrxBSS = NADP + TrxBSH
kcat1*TR*(NADPH/K1nadph)*(TrxBSS/K1trxbss)/((1+NADPH/K1nadph)*(1+TrxBSS/K1trxbss))

R2: NADPH + TrxCSS = NADP + TrxCSH
kcat2*TR*(NADPH/K1nadph)*(TrxCSS/K2trxcss)/((1+NADPH/K1nadph)*(1+TrxCSS/K2trxcss))

# TrxB and TrxC, Thioredoxin Reactions:
# TrxB reactions with TpxSH/SS and BcpSH/SS below:

R3: TrxBSH + TpxSS = TrxBSS + TpxSH
    K3*TrxBSH*TpxSS

R4: TrxBSH + BcpSS = TrxBSS + BcpSH
    K4*TrxBSH*BcpSS

# TrxC reactions with TpxSH/SS and BcpSH/SS below:

R5: TrxCSH + TpxSS = TrxCSS + TpxSH
    K5*TrxCSH*TpxSS

R6: TrxCSH + BcpSS = TrxCSS + BcpSH
    K6*TrxCSH*BcpSS

#H2O2 reactions with Prx's TpxSH and BcpSH:

R7: TpxSH + H2O2 = TpxSS + {2} H2O
    K7*TpxSH*H2O2

R8: BcpSH + H2O2 = BcpSS + {2} H2O
    K8*BcpSH*H2O2

#Species:
NADPH = 5
NADP = 0
TrxBSH = 0.5
TrxBSS = 0.5
TrxCSH = 0.5
TrxCSS = 0.5
TR = 5
TpxSH = 0.5
TpxSS = 0.5
BcpSH = 0.5
BcpSS = 0.5
H2O2 = 1
H2O = 0.5

#Rate Parameters:
kcat1 = 1
kcat2 = 1
K1nadph = 1
```

K1trxbss = 1  
 K2trxcss = 1  
 K3 = 1  
 K4 = 1  
 K5 = 1  
 K6 = 1  
 K7 = 1  
 K8 = 1

## **Computational model script S2: Bi-parallel motif for comparison to Bi-Fan motif**

```

#Core model of the Bi-parallel motif to compare to the Mtb Bi-Fan motif
#####
#Reactions with rate expressions#
#####

FIX: NADPH NADP H2O2 H2O

# TR, thioredoxin reductase reactions with TrxBSS and TrxCSS:

R1: NADPH + TrxBSS = NADP + TrxBSH
kcat1*TR*(NADPH/K1nadph)*(TrxBSS/K1trxbss)/((1+NADPH/K1nadph)*(1+TrxBSS/K1trxbss))

R2: NADPH + TrxCSS = NADP + TrxCSH
kcat2*TR*(NADPH/K1nadph)*(TrxCSS/K2trxcss)/((1+NADPH/K1nadph)*(1+TrxCSS/K2trxcss))

# TrxB side, thioredoxin reaction with Tpx:

R3: TrxBSH + TpxSS = TrxBSS + TpxSH
    K3*TrxBSH*TpxSS

R4: TpxSH + H2O2 = TpxSS + {2} H2O
    K4*TpxSH*H2O2

# TrxC side, thioredoxin reaction with Bcp:

R5: TrxCSH + BcpSS = TrxCSS + BcpSH
    K5*TrxCSH*BcpSS

R6: BcpSH + H2O2 = {2} H2O + BcpSS
    K6*BcpSH*H2O2

# Species
NADPH = 5
NADP = 1
TrxBSH = 0.5
TrxBSS = 0.5
TrxCSH = 0.5
TrxCSS = 0.5
TR = 5
TpxSH = 0.5
TpxSS = 0.5
BcpSH = 0.5
BcpSS = 0.5
H2O2 = 1
H2O = 1

#Rate Parameters:
kcat1 = 1
kcat2 = 1
K1nadph = 1
  
```

K1trxbss = 1  
K2trxcss = 1  
K3 = 1  
K4 = 1  
K5 = 1  
K6 = 1

**Table S1:** FANMOD 3 Node Output using 2000 randomizations for *E. coli* for the motif detection analysis.

Motif ID	Frequency % (Original)	Mean-Frequency % (Random)	Standard deviation (Random)	z-Score	p-Value	Motif (Sub-graph)
6	16.216	15.836	0.0177	0.215	0.277	
12	35.135	33.975	0.0253	0.458	0.183	
36	45.946	46.259	0.0100	-0.3123	0.318	
38	2.703	3.523	0.0269	-0.3045	0.421	

**Table S2:** FANMOD 3 Node Output using 2000 randomizations for *S. cerevisiae* for the motif detection analysis.

Motif ID	Frequency % (Original)	Mean-Frequency % (Random)	Standard Deviation (Random)	z-Score	p-Value	Motif (Sub-graph)
6	25.714	24.046	0.0114	1.459	0.0725	
12	28.571	26.095	0.0188	1.320	0.0085	
36	44.286	44.16	0.0067	0.188	0.221	
38	1.429	5.352	0.0227	-1.732	0.940	

**Table S3:** FANMOD 3 Node Output using 2000 randomizations for *M. tuberculosis* for the motif detection analysis.

Motif ID	Frequency % (Original)	Mean-Frequency % (Random)	Standard deviation (Random)	z-Score	p-Value	Motif (Sub-graph)
6	11.11	11.925	0.0170	-0.480	0.584	
12	52.778	50.847	0.0321	0.6008	0.0995	
36	33.33	34.237	0.0130	-0.696	0.620	
38	2.778	2.02	0.0227	0.335	0.258	

**Table S4:** MAVisto 3 Node Output using 2000 randomizations for *E. coli* for the motif detection analysis.

Motif ID	Frequency	Frequency %	Standard deviation	z-Score	p-Value	Motif (Sub-graph)
F7F	7	17.5	0	0	1	
F8R	14	35	1.06	0.579	0.726	
FKX	1	2.5	0.91	-0.171	0.742	
GCR	18	45	0	0	1	

**Table S5:** MAVisto 3 Node Output using 2000 randomizations for *S. cerevisiae* for the motif detection analysis.

Motif ID	Frequency	Frequency %	Standard deviation	z-Score	p-Value	Motif (Sub-graph)
F7F	16	23.88	0	0	1	
F8R	19	28.36	1.05	0.621	0.702	
FKX	1	1.49	1.289	-1.316	0.962	
GCR	31	46.27	0	0	1	

**Table S6:** MAVisto 3 Node Output using 2000 randomizations for *M. tuberculosis* for the motif detection analysis.

Motif ID	Frequency	Frequency %	Standard deviation	z-Score	p-Value	Motif (Sub-graph)
F7F	5	12.82	0	0	1	
F8R	20	51.28	1.265	0.688	0.635	
FKX	1	2.56	0.754	0.417	0.53	
GCR	13	33.33	0	0	1	

**Table S7:** FANMOD 4 Node Output using 2000 randomizations for *E. coli* for motif detection analysis.

<b>Motif ID</b>	<b>Frequency % (Original)</b>	<b>Mean-Frequency % (Random)</b>	<b>Standard deviation (Random)</b>	<b>z-Score</b>	<b>p-Value</b>	<b>Motif (Sub-graph)</b>
14	1.389	1.388	0.0083	0.0007	0.459	
28	6.944	5.415	0.0173	0.8836	0.145	
74	8.333	8.234	0.0392	0.0253	0.44	
140	6.944	17.094	0.0621	-1.635	0.925	
142	1.389	1.128	0.0103	0.253	0.308	
392	29.167	24.83	0.0461	0.941	0.172	
536	13.889	9.492	0.0302	1.456	0.073	
2076	1.389	1.260	0.0117	0.110	0.334	
2182	1.389	0.441	0.00811	1.168	0.1005	
2184	27.778	22.5	0.0264	2.00	0.024	
2188	1.389	5.572	0.0449	-0.932	0.698	

**Table S8:** FANMOD 4 Node Output using 2000 randomizations for *S. cerevisiae* for the motif detection analysis.

Motif ID	Frequency % (Original)	Mean-Frequency % (Random)	Standard Deviation (Random)	z-Score	p-Value	Motif (Sub-graph)
14	7.22	4.755	0.011	2.286	0.012	
28	8.33	5.865	0.0151	1.631	0.01	
74	7.778	9.596	0.0350	-0.520	0.671	
140	7.22	17.659	0.0498	-2.095	0.971	
142	1.11	3.015	0.0131	-1.455	0.908	
392	22.22	16.143	0.0371	1.637	0.05	
536	9.44	5.571	0.0188	2.062	0.014	
2076	0.556	1.158	0.00748	-0.805	0.753	
2116	0.556	0.279	0.00280	0.99	0.2245	
2182	3.889	0.485	0.00720	4.730	0.002	
2184	31.111	23.465	0.0215	3.554	0.0005	
2188	0.556	7.88	0.0346	-2.118	0.968	

**Table S9:** FANMOD 4 Node Output using 2000 randomizations for *M. tuberculosis* for the motif detection analysis.

<b>Motif ID</b>	<b>Frequency % (Original)</b>	<b>Mean-Frequency % (Random)</b>	<b>Standard deviation (Random)</b>	<b>z-Score</b>	<b>p-Value</b>	<b>Motif (Sub-graph)</b>
28	4.762	4.10	0.0133	0.4996	0.397	
74	4.762	10.015	0.0268	-1.958	0.974	
204	1.587	0.055	0.0028	5.497	0.0075	
392	38.095	30.189	0.0516	1.531	0.058	
536	22.22	21.73	0.0422	0.116	0.449	
2076	1.587	0.8181	0.010	0.763	0.175	
2116	3.175	3.41	0.011	-0.217	0.622	
2118	1.587	0.222	0.00573	2.383	0.053	
2182	6.349	0.436	0.0075	7.842	0	
2184	15.873	12.187	0.0215	1.714	0.027	

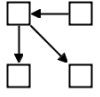
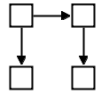
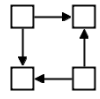
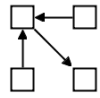
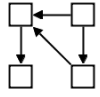
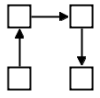
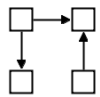
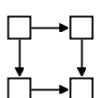
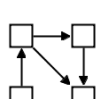
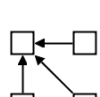
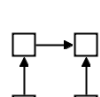
**Table S10:** MAVisto 4 Node Output using 2000 randomizations for *E. coli* for the motif detection analysis.

Motif ID	Frequency	Frequency %	Standard deviation	z-Score	p-Value	Motif (Sub-graph)
PMN4F	2	2.35	0	0	1	
PMN8R	6	7.06	1.097	0.479	0.79	
PMO8X	1	1.18	0.865	-0.001	0.686	
PMQGF	9	10.59	3.276	-0.113	0.576	
PN0KF	11	12.94	2.226	0.99	0.232	
PNHHF	7	8.24	6.491	-1.87	0.968	
PUBTX	1	1.18	0.678	0.808	0.372	
Q9GBX	1	1.18	0.849	0.034	0.677	
Q9PFR	21	24.71	0	0	1	
Q9QK9	1	1.18	3.397	-0.926	0.772	
RJ9KF	25	29.41	3.874	-0.016	0.554	

**Table S11:** MAVisto 4 Node Output using 2000 randomizations for *S. cerevisiae* for the motif detection analysis.

Motif ID	Frequency	Frequency %	Standard deviation	z-Score	p-Value	Motif (Sub-graph)
PMN4F	12	6.32	0	0	1	
PMN8R	13	6.84	1.977	0.548	0.741	
PMO8X	1	0.53	2.944	-1.593	0.97	
PMQGF	25	13.16	6.557	0.033	0.528	
PN0KF	16	8.42	2.947	1.232	0.186	
PNHHF	11	5.79	12.849	-2.87	0.994	
PUBTX	6	3.16	1.377	3.22	0.021	
Q9GBX	1	0.53	1.138	-0.884	0.906	
Q9PFR	57	30	0	0	1	
Q9QK9	1	0.53	7.19	-1.856	0.97	
RJ9KF	47	24.74	5.145	-0.008	0.489	

**Table S12:** MAVisto 4 Node Output using 2000 randomizations for *M. tuberculosis* for the motif detection analysis.

Motif ID	Frequency	Frequency %	Standard deviation	z-Score	p-Value	Motif (Sub-graph)
PMN8R	4	4.49	0.666	0.544	0.732	
PMQGF	12	13.48	1.81	1.883	0.05	
PMRM9	1	1.12	0.216	4.404	0.049	
PMXCR	3	3.37	0.571	0.505	0.768	
PMYH9	1	1.12	0.359	2.4	0.134	
PN0KF	16	17.98	2.817	-0.192	0.666	
PNHHF	4	4.49	3.43	-1.998	0.982	
PUBTX	4	4.49	0.516	7.186	0	
Q9GBX	1	1.12	0.671	0.678	0.452	
Q9PFR	10	11.24	0	0	1	
RJ9KF	33	37.08	4.414	2.012	0.033	

**Equation S1:** Differential equation solved for  $dTpxSH$  in the Bi-Fan motif.

$$\frac{dTpxSS}{dt} = k_{c1} \cdot H_2O_2 \cdot TpxSH - v_2 - v_5 \quad (27)$$

At steady state,  $\frac{dTpxSS}{dt} = 0$  therefore:

$$k_{c1} \cdot H_2O_2 \cdot TpxSH - v_2 - v_5 = 0$$

where  $v_2$  and  $v_5$  are equations (25) and (26) (Page 56) above respectively,

solving for  $TpxSH$  yields the following equation:

$$TpxSH = \frac{((k_2k_5TpxSS + k_2k_6BcpSS)(k_1TrxB_{tot}NADPH)(TpxSS) + (k_2k_5TpxSS + k_3k_5BcpSS)(k_4TrxC_{tot}NADPH)(TpxSS) + (k_1k_5(k_4TrxC_{tot}NADPH)(TpxSS) + k_2k_4(k_1TrxB_{tot}NADPH)(TpxSS))NADPH)}{(k_1k_4k_{c1}H_2O_2NADPH^2 + H_2O_2NADPH(k_{c1}(k_1k_6BcpSS + k_3k_4BcpSS) + k_{c1}TpxSS(k_1k_5 + k_2k_4)) + k_3k_6k_{c1}BcpSS^2 + k_{c1}TpxSS(k_2k_6BcpSS + k_3k_5BcpSS) + k_2k_5k_{c1}TpxSS^2)H_2O_2)}$$

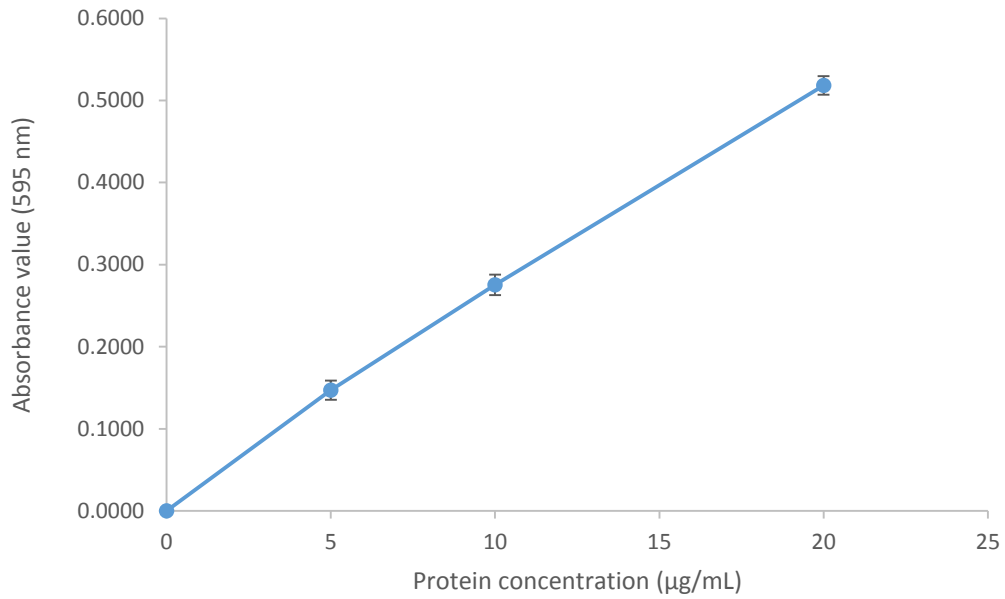


**Figure S1.** The Bradford standard curve constructed using a 1 mg/mL bovine serum albumin stock solution diluted to concentrations ranging from 0 to 20 µg/mL. Absorbance values were measured in triplicate for each concentration (595 nm) and standard error bars are shown. This is the linear portion of the original curve (0 to 100 µg/mL) and served to be sufficient for this study as protein concentrations never exceeded 20 µg/mL.